Studies of Molecules and Molecular Complexes Using Microwave Spectroscopy

A DISSERTATION
SUBMITTED TO THE FACULTY OF THE
UNIVERSITY OF MINNESOTA
BY

Christopher J. Smith

IN PARTIAL FULFILLMENT OF THE REQUIREMENTS
FOR THE DEGREE OF
DOCTOR OF PHILOSOPHY

Dr. Kenneth R. Leopold, Advisor

September, 2019

Acknowledgments

Much, if not most, of my success in graduate school is due to my advisor, Ken Leopold. His kindness, support, and passion for science made me strive to be a better scientist, spectroscopist, and ultimately, a better person. He was always available whenever I needed to talk, whether it be about science or about life. He cared about me as a student, a fellow scientist, and as a person. I will forever be grateful of his contributions in my life and a better advisor could not be asked for.

Thank you to my lab mates, Chris, Becca, Anna, and Nathan. You are terrific colleagues and wonderful friends. Chris and Becca, much thanks to you both for your lessons about the instrumentation and about microwave spectroscopy in general. Anna, thank you for all your help over the last few years and helping me answer questions that I had, especially those pertaining to computational chemistry. To the rest of my physical chemistry professors and graduate students, thank you for your never-ending support, your welcoming community, and helpful criticism of my work.

To all my friends, especially those who did CrossFit and played baseball with me, thank you. You always knew how to cheer me up and make me laugh whenever I was feeling down and pushed me to always look on the brighter side of any situation.

Finally, to my family. Words cannot describe how much your love, support, and unwavering faith in me helped me get to where I am today. Rigby, your unconditional love and constant kisses always made the day shine brighter. Claude and Julie, thank you for showing me what really matters in life and for welcoming me into your family. Nana and Papa, for calling just to check in with me. It always made the day a little brighter. Mom and dad, your care, support, and the lessons you have taught me over the years are invaluable and will never be forgotten. Most importantly, to my wife, Ciara Louise Smith, thank you from the bottom of my heart. You taught me to keep the bigger picture in perspective whenever I became too focused. Your constant push, both in my school work and at home, helped me more than you can imagine. You have always been there for me and put a smile on my face, no matter what type of day you were having. Your love for me never faltered and for that, I am forever grateful.

Dedication

For James Reuben Smith Jr. and Barbara Helen Davis Smith

Table of Contents

List of Tables

List of Figures

Introduction

Molecular clusters play an important role in many aspects of chemistry. They serve as the link between microscopic and macroscopic states of matter because their sizes and properties are intermediate between those of individual molecules and the bulk phase. Studying small molecular clusters allows for a better understanding of the fundamental interactions that govern molecules as they assemble to form bulk matter. From simple systems, such as hydrogen-bonded water molecules, to multicomponent systems, like precursors to aerosol particles, the constituents and their orientation in molecular clusters is crucial to understand if insight is to be gained in how macroscopic properties evolve with size. By focusing on molecular clusters that potentially form in the atmosphere, insight can be gained regarding atmospheric processes like aerosol formation.

The broad impact that molecular clusters have in chemistry has made them targets of scientific research, and many techniques are available to study them. For example, Fourier Transform Infrared Spectroscopy (FTIR) and intracavity laser absorption spectroscopy have been used to study the dynamics of molecular clusters,[1,2] time-of-flight mass spectrometry has been used to study the reactivity of charged clusters,[3] and the properties of atomic and molecular clusters have been determined using negative ion photoelectron spectroscopy[4,5] and microwave spectroscopy.[6-8] This thesis employs microwave spectroscopy to gain a great amount of detail about a cluster's molecular and electronic structure, as well as internal dynamics. For instance, it has provided insight to how the process of proton dissociation is initiated, elucidated hydrogen bonding networks, and described the structure of atmospheric complexes and intermediates in reactions.[9]

The Leopold group uses Fourier transform microwave spectroscopy (FTMW) to obtain information regarding the physical and electronic structure of molecules and molecular complexes. Since World War II[10], microwave spectroscopy, as implemented via waveguide cells,[11] molecular beam electric resonance,[12] and the Ball-Flygare spectrometer,[13] has proven a powerful tool for studying molecules and molecular clusters. One of the latest advancements in microwave spectroscopy is the broadband chirped-pulse

spectrometer. Originally developed in the Pate lab in 2008, the chirped-pulse FTMW is capable of collecting broadband regions of rotational spectra in a single acquisition.[14] While its counterpart, the Balle-Flygare spectrometer, a Fabry-Perot cavity instrument, provides high resolution and sensitivity, the cavity method is greatly restricted by the speed with which data can be collected. The two techniques function synergistically and have greatly added to the practice and impact of rotational spectroscopy.

The cavity FTMW spectrometer in the Leopold lab was renovated to include a chirped-pulsed spectrometer in 2013.[15] Microwave horns and associated circuitry were added along an axis perpendicular to that of the microwave cavity, and a microwave absorbing foam arm was installed between the mirrors in the cavity to stop the microwave radiation from producing unwanted reflections between them. Briefly, our chirped-pulse spectrometer collects spectra between 6 and 18 GHz, in 3 GHz segments. A 3 GHz sweep between 0.2 and 3.2 GHz is mixed with a microwave signal and the resulting radiation is emitted through a microwave horn into a vacuum chamber, whereupon molecular excitation ensues. The resulting molecular emission is collected via a second microwave horn, down converted using a local microwave frequency, and recorded on an oscilloscope. The resulting signal is Fourier transformed and a frequency spectrum is thus generated. The instrument is designed for switching between the chirped-pulse and cavity experiments while the molecule source can remain unchanged.

Alongside the experimental data collected using the University of Minnesota's dual chirped-pulse and cavity FTMW, every project was complemented with theoretical work. Both density functional theory and *ab initio* methods were utilized in predicting the structure, energies, and other electronic properties of the small molecules and molecular complexes.

The work presented in this thesis covers a variety of small molecules and complexes, which can roughly be grouped into two categories: molecules with different conformations and molecules/complexes potentially relevant to atmosphere aerosol nucleation.

The conformation of molecules has been a topic of interest for many years, as essential biological and chemical processes, such as transport and recognition, are determined by the shape of a molecule and weak interactive forces between them and the surrounding environment.[16] For example, enzymes play important functional roles in substrate binding and release, as well as formation of catalytically competent configurations.[17] Without their ability to change conformation, many biological processes would not be possible as these enzymes could not bind or release specific substrates. Additionally, molecules can exhibit interesting internal dynamics, which can provide useful information about the physical and electronic structure of the molecule. For example, studying molecules that contain methyl rotors offers insight into their barrier heights[18-21], which not only allows for a better understanding of the molecular flexibility of the molecule, but also provides benchmarks for theoretical chemists.

Chapter 1 presents work on the *syn*- and *anti* conformers of thioacetic acid, where we discovered that the methyl group internal rotation barrier differed between the two forms by a nearly a factor of five. With the collaboration of Yirong Mo (Western Michigan University) and Huaiyu Zhang (Hebei Normal University), we aimed to explain this unusually large difference.[22]

In regard to the second subject, atmospheric aerosols have become of great interest in recent years. Aerosols are ubiquitous in the atmosphere and can affect the quality of life in several ways, such as negatively affecting human health, decreasing visibility and influencing climate.[23] While the mechanism(s) by which particles nucleate and grow in the atmosphere is not yet fully understood,[23-26] homogenous nucleation is one possible route for particle formation. Homogeneous nucleation is a process by which individual gas molecules aggregate together to first form complexes, then a stable cluster, and finally an aerosol particle through continued spontaneous growth.[27] Sulfuric acid has long been known to be a key component in particle formation. It is formed in the atmosphere by the oxidation of sulfur dioxide (SO_2) to sulfur trioxide (SO_3), followed by hydrolysis. Sulfuric

acid is highly hygroscopic, however, binary models involving sulfuric acid and water do not accurately predict new particle formation rates. Therefore, other constituents must be involved and scientists have started to incorporate common atmospherically relevant organic species, such as amines, carboxylic acids, and oxidative products of hydrocarbons into their models.[28,29] However, while much has been learned about aerosols and their formation over the past few decades, a full understanding of the nucleation pathways, new particle formation rates, and aerosol composition at various stages, is still unclear.

Recent theoretical research incorporating carboxylic acids in the early stages of nucleation, which showed that formic acid (HCOOH) catalyzes the hydration of SO_3, converting SO_3 to sulfuric acid, caught our attention. Furthermore, calculations showed that the activation barrier of this formic acid catalyzed reaction was not only lowered, but essentially zero. Finally, the authors proposed that this alternative pathway for generating atmospheric sulfuric acid could be competitive with current proposed mechanisms.[30] When our group set out to investigate related complexes such H_2SO_4 – HCOOH and SO_3 – HCOOH, a new project transpired, as an entirely new molecule was discovered, FSA (formic sulfuric anhydride).[31]

While this new class of molecules, carboxylic sulfuric anhydrides, is relatively unknown in the chemical literature, they could have great importance in the mechanisms for formation of atmospheric aerosols. Chapter 2 presents work on *s-cis*- and *s-trans*-acrylic sulfuric anhydride (*s-cis*-AcrSA and *s-trans*-AcrSA), which are formed from *trans*- and *cis*-acrylic acid, respectively, and provides experimental evidence that a variety of carboxylic acids can react with SO_3 to generate their corresponding carboxylic sulfuric anhydrides[32] Chapter 3 illustrates our work on the acetic sulfuric anhydride – water complex. Our aim was to hydrate a carboxylic sulfuric anhydride in order to understand its interaction with water, a first step in understanding anhydride hydrolysis, which would result in the generation of the sulfuric acid – acetic acid complex.[33] Chapter 4 contains a study of propiolic sulfuric anhydride (PSA) and reviews all the carboxylic sulfuric anhydrides characterized by our lab to date, both experimentally and theoretically.

Comparisons among their structures and energetics are made and detailed statistical thermodynamic calculations are carried out to estimate their equilibrium constants and concentrations over a range of atmospherically relevant temperatures. Comparisons between their concentrations and the concentrations of other atmospherically relevant species are also highlighted.[34]

Chapter 1: A Strong Dependence of the CH3 Internal Rotation Barrier on Conformation in Thioacetic Acid: Microwave Measurements and an Energy Decomposition Analysis

Reproduced from C. J. Smith, Anna K. Huff, Huaiyu Zhang, Yirong Mo, Kenneth R. Leopold, *J. Chem Phys.*, **150**, 134302 (2019)
With the permission of AIP Publishing

Overview

Rotational spectra of thioacetic acid (CH3COSH) have been observed by pulsed-nozzle Fourier transform microwave spectroscopy. Spectroscopic constants are reported for both the syn and anti conformers of the parent species, as well as the ^{34}S and ^{13}C carbonyl isotopologues. Transitions arising from the lowest A and E internal rotor states of the methyl group have been observed and analyzed. Experimental values of the three-fold internal rotation barrier, V_3, for the *syn* and *anti* conformers of the parent isotopologue are 76.300(12) and 358.056(51) cm^{-1}, respectively, indicating a large effect of the S−H orientation on the CH_3 internal rotation potential. M06-2X/6-311+G(d,p) calculations are in good agreement with these results. The block localized energy decomposition method has been applied to understand the origins of this strong dependence of V_3 on conformation. The results indicate that π conjugation from the SH to the carbonyl group and steric repulsion between the SH and the methyl group in the *anti* form are main contributors to the difference.

Introduction

Interest in the internal rotation barriers in molecules has spanned many decades.[35] Rigorous methods for the analysis of their spectroscopic manifestations have long been available,[36] and continuing improvements in experimental capabilities continue to drive modern research aimed at improving the accuracy with which spectra can be analyzed.[37-42] Along separate lines, the development of a general understanding of the physical origins of internal rotation barriers has been the subject of much discussion.[43-48] The topic is complex due to the interplay between steric repulsion, structural relaxation, and electronic delocalization effects which, together, conspire to produce barriers that can be the net result of large and sometimes competing terms. Further complications arise, moreover, when molecules are flexible and subject to multiple conformations. Indeed, surprising conformational dependences of CH_3 group internal rotation barriers have been well established in a number of recent microwave studies.[18-20]

In this paper, we report the microwave spectroscopic determination of the CH_3 internal rotation barriers for the *syn* and *anti* conformers of thioacetic acid, CH_3COSH (Figure 1.1). While the barrier for the *syn* form has been determined by microwave spectroscopy,[49] to the best of our knowledge, the *anti* form has not been directly observed in the gas phase. Vibrational spectra of the liquid and vapor of thioacetic acid have been recorded,[50] and both conformers have been observed in cryogenic matrices.[51] Gas phase electron diffraction[52] and solution phase nmr spectroscopy[53] have also been reported. However, none of these methods have allowed the internal rotation barrier of the *anti* conformer to be determined. The ability to observe microwave spectra of both conformers in the gas phase affords the opportunity to study the effect of conformation on the CH_3 internal rotation barrier in a particularly simple system. The experimental results indicate a striking dependence of the barrier on the orientation of the SH group, with that of the *anti* conformer nearly five times that of the *syn* conformer. This difference is unusually large, and its

physical origins are investigated computationally using a Block Localized Wavefunction energy decomposition approach.

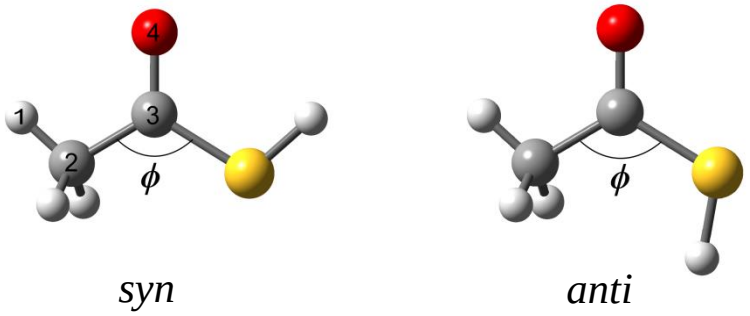

Figure 1.1 The *syn* and *anti* Forms of CH_3COSH

Experimental Methods and Results

Rotational spectra of thioacetic acid were obtained using a Fourier transform microwave spectrometer with dual cavity[13] and chirped-pulse[14] capabilities. The chirped-pulse spectrometer records spectra in 3 GHz segments at a resolution of ~30 kHz, thus enabling rapid exploration of frequency space. The cavity system offers higher sensitivity, albeit in a much narrower spectral bandwidth (~1 MHz). Further instrumental details have been described elsewhere.[15,54] Thioacetic acid was introduced into the spectrometer by entraining the vapor above the pure liquid (96%, Sigma Aldrich) in argon at a stagnation pressure of 1.7 atm. The resulting gas mixture was expanded through a 0.8 mm diameter nozzle, and was immediately guided through a 0.5 in. stainless steel cone terminating in a 0.19 in. diameter orifice. Initial chirped-pulse experiments enabled the determination of a preliminary set of spectral assignments, and subsequent cavity experiments were performed to re-measure transitions at higher resolution and observe weaker lines that were predicted on the basis of those assignments. In addition to spectra of the parent species, A and E state spectra of the *syn* and *anti* conformers of the ^{34}S and ^{13}C carbonyl isotopologues were also measured in natural abundance on the cavity system. Reported frequencies are typically accurate to ~6 kHz.

The observed chirped-pulse spectrum, recorded in 3 GHz segments, is shown in Figure 1.2 and represents the average of 10,000 free induction decay signals with a 90 μs data collection time. Under these conditions, only the *b*-type transitions were readily identified, though several weaker *a*-type lines were predicted and later recorded on the cavity spectrometer. Several *c*-type transitions in the E state were also observed for both conformers. Although formally forbidden since μ_c = 0 for both conformers, these transitions gain intensity through mixing of the *K*-doublet states, as described previously.[55,56] The set of recorded transitions for the parent species spanned 3.6 to 17.1 GHz, and included transitions involving levels up to J'' = 7 and J'' = 5 for the parent *syn* and *anti* forms, respectively. Somewhat lower J values were analyzed for the ^{34}S and ^{13}C carbonyl species. For all these species, however, transitions from K_{-1}'' = 0 to K_{-1}'' = 2 were

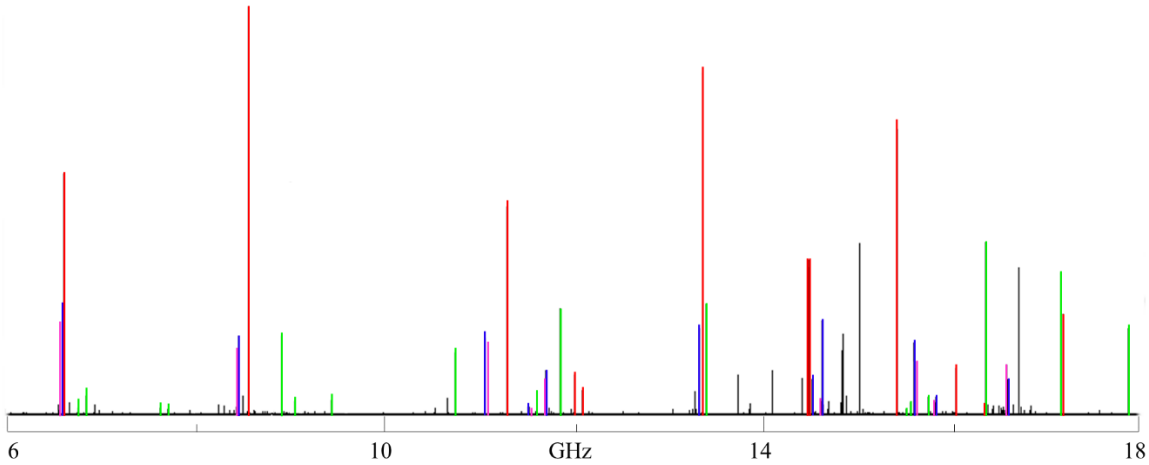

Figure 1.2 A 6-18 GHz Chirped-Pulse Microwave Spectrum of Thioacetic Acid in Argon.
The spectrum is an average of 10,000 free induction decay signals. *Syn* A and E states and *anti* A and E states of thioacetic acid are highlighted in red, green, blue, and pink, respectively. Known instrumental artifacts have been removed from the spectrum.

assigned, as were a few transitions involving K_{-1}'' = 3 for the parent species. Typically, A/E splittings for the *anti* form were between 1 and 10 MHz, whereas for the *syn* conformer, the splittings were on the order of hundreds of MHz to a few GHz. Qualitatively, this reflects the large difference between the internal rotation barriers of the two forms. Figure 1.3 shows a cavity spectrum containing A and E state transitions of the *anti* parent

conformer, which fortuitously lie within the span of a single data collection window. Tables of observed transition frequencies, assignments, and residuals from the least squares fits (see below) are provided in Appendix A. Note that in addition to the parent, ^{34}S, and ^{13}C carbonyl isotopologue spectra reported here, eight A state transitions were also observed for the *syn*-^{13}C methyl species. However, no E state lines were recorded and no internal rotation barrier could be determined. Thus, further analysis of those spectra was not pursued.

Preliminary spectral analysis of the parent isotopologue employed the program XIAM of Hartwig,[37] which implements the extended internal axis method introduced by Woods[57,58] and

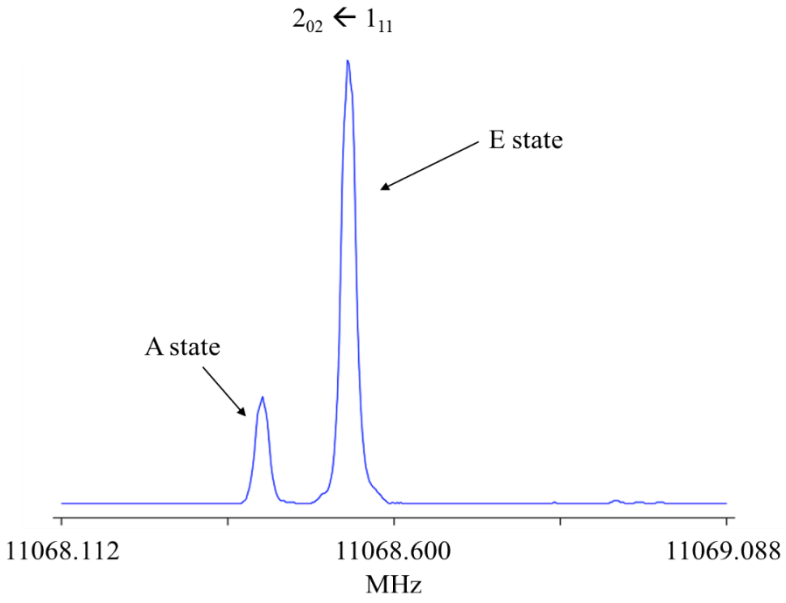

Figure 1.3 A Trace of the $2_{02} \leftarrow 1_{11}$ A and E State Transitions of *anti*- Thioacetic Acid Recorded on the Cavity Spectrometer

modified by Vacherand et al.[59] While a satisfactory fit was obtained for the *anti* conformer, the root means squared (rms) residual obtained for the *syn* conformer was approximately 85 kHz, a value that is significantly larger than the experimental uncertainties. Recognizing that the difficulty likely originated with the low barrier for the *syn* form, further trial fits were performed for both conformers using Kleiner's program BELGI-Cs[41] which has

previously demonstrated better success with low barrier problems.[40,60-63] This analysis applies the Rho-Axis Method ("RAM") and is based on the internal rotation Hamiltonian from the work of Kirtman[64], Lees and Baker,[65] and Herbst et al.[66] Details are given elsewhere.[41] Parameters involving progressively higher powers of the angular momentum operators were added as needed until a satisfactory fit was obtained in which all floated parameters were statistically determined.

Table 1.1 provides a comparison of the rotational constants (*A*, *B*, and *C*), internal rotation barrier (V_3), and rms residuals for both conformers of the parent species obtained from the XIAM and BELGI-Cs fits. Since BELGI-Cs outputs rotational constants in the rho-axis system, *A*, *B*, and *C* in this table have been transformed into the principal axis system for comparison with the XIAM values.[60] It is seen that there is quite reasonable agreement between the two methods, but that the constants obtained are not within the calculated standard errors. Similar results have been reported by others.[67] This may be due to the increased flexibility of the BELGI-Cs Hamiltonian, which allows for more terms to contribute to the rotational energy. Nevertheless, there is a pronounced improvement in the rms residuals for the *syn* species using BELGI-Cs and thus we use the values determined by BELGI-Cs for both conformers throughout the remainder of this work. Full sets of fitted spectroscopic constants for the *syn* and *anti* conformers produced by BELGI-Cs are provided in Table 1.2.A and 1.2.B, respectively, where it may be observed that (not surprisingly) a smaller set of constants is required to fit the spectrum of the higher barrier species. Definitions of these constants are given elsewhere.[68] We note that low barrier internal rotation problems are notoriously difficult, and that the particular choice of sets of distortion-like parameters may not be unique. Nevertheless, V_3 showed stability with respect to the choice of these smaller parameters through the sequence of trial fits and, moreover, is seen to be quite consistent across isotopologues. Even for the *anti* ^{13}C carbonyl species, for which nine parameters were used to fit only ten transitions, and with large standard errors on *A* and *B*, the value of V_3 is remarkably consistent with the other determinations.[69]

Table 1.1 Comparison of Spectroscopic Constants between XIAM and BELGI-Cs for *syn*- and *anti*-Thioacetic Acid[a]

***syn*-Thioacetic Acid**						
	XIAM			**BELGI-Cs[b]**		
	Parent	^{34}S	^{13}C-carbonyl	Parent	^{34}S	^{13}C-carbonyl
A [MHz]	9913.196(12)	9907.555(28)	9910.702(29)	9888.32(28)	9884.92(75)	9885.704(33)
B [MHz]	4923.132(10)	4777.292(13)	4911.381(21)	4923.96(17)	4778.68(45)	4911.935(37)
C [MHz]	3354.778(10)	3285.775(12)	3349.035(19)	3355.187(16)	3286.026(23)	3349.467(26)
V_3 [cm^{-1}]	77.81940(64)	77.72316(55)	77.7930(50)	76.300(12)	76.378(31)	76.2796(23)
N_A/N_E[c]	20, 23	12, 15	9, 7	20, 23	12, 15	9, 7
N_{param}[d]	11	11	10	20	20	13
rms [kHz][e]	85.2	102.8	46.1	3.0	0.8	1.7
***anti*-Thioacetic Acid**						
	XIAM			**BELGI-Cs[b]**		
	Parent	^{34}S	^{13}C-carbonyl	Parent	^{34}S	^{13}C-carbonyl
A [MHz]	9975.6935(98)	9974.5095(12)	9974.574(46)	9978.0(12)	9976.5(16)	9977(52)
B [MHz]	4884.8551(56)	4738.98574(70)	4801.096(27)	4887.04(57)	4740.82(89)	4803(24)
C [MHz]	3344.53002(89)	3275.36077(53)	3306.049(22)	3346.59(22)	3277.05(56)	3308.034(57)
V_3 [cm^{-1}]	354.56(35)	354.578(22)	349.34(56)	358.056(51)	358.498(57)	356.1(50)
N_A/N_E[c]	15, 16	10, 10	6, 4	15, 16	10, 10	6, 4
N_{param}[d]	13	8	7	12	12	9
rms [kHz][e]	5.3	8.2	15.0	4.5	3.2	13.5

(a) Numbers in parentheses represent the uncertainty in the last digit. The table does not report all spectroscopic constants included in the fits. Complete fits are provided as Supplementary Material.

(b) *A*, *B*, and *C* from the output of BELGI-Cs have been transformed to the principal axis system for comparison with XIAM results.

(c) Number of A and E state transitions, respectively, included in the fit.

(d) Number of fitted parameters.

(e) Unweighted rms was calculated as $[\Sigma(\nu_{obs} - \nu_{calc})^2/(N_A+N_E)]^{1/2}$ for direct comparison with the output of BELGI-Cs.

Table 1.2.A Spectroscopic Constants for *syn*-Thioacetic Acid Determined from BELGI-Cs[a]

	syn		
Parameter[b]	CH_3COSH	$CH_3CO^{34}SH$	$CH_3{}^{13}COSH$
A [MHz]	8036.32(25)	8026.91(29)	8028.687(20)
B [MHz]	6775.96(20)	6636.68(90)	6768.952(50)
C [MHz]	3355.187(16)	3286.026(23)	3349.467(26)
Δ_J [kHz]	19.44(97)	-104(14)	16.6(12)
Δ_{JK} [kHz]	-106.6(43)	651(86)	-85.7(82)
Δ_K [kHz]	69.4(57)	-685(75)	53.4(61)
V_3 [cm^{-1}]	76.300(12)	76.378(31)	76.2796(23)
ρ^c	0.042818(11)	0.042218(30)	0.0427214(22)
D_{ab} [MHz]	2400.851(56)	2456.67(24)	2405.7985(18)
δ_J [kHz]	6.65(62)	-36.0(56)	5.76(44)
δ_K [kHz]	2.240(57)	1.08(18)	-4.7(26)
D_{abJ} [kHz]	0.51(31)	-14.0(13)	0.51[f]
F_V [MHz]	-0.97(25)	5.3(12)	-0.642(52)
c_2 [MHz]	0.36(27)	6.3(12)	0.732(63)
k_5 [MHz]	56.85(56)	31.8(15)	56.85[f]
d_{ab} [MHz]	22.43(14)	24.52(63)	22.43[f]
f_V [kHz]	53.0(19)	-273(36)	53.0[f]
k_{5J} [MHz]	-0.2926(89)	1.55(20)	-0.2926[f]
k_{5K} [MHz]	0.157(13)	-1.52(17)	0.157[f]
c_{2J} [kHz]	40.6(20)	-0.203(29)	41[f]
F [cm^{-1}][d]	5.43113	5.43113	5.43113
N_A/N_E[e]	20, 23	12, 15	9, 7
rms [kHz]	3	0.8	1.7

(a) Numbers in parentheses are one standard error in the least squares fit. *A*, *B*, and *C* are in the rho-axis system.
(b) Notation from Reference [68].
(c) ρ is dimensionless.
(d) Fixed at the value derived from the M06-2X/6-311+G(d,p) structure
(e) Number of A and E state transitions, respectively, included in the fit.
(f) Fixed at parent value.

Table 1.2.B Spectroscopic Constants for *anti*-Thioacetic Acid Determined from BELGI-Cs[a]

anti			
Parameter[b]	CH_3COSH	$CH_3CO^{34}SH$	$CH_3{}^{13}COSH$
A [MHz]	8446.19(76)	8457.38(88)	8349(38)
B [MHz]	6418.89(97)	6259.9(16)	6431(38)
C [MHz]	3346.59(22)	3277.05(56)	3308.034(57)
Δ_J [kHz]	-2.21(18)	-2.03(46)	-10.8(35)
Δ_{JK} [kHz]	19.5(11)	18.8(28)	41.7(97)
Δ_K [kHz]	-2.65(56)	-3.3(17)	-2.65[f]
V_3 [cm^{-1}]	358.056(51)	358.498(57)	356.1(50)
ρ[c]	0.046110(28)	0.045631(28)	0.0456(14)
D_{ab} [MHz]	2334.97(37)	2376.10(53)	2403(15)
δ_J [kHz]	-1.306(86)	-1.17(24)	-7.0(22)
δ_K [kHz]	2.62(13)	2.39(63)	2.62[f]
D_{abJ} [kHz]			
F_V [MHz]	-11.8(12)	-9.9(30)	-11.8[f]
c_2 [MHz]			
k_5 [MHz]			
d_{ab} [MHz]			
f_V [kHz]			
k_{5J} [MHz]			
k_{5K} [MHz]			
c_{2J} [kHz]			
F [cm^{-1}][d]	5.52779	5.52779	5.52779
N_A/N_E[e]	15, 16	10, 10	6, 4
rms [kHz]	4.5	3.2	13.5

(a) Numbers in parentheses are one standard error in the least squares fit. *A*, *B*, and *C* are in the rho-axis system.
(b) Notation from Reference [68].
(c) ρ is dimensionless.
(d) Fixed at the value derived from the M06-2X/6-311+G(d,p) structure
(e) Number of A and E state transitions, respectively, included in the fit.
(f) Fixed at parent value.

Table 1.3 Observed and Calculated Spectroscopic Constants for the Parent *syn*- and *anti*-Thioacetic Acid and Comparison with Literature Values for the *syn* Form

	***syn*-Thioacetic Acid**			***anti*-Thioacetic Acid**	
	Experimental[a]	Theoretical[b]	Reference **Error! Bookmark not defined.**[c]	Experimental[a]	Theoretical[b]
A [MHz]	9888.32(29)	9967	9913.29(56)	9978.0(12)	10017
B [MHz]	4923.96(17)	4909	4923.11(23)	4887.04(57)	4868
C [MHz]	3355.187(16)	3358	3354.60(24)	3346.59(23)	3344
V_3 [cm^{-1}]	76.300(12)	86	77.86(49)	358.056(51)	370
μ_a [D]		0.15	0.191(10)		0.14
μ_b [D]		1.79	1.811(13)		3.72

(a) Microwave spectroscopic value determined in this work using BELGI-Cs. Values have been transformed into the principal axis system. Numbers in parentheses are one standard error in the least squares fit.
(b) M06-2X/6-311+G(d,p) value obtained in this work.
(c) Microwave spectroscopic value from reference 49.

Table 1.3 compares the results obtained with the literature values for the *syn* form, as well as with the values derived computationally for both forms in the next section. The qualitatively striking feature of these results is that the internal rotation barrier in the *anti* conformer is approximately 4.7 times larger than that in the *syn* conformer. Tables 1.1, 1.2.A, 1.2.B, and 1.3 provide convincing evidence that the difference is real and does not result from artifacts related to the method of spectroscopic analysis.

Computational Methods and Results

Calculations were performed in order to develop a physical understanding of the large difference between the internal rotation barriers described above. Rotations along bonds do not involve bond making or breaking, and thus the barriers can be computed quite accurately even at relatively low theoretical levels, largely due to the comparability of the electron correlation effect on isomers of the same molecule.[70,71] However, the exact nature of barriers can be better understood with more advanced computational approaches, as there are several stereoelectronic factors that contribute to the energy variation along the internal rotation pathway.[47,72-79] Thus, a series of calculations using the Block Localized Wavefunction (BLW) approach[80-83] was performed. The BLW method is a variant of *ab initio* valence bond (VB) theory[84-86] and calculations were implemented using the Xiamen Valence Bond (XMVB) program with the M06-2X/6-311+G(d,p) geometries and the 6-311+G(d,p) basis set.[87]

Initial geometry optimizations for both the *syn* and *anti* conformers of the acid were conducted at the M06-2X/6-311+G(d,p) level with Gaussian09[88] in order to establish the relative energies of the two forms. At this level of theory, the *anti* conformer lies 1.7 kcal/mol higher in energy than the *syn* form (1.4 kcal/mol with zero-point energy correction). Additional calculations at the M06-2X/6-311++G(3df,3pd) level place the *anti* conformer only 0.9 kcal/mol higher in energy (0.7 kcal/mol with zero-point corrections). The BLW calculations, however, were carried out at the former level of theory. Tables of Cartesian coordinates for the minimum energy structures of the *syn* and *anti* forms, obtained from the M06-2X/6-311+G(d,p) calculations, are provided in Appendix A.

Next, the difference between the CH_3 internal rotation barriers of the *anti* and *syn* forms were examined using both HF and M06-2X methods, with the geometries optimized at the M06-2X/6-311+G(d,p) level. Table 1.4 lists the energies obtained relative to the bottom of the potential well at several points along the internal rotation coordinate. It is clear from the table that the theoretical results are in accord with experiment using either method: The barrier for the *anti* form is in the 340-380 cm^{-1} range, while that for the *syn* form is in the 80-110 cm^{-1} range. The HF rotation barriers are larger than M06-2X values by 28-36 cm^{-1} (0.08-0.10 kcal/mol), which is understandable because the sterically hindered (crowded) molecules tend to have higher electron correlation. The difference between the internal rotation barriers at HF/6-311+G(d,p) and M06-2X/6-311+G(d,p) levels are level 268 and 260 cm^{-1}, respectively. These compare well with the experimentally observed value of 282 cm^{-1}.

The classical Lewis structure for the *syn* form of thioacetic acid is shown below (I). Here, the C=O bond is understood to be polarized, so that the resonance structure with a negative charge on oxygen and a positive charge on the carbonyl carbon is contained in (I). In addition to this structure, however, there is the possibility of π conjugation from the lone pair on the S atom to the carbonyl group (II), as well as structures involving hyperconjugation from the methyl group adjacent to the π system, represented by (III).

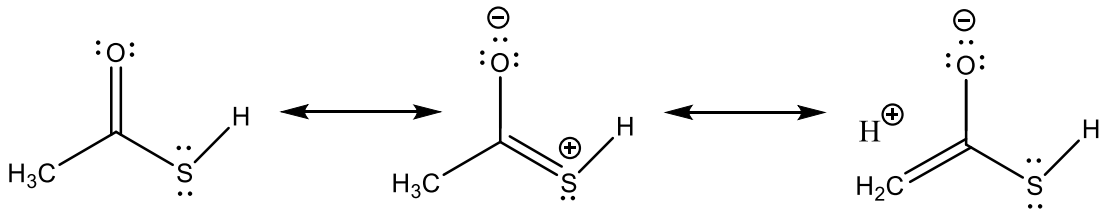

(I) (II) (III)

Table 1.4 Relative Energies (cm^{-1}) of Thioacetic Acid with the Rotation of CH_3

θ [a]	M06-2X		HF		BLW[b]		BLW(π)[c]		ϕ[a]	
	anti	syn	anti	syn	anti	syn	anti	syn	anti	syn
0	0.00	0.00	0.00	0.00	0.00	0.00	0.00	0.00	116.95	113.06
30	192.00	42.25	216.68	62.69	280.41	214.40	190.97	67.66	117.93	113.40
60	**343.70**	**83.82**	**379.59**	**111.74**	**493.45**	**342.71**	**310.60**	**88.66**	**118.86**	**113.66**
90	170.75	38.78	195.99	54.96	270.05	190.96	182.78	61.82	117.81	113.30
120	0.00	0.00	0.00	0.00	0.00	0.00	0.00	0.00	116.95	113.06

(a) θ is dihedral angle H1-C2-C3-O4. ϕ is the C2-C3-S angle (Figure 1.1).
(b) All σ and π electrons are localized.
(c) Only π electrons are delocalized.

To implement the BLW decomposition scheme, we initially examine the internal rotation barriers without any electronic contributions, i.e., we initially disable the intramolecular electron delocalization and calculate the energies of the classical Lewis structure (I) along the internal rotation coordinate. The resulting barriers are attributed to the steric effect that is composed of the electrostatic and Pauli repulsive interactions. Next, starting from this reference Lewis (or BLW) state, we then allow delocalization of the π electrons to arrive at a "BLW(π)" state (II). Finally, we continue to delocalize σ electrons (i.e., hyperconjugation) and arrive at the delocalized state, which is that computed from regular molecular orbital (MO) methods. At each step in these calculations, the molecular geometry is fixed at that obtained by constraining the internal rotation angle and re-optimizing the other structural parameters of the system. In this way, the molecular frame is allowed to relax at each value of the internal rotation angle.

The BLW results are depicted in two ways in Figure 1.4. The top portion of the figure shows the torsional energy profiles at different levels of theory. The bottom portion provides a "sequential" representation of the barriers along the steps of the BLW decomposition. Vertical lines (black) represent the changes in V_3 at different stages of the decomposition, beginning with the BLW state and following the arrows to the M06-2X energy. Diagonal lines (red) indicate the difference between internal rotation barriers of the *anti* and *syn* forms at each stage. With all electrons strictly localized on bonds or atoms, the BLW difference in internal rotation barriers between the *syn* and *anti* forms is only 151 cm^{-1}. However, if we allow π electrons to delocalize (i.e. by computing energies of the BLW(π) state), the difference increases remarkably to 222 cm^{-1}, quite close to the 268 cm^{-1} value obtained at the Hartree-Fock level with all electrons delocalized. Note that the π conjugation redistributes electrons within the COSH fragment and thus changes the local dipole moment of that moiety. This is usually regarded as a component of the steric effect to the methyl rotation barrier. Only a small difference (268 – 222 = 46 cm^{-1}) is contributed by the hyperconjugation (electronic) effect between the methyl and COSH groups. At the

M06-2X level, the difference is 260 cm^{-1}, only 8 cm^{-1} less than the Hartree-Fock result. This provides an estimate of the effect of electron correlation. Overall, these computations thus suggest that the difference between the methyl group internal rotation barriers in *syn* and *anti* forms of thioacetic acid results primarily (>80%) from the steric effect.

Further evidence for this steric effect is revealed by monitoring the variation of the bond angle ϕ ($\angle$CCS, Figure 1.1) along the methyl group internal rotation pathway. As seen in Table 1.4, for the *syn* form, ϕ is small and changes very little as the internal rotation takes place. In contrast, for the *anti* form, ϕ is large and increases linearly with energy, as shown in Figure 1.5. Moreover, further calculations indicate that when ϕ is fixed at its maximum value (118.86º at $\theta = 60º$), the internal rotation barrier for the *anti* form is reduced to 46.4 cm−1, a value close to that of the *syn* form. These results confirm the above conclusion that there is steric repulsion between the SH group and CH_3 groups in the *anti* conformer. This steric repulsion is most likely electrostatic in origin. To support this hypothesis, we plot the molecular electrostatic potential (ESP) in Figure 1.6. Obviously, the regions around H atoms are positive (attractive to electrons). Therefore, for the *anti* form, there is repulsion between the SH group and CH_3 groups, and the repulsion is largest when one of the H atoms on the CH_3 is coplanar with the H atom on the SH group.

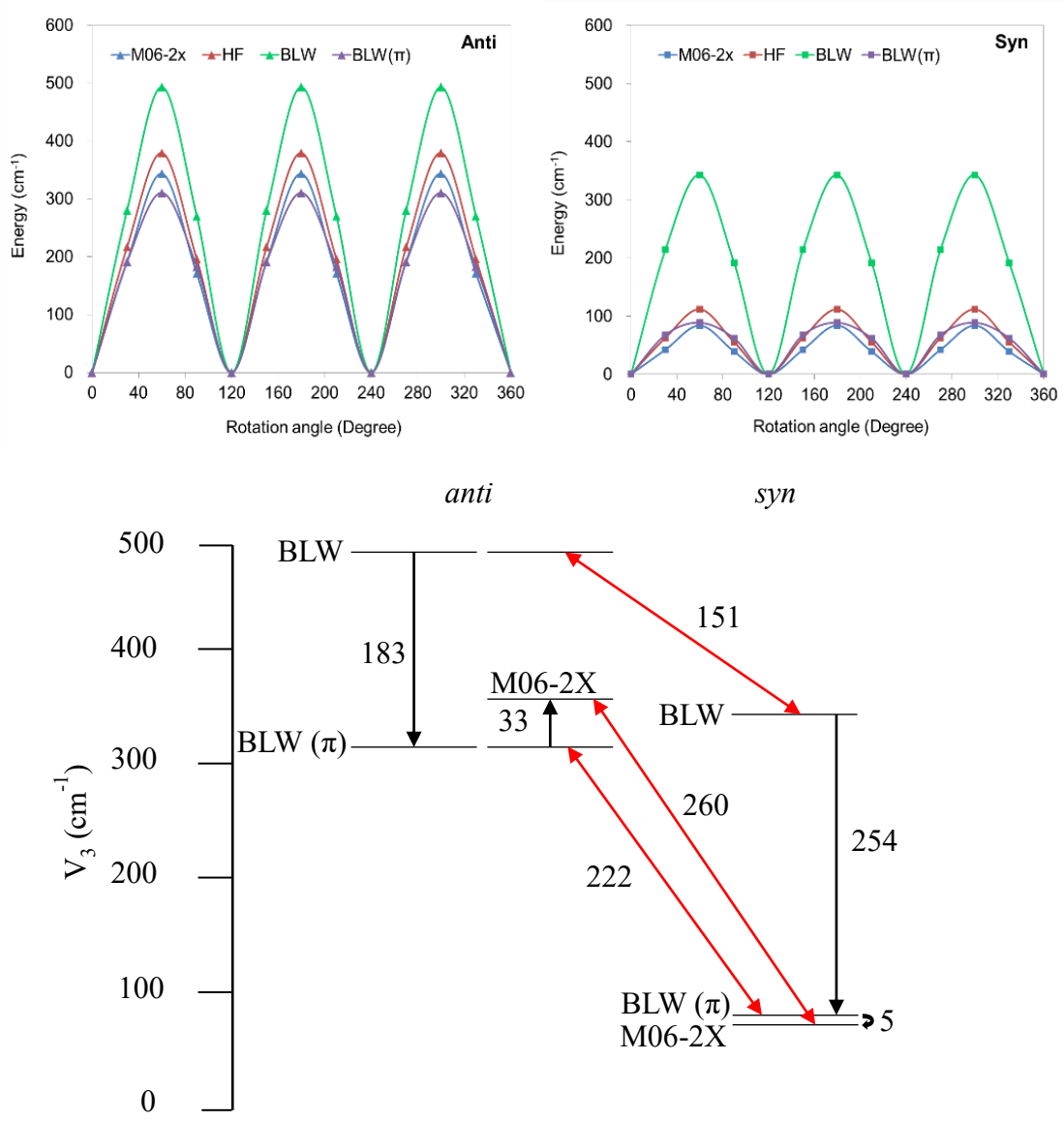

Figure 1.4 Two Representations of the BLW Energy Decomposition Results. Top: The torsional energy profiles at different levels of theory. Bottom: A "sequential" representation of the barriers. Vertical lines (black) represent the changes in V_3 at different stages of the BLW decomposition. Diagonal lines (red) indicate the difference between internal rotation barriers of the *anti* and *syn* forms of thioacetic acid at different stages of the BLW decomposition. All differences are in cm^{-1}. The changes from BLW(π) to M06-2X reflect the combined effects of hyperconjugation and electron correlation.

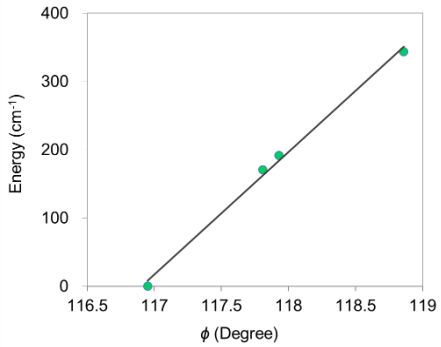

Figure 1.5 Correlation Between the Energy and the CCS Bond Angle(ϕ) for *anti*-Thioacetic Acid. Data are from Table 1.4.

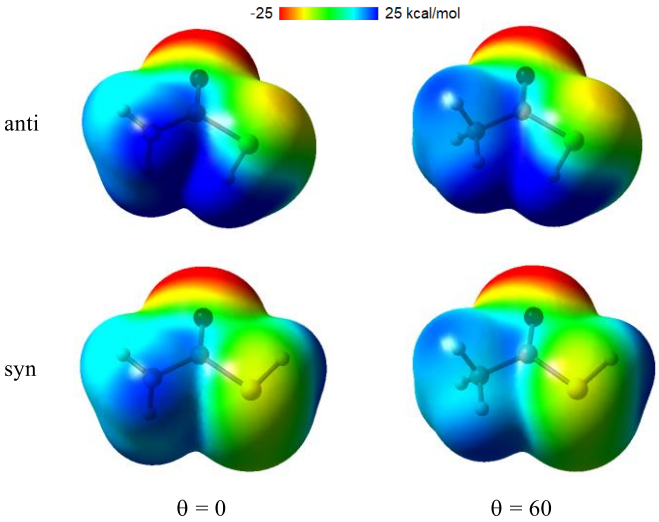

Figure 1.6 ESP Maps on the 0.001 a.u. Electron Eensity Surfaces of Molecules Computed at the M06-2X/6-311+G(d,p) Theoretical Level

Discussion

This work has established that the methyl group internal rotation barrier in the *anti* form of thioacetic acid is 4.7 times larger than that of the *syn* form. This is a large effect, even in comparison with other recent experimental studies that have demonstrated conformational effects on internal rotation barriers. For example, in 4-hexyn-3-ol, the barriers were

determined to be 7.16102(7), 4.2365(26), and 7.9016(39) cm^{-1} for the three conformers studied,[19] whereas in m-methylanisol,[18] the measured barriers for two conformers studied were 55.7693(90) and 36.6342(84) cm^{-1}. Here, we find that the internal rotation barrier increases from 76.300(12) to 358.056(51) cm^{-1} when the S–H bond is rotated from the *syn* to the *anti* position. Interestingly, calculations have indicated that the CF_3 internal rotation barrier in the *syn* and *anti* conformers of methyl trifluoroacetate differ by about a factor of six, though only the barrier for the *anti* conformer was determined experimentally.[89]

Much has been written about the complexity of internal rotation barriers. The difficulty appears to be that these barriers, in general, arise from complex combinations of competing terms, in a way that is largely system-specific. Moreover, the total energy is the observable, while the individual terms themselves are theoretical constructs designed to offer intuitive understanding. As a result, different approaches have been used to break the problem down into physically meaningful contributions. As noted above, the BLW scheme provides useful insight into this problem, indicating that, in this case, ~80% of the difference arises from steric repulsion between the SH hydrogen and the methyl group.

In principle, acetic acid should provide an opportunity to examine the internal rotation barriers in a very similar system, but microwave spectra[90-93] and gas phase electron diffraction[94,95] of only the *syn* form have been reported. The *anti* conformer of acetic acid has been observed by infrared spectroscopy in cryogenic matrices[96-98] but gas phase spectra appear to be lacking. Calculations indicate that the *anti*- conformer of CH_3COOH lies ~5.4 kcal/mol higher in energy than the *syn* form,[99] which corresponds to an *anti/syn* ratio of about 1×10^{-4} at 300 K. For thioacetic acid, however, the *anti* conformer is only 0.7 kcal/mol more energetic at the highest level of theory employed in this work, which suggests that the *anti/syn* ratio at 300 K is ~0.3. The predicted percent of the *anti* form, therefore, is 24%, which is in quite reasonable agreement with the 16% value estimated by Romano et al.[51]**Error! Bookmark not defined.** from infrared intensities after matrix deposition. High sensitivity searches for the *anti* conformer of acetic acid in the gas phase would be most interesting.

Conclusion

The *syn*- and *anti*- forms of thioacetic acid, as well their ^{34}S and ^{13}C carbonyl substituted isotopologues, have been observed using microwave spectroscopy. The internal rotation barriers for the parent *syn* and *anti* conformers are dramatically different, 76.300(12) and 358.056(51) cm^{-1}, respectively. BLW calculations show that both steric repulsion between the SH and CH_3 groups and π conjugation from the SH to the carbonyl group account for most of the difference. Zero-point corrected M06-2X/6-311+G(d,p) calculations indicate that *syn*-thioacetic acid is 1.4 kcal/mol lower in energy than *anti*-thioacetic acid (0.7 kcal/mol at the M06-2X/6-311++G(3df,3pd) level). This study has also provided occasion to compare the performance of the XIAM and BELGI-Cs programs for treating the effects of internal rotation in microwave spectra, and corroborates previous experience that (a) either program is suitable for high barrier problems and (b) BELGI-Cs has the additional flexibility needed to satisfactorily fit the spectra in low barrier cases.

Acknowledgements

This work was supported by the National Science Foundation (Grant No. CHE 1563324) and the Minnesota Supercomputing Institute. Anna Huff was supported by a Lester C. and Joan M. Krogh Fellowship, administered through the University of Minnesota.

Chapter 2: Observation of Two Conformers of Acrylic Sulfuric Anhydride by Microwave Spectroscopy

Adapted with permission from C. J. Smith, Anna K. Huff, Rebecca B. Mackenzie, Kenneth R. Leopold, *J. Phys. Chem A.*, **121**, 9074-9080, (2017).

Overview

The rotational spectrum of acrylic sulfuric anhydride (CH_2=CHCOOSO_2OH, AcrSA), has been observed using pulsed-nozzle Fourier transform microwave spectroscopy. The species was produced from the reaction between acrylic acid and sulfur trioxide in a supersonic jet. Spectroscopic constants are reported for both the *s-cis*- and *s-trans*-AcrSA conformers of the parent and monodeuterated (OD) isotopologues. Geometries were optimized for both conformers using M06-2X/6-311++G(3df,3pd) methods. Single point energy calculations at the M06-2X geometries were calculated using the CCSD(T)/complete basis set method with double and triple extrapolation [CBS(D-T)]. Further calculations indicate that the anhydride results from a π_2 + π_2 + σ_2 cyloaddition reaction within the acrylic acid – SO_3 complex. Because the C=O double bond of the acrylic acid migrates from one of the COOH oxygens to the other during the reaction, the *s-cis* form of acrylic acid leads to the *s-trans* form of the anhydride and vice versa. With zero point energy corrections applied to the CCSD(T) energies, the *s-cis* and *s-trans* forms of CH_2=CHCOOSO_2OH are 19.0 kcal/mol and 18.8 kcal/mol lower in energy than that of SO_3 + their corresponding CH_2=CHCOOH precursor conformation. The zero point corrected transition state energies for formation of the *s-trans* and *s-cis* anhydrides are 0.22 kcal/mol and 0.33 kcal/mol lower than those of the complexes of SO_3 with *s-cis* and *s-trans* acrylic acid, respectively, indicating that the reaction is essentially barrierless. This system adds to a growing body of examples which demonstrate that carboxylic acids readily add to SO_3 in the gas phase to produce the corresponding carboxylic sulfuric anhydride.

Introduction

The formation and activity of atmospheric aerosol is an active area of research.[100-103] Interest in this topic stems from the ability of aerosol particles to modulate the earth's energy budget via reflection and absorption of solar radiation, their function as cloud condensation nuclei, and their role as sites for heterogeneous chemistry. There is now considerable evidence that aerosol formation in the atmosphere is a multi-component process, and that a wide range of substances can serve to stabilize precursor clusters during the early stages of nucleation.[104-107] Indeed, while great strides have been made in understanding the chemical composition of aerosol precursors,[3] the chemical and dynamic complexity of the atmosphere is such that the modeling of new particle formation remains a challenging problem.

Despite the difficulties, sulfuric acid is widely recognized as a key component in atmospheric aerosol nucleation.[3,108,109] Early work suggested the $H_2O–SO_3$ complex as the primary precursor to the formation of H_2SO_4 from H_2O and SO_3,[110,111] but subsequent studies concluded that the activation energy for intramolecular proton transfer within the 1:1 complex was too large for the direct reaction to be of importance.[112,113] Further theoretical and experimental work later indicated, that the hydration of SO_3 can be catalyzed by the addition of a second H_2O molecule to form an $SO_3–(H_2O)_2$ intermediate,[114-117] and more recent computational studies suggest that atmospheric species other than water can also catalyze the process.[30,118-121] Most relevant to the present report is work by Hazra and Sinha[30] and Long et al.[120] indicating that replacement of the second water by formic acid to produce an $SO_3–H_2O–HCOOH$ intermediate yields H_2SO_4 with essentially no barrier at all. Hazra and Sinha further argued that since the immediate product is a hydrogen bonded complex between HCOOH and H_2SO_4, the process may be a preliminary step en route to the formation of a critical nucleation cluster.

With this idea in mind, we recently set out to investigate complexes containing SO_3, HCOOH, and H_2SO_4 by microwave spectroscopy in a supersonic jet. To our surprise, however, upon expanding a mixture of HCOOH and SO_3 in argon, the most prominent

spectral features observed were not due to weakly bound complexes, but rather to a new molecule, $HCOOSO_2OH$ (formic sulfuric anhydride, FSA), which we concluded was formed from a cycloaddition reaction between SO_3 and HCOOH.[31] Theoretical calculations suggested that the activation energy for the process is only 0.2 kcal/mol after zero point corrections, and furthermore that benzoic and pinic acids whould undergo similar reactions with slightly negative activation energies. We speculated that the formation and subsequent hydrolysis of FSA(or other carboxylic sulfuric anhydrides) either in a water cluster or a pre-existing droplet, could provide a pathway for the incorporation of organic matter into atmospheric aerosol.[31]

Further experimental and theoretical work in our laboratory has identified the acetic acid analog of FSA (CH_3COOSO_2OH, ASA),[122] providing additional experimental evidence that the reaction of SO_3 + RCOOH can occur with a carboxylic acid other than HCOOH. Internal rotation of the methyl group raised some interesting issues insofar as its equilibrium orientation changes when CH_3COOH is converted to ASA. Specifically, because the equilibrium orientation of the methyl group differs between acetic acid and acetic sulfuric anhydride, the cycloaddition reaction that forms the anhydride must be accompanied by internal rotation. Whether the two processes are sequential or simultaneous could not be addressed, but both paths were shown to have a negligible activation barrier.

In this paper, we examine the reaction of SO_3 with acrylic acid (CH_2=CHCOOH). Acrylic acid has two conformers, *s-cis* and *s-trans* (Figure 2.1), where the nomenclature follows the IUPAC designations in which *s-cis* and *s-trans* refer to the relative orientation of two double bonds separated by a single bond.[123] The *s-cis* form is slightly more stable than the *s-trans* form, with estimates of the relative energies lying in the 0.2 to 0.6 kcal/mol range.[124-127] Note that for both of these forms, the *syn* orientation of the OH and carbonyl group is the energetically preferred arrangement. We show that the reaction of SO_3 with acrylic acid produces both *s-cis* and *s-trans* conformers of acrylic sulfuric anhydride

(AcrSA), though our calculations identify transition states that connect the *s-cis* form of the monomer with the *s-trans* form of the anhydride and vice versa.

Acrylic acid is an important industrial chemical, and while we are unaware of specific determinations of its concentration in the atmosphere, numerous reports of its release appear on the EPA's Toxic Release Inventory.[128,129] Studies aimed at understanding its atmospheric degradation have also been reported.[130] Moreover, carboxylic acids in general are abundant in the atmosphere and their chemistry is of broad interest.[131-134] This system provides an additional example of the formation of a carboxylic sulfuric anhydride and, as such, contributes to a general characterization of what appears to be a relatively unrecognized reaction of carboxylic acids with SO_3.

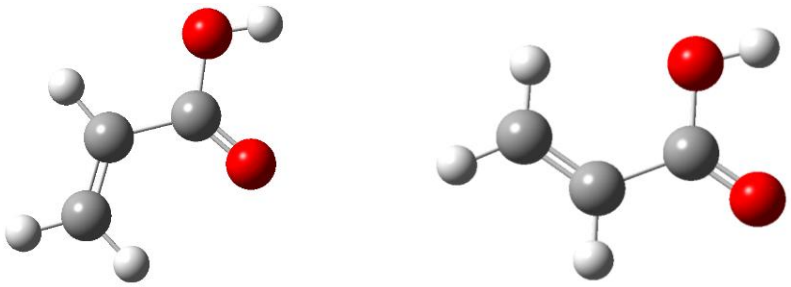

***s-cis*-Acrylic Acid** ***s-trans*-Acrylic Acid**

Figure 2.1 M06-2X/6-311++G(3df,3pd) minimum energy structures of the *s-cis* and *s-trans* forms of acrylic acid

Experimental Methods and Results

Rotational spectra of AcrSA were obtained using a Fourier transform microwave (FTMW) spectrometer with combined cavity[13] and chirped-pulse[14] capabilities. Details of the instrument have been described elsewhere,[15,54] and the molecular source design was the same as that used in our previous work on acetic sulfuric anhydride.[122] SO_3 was introduced into the system by passing argon over a reservoir of solid, polymerized SO_3, which was then expanded at a stagnation pressure of 1.3 atm through a 0.8 mm diameter nozzle into the spectrometer. Acrylic acid vapor entrained in argon, at a pressure of 0.7 atm, was added

through a continuous flow line, which terminates in an "injection needle" of inner diameter 0.012 inches.[135] The needle was placed a few millimeters downstream of the nozzle orifice so as to introduce the sample along the axis of the expansion. A 5:1 acrylic acid/D_2O mixture was used to collect H_2C=CHCOOSO_2OD rotational spectra with the same apparatus. Acrylic acid and SO_3 were obtained from Sigma-Aldrich and D_2O was obtained from Cambridge Isotope Laboratories, Inc.

Initially, spectra were collected from 6 – 18 GHz in 3 GHz segments using our broadband chirped-pulse system. For each segment, 10,000 free induction decay signals were averaged, each with a 90 μs data collection time. The observed spectrum is shown in Figure 2.2.A. Spectra of the *s-cis* and *s-trans* forms of the anhydride were identified using predicted structures (see next section) and were each fit to the A-reduced Watson Hamiltonian[10] using the SPFIT program of Pickett.[136] Fewer than 4 unassigned features remained in the chirped-pulse spectrum, none of which could be assigned to the SO_3—acrylic acid van der Waals complex. Preliminary fits utilized only *a*-type transitions, but with non-zero dipole moment components predicted along all three inertial axes for both conformers, *b*- and *c*-type transitions were also anticipated. After switching to our narrowband cavity spectrometer, the weaker *b*- and *c*-type transitions were readily observed, and higher resolution measurements of the *a*-type transitions were obtained. The monodeuterated isotopologue was also readily observed with the cavity system, with which transitions were recorded between 5.6 and 10.6 GHz. Deuterium hyperfine structure was not resolved in these spectra and therefore no nuclear quadrupole coupling constants were obtained. For all measurements using the cavity mode, the sample was pulsed at a rate of 4 Hz and four free induction decay signals were collected per pulse, each with a data collection time of 140.8 μs. Transition frequencies measured on the chirped-pulse system were typically accurate to ~30 khz. Measurements made on the cavity system were accurate to ~4 kHz. A recording of the $3_{12} \leftarrow 2_{02}$ transition of the *s-cis* conformer taken on the cavity spectrometer is shown in Figure 2.2.B. Spectroscopic constants are given in Table 2.1. The slightly larger rms residual for the *s-trans* parent species appears to be related to a number of the higher J, K_{-1} transitions included. However, since it is still significantly less than the

estimated uncertainty in the chirped-pulse measurements, no attempts were made to pursue the issue. The centrifugal distortion constants appear to show a curious isotope dependence, though this, too, may be an artifact of the number and identity of measured transitions. Observed frequencies, assignments, and residuals from the least squares fits are provided in Appendix B.

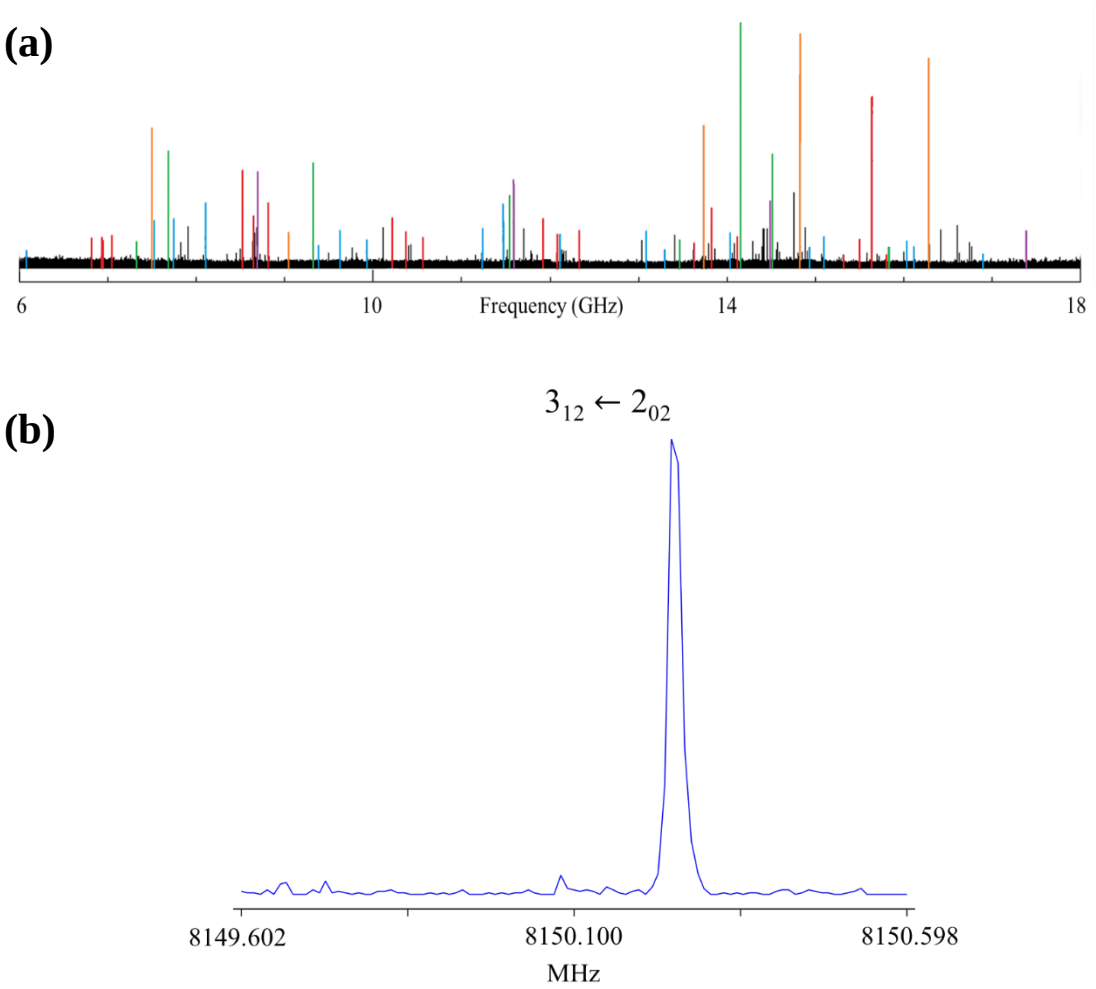

Figure 2.2 Chirped-Pulse and Cavity Microwave Spectra of *s-cis*- and *s-trans*-AcrSA **(a)** A 6-18 GHz chirped-pulse microwave spectrum of SO_3 and acrylic acid in Ar. The spectrum is an average of 10,000 free induction decay signals. *s-cis*- and *s-trans*-AcrSA, Ar-SO_3, as well as *s-cis*- and *s-trans*-acrylic acid monomer transitions are highlighted in red, blue, purple, green, and orange, respectively. Known instrumental artifacts have been removed from the spectrum. **(b)** A trace of the $3_{12} \leftarrow 2_{02}$ transition of the *s-cis* conformer recorded on the cavity spectrometer.

Table 2.1 Spectroscopic Constants of Conformers and Isotopologues of AcrSA[a]

Parameter	*s-trans*-AcrSA	*s-cis*-AcrSA	*s-trans*-OD-AcrSA	*s-cis*-OD-AcrSA
A (MHz)	2852.59731(50)	3639.31630(57)	2801.452(38)	3557.207(70)
B (MHz)	1052.22420(32)	896.25135(15)	1049.76868(45)	895.21100(11)
C (MHz)	905.04333(30)	837.56260(21)	899.14677(13)	833.24420(11)
Δ_J (kHz)	0.0722(37)	0.0349(10)	0.0547(46)	0.0308(12)
Δ_{JK} (kHz)	0.360(37)	0.595(20)	0.23(10)	0.671(24)
N[b]	42	41	15	15
RMS (kHz)	10	3	4	1

[a] Numbers in the parentheses are one standard error in the least squares fit.
[b] Number of transition frequencies in the least squares fit.

Computational Methods and Results

All structures were optimized at the M06-2X/6-311++G(3df,3pd) level of theory[137] using the Gaussian suite of programs.[88] This level proved successful in our prior work on the formic[31] and acetic[122] sulfuric anhydrides and was applied here to be consistent with the previous studies. The equilibrium structures of *s-cis*- and *s-trans*-AcrSA, as well as those of both conformers of the acrylic acid – SO_3 weakly bound complex, are shown in Figure 2.3. Chemically significant results for *s-cis*- and *s-trans*- AcrSA are summarized in Table 2.2 and Cartesian coordinates for all relevant structures are given in Appendix B. To improve the quality of the computed energies, single-point calculations were performed using M06-2X geometries with the CCSD(T)/complete basis set with double and triple extrapolation [CBS(D-T)] method.[138] Zero-point energy corrections were applied using the frequencies obtained from the M06-2X calculations. A summary of the energy calculations is presented in Table 2.3.

Computational searches for transition states connecting the putative CH_2=CH-COOH–SO_3 complexes with their corresponding anhydrides were also conducted. Cyclic transition state structures analogous to those previously found for the RCOOH–SO_3 → $RCOOSO_2OH$ (R = H, CH_3) reaction were identified for both the *s-cis*- and *s-trans*-acrylic acid reactions. Transition state energies relative to the weakly bound SO_3 complexes are included in Table 2.3, and key points on the potential energy surface are shown in Fig 2.4. The CCSD(T) barriers without zero point corrections are 1.8 and 1.9 kcal/mol for the formation of *s-cis*- and *s-trans*-AcrSA, respectively. Both barriers are eliminated with the inclusion of zero point energy, with the transition state energies 0.22 and 0.33 kcal/mol below that of the acrylic-SO_3 complexes for *s-cis* and *s-trans*-acrylic acid, respectively. The imaginary frequencies at the transition states for the *s-cis* and *s-trans* conformers both correspond to a concerted reaction, fully analogous to that of the $\pi_2+ \pi_2+\sigma_2$ cycloaddition mechanism previously proposed for the HCOOH[31] and CH_3COOH[124] reactions. The overall formation energies for *s-cis*-AcrSA and *s-trans*-AcrSA from *s-trans*- and *s-cis*-acrylic acid are −19.0 and −18.8 kcal/mol, respectively. At the level of theory used, the *s-cis*/*s-trans* energy difference for the acrylic acid monomer is 0.25 kcal/mol, in agreement

with the range reported in the literatue.[124-127] In contrast, the energy difference between the *s-trans* and *s-cis* conformers of AcrSA is virtually zero (0.02 kcal/mol).

The barrier to interconversion from the *s-cis* to *s-trans* form via rotation about the C–C single bond was also estimated by locating a transition state along the coordinate corresponding to O=C–C=C dihedral angle. For the acrylic acid monomer, the value obtained from CCSD(T) calculations with zero point energy corrections was 5.6 kcal/mol (6.3 kcal/mol uncorrected), in good agreement with previous estimates.[124-127] For the anhydride at the same level of theory, a value of 6.2 kcal/mol (6.7 kcal/mol uncorrected) was obtained. For both acrylic acid and the anhydride, the dihedral angle at the transition state is very close to 90° (within 1°).

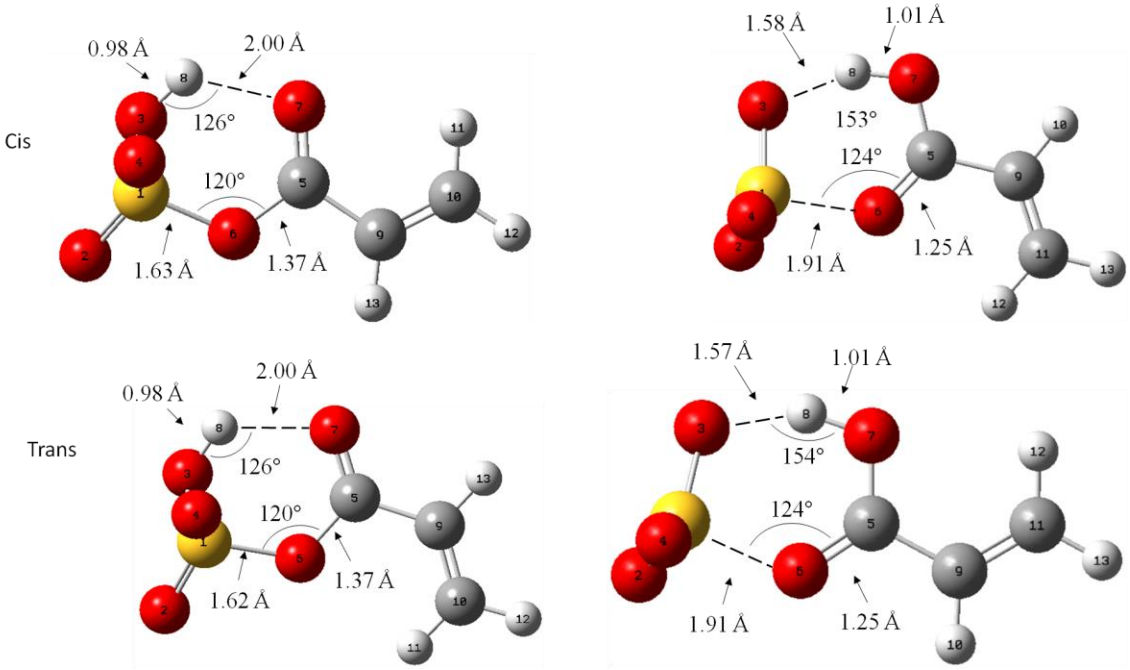

Figure 2.3 Equilibrium structures of the *s-cis* and *s-trans* conformers of AcrSA and the acrylic acid–SO_3 complex obtained from M02-2X/6-311++G(3df, 3pd) calculations

Table 2.2 Computational Results for AcrSA and Comparison with Experimental Values

s-cis-AcrSA	M06-2X/6-311++G(3df,3pd)	Experimental
A [MHz]	3667	3639.31630(57)
B [MHz]	901	896.25135(15)
C [MHz]	842	837.56260(21)
μa [D]	5.08	
μb [D]	0.26	
μc [D]	0.9	
Internal H-bond length (O7-H8) [Å]	1.997	
Internal H-bond angle (O7-H8-O3) [deg]	125.92	
C5-O6-S1 angle [deg]	119.74	
S1-O6 bond length [Å]	1.627	
C5-C9 bond length [Å]	1.475	

[a] M06-2X/6-311++G(3df,3pd)
[b] Values for the parent isotopologue

Table 2.3 Summary of Energetics for Complexes and Anhydrides of SO_3 with Acrylic Acid[a]

Species	**Energy Difference (kcal/mol)**				**Description**	
	M06-2X	M06-2X + Zero Point Corrections	CCSD	CCSD + Zero Point Corrections		
s-trans-Acrylic + SO_3 *s-trans*-Acrylic···SO_3	18.9	17.4	17.6	16.1	Complexation Energy, SO_3 + *s-trans-Acrylic Acid*	C
s-cis-Acrylic + SO_3 *s-cis*-Acrylic···SO_3	18.9	17.4	17.6	16.1	Complexation Energy, SO_3 + *s-cis-Acrylic Acid*	B
s-trans-Acrylic + SO_3 *s-cis*-AcrSA	22.3	20.5	20.8	19.0	*s-cis*-Anhydride Formation Energy	H
s-cis-Acrylic + SO_3 *s-trans*-AcrSA	22.2	20.3	20.7	18.8	*s-trans*-Anhydride Formation Energy	G
s-trans-Acrylic···SO_3(TS) *s-trans*-Acrylic···SO_3 [b]	1.6	–0.55	1.8	–0.33	Barrier Relative to *s-trans* Complex	E
s-cis-Acrylic···SO_3(TS) *s-cis*-Acrylic···SO_3[c]	1.7	–0.44	1.9	–0.22	Barrier Relative to *s-cis* Complex	D
s-trans-Acrylic Acid *s-cis*-Acrylic Acid	0.20	0.22	0.24	0.25	Acrylic Acid *s-cis/s-trans* Difference	A
s-trans-AcrSA *s-cis*-AcrSA	–0.12	–0.002	–0.10	+0.02	Acr-SA *s-cis-/s-trans* Difference	F

(a) Entry in the Table gives the energy difference between the species listed in the left-most column (top species minus bottom species, i.e., a positive number indicates that the top species listed in the row is higher energy). "+" refers to the isolated monomers. "···" refers to the weakly bound complex. Letters in the right-most column refers to the energy difference indicated in Figure 2.4.
(b) Leads to *s-cis*-AcrSA.
(c) Leads to *s-trans*-AcrSA.

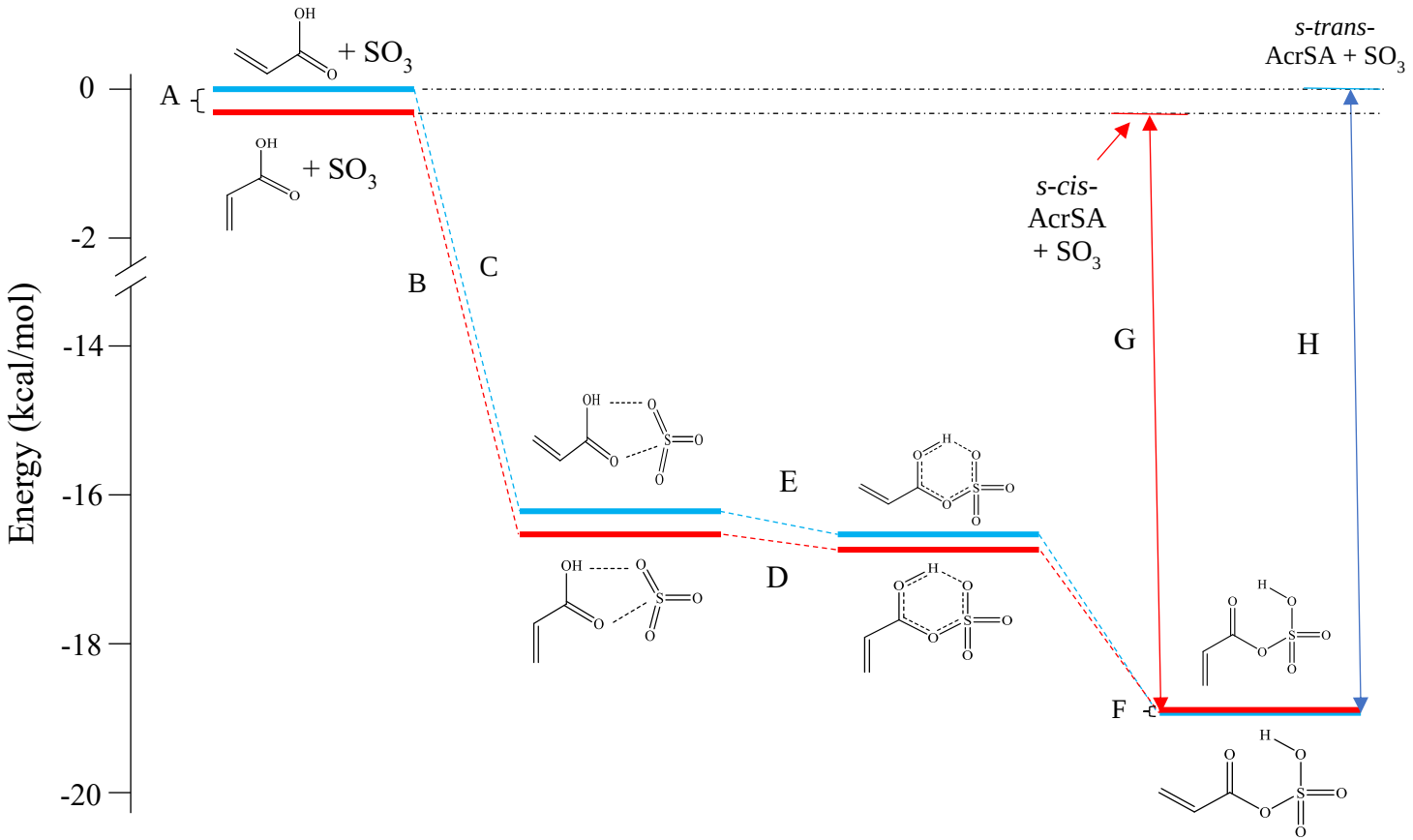

Figure 2.4 Zero Point Corrected CCSD(T)/CBS Energies for Key Points on the SO_3 + Acrylic Acid Potential Energy Surface. The transformation of *s-cis*-acrylic acid + SO_3 to *s-trans*-AcrSA is depicted in red. The transformation of *s-trans*-acrylic acid + SO_3 to *s-cis*-ASA is depicted in blue. Zero point corrections were obtained from M06-2X/6-311++G(3df,3pd) calculations. See Table 2.3 for the energies A-H.

Discussion

Table 2.4 compares the experimental rotational constants and their H/D shifts with those calculated for the four structures in Figure 2.3. Inspection of the table reveals that the values obtained for their species assigned to the *s-cis* anhydride are in excellent agreement with the computational results whereas, overall, in rather poor agreement with calculated values for the van der Waals complexes or the *s-trans* anhydride. The values for the *A* and *B* rotational constants, as well as their isotope shifts, are particularly compelling. We note that the *C* rotational constant for the deuterated species, and hence the isotope shift, do not provide as clean a comparison. (The calculated values for either the *s-cis* anhydride or the *s-cis* van der Waals complex could be construed as being reasonably commensurate with the experiment.) However, the other constants clearly rule out the van der Waals complex. Similar comparisons confirm the assignment for the *s-trans* anhydride. Thus, these results leave little doubt that the observed spectra correspond to the *s-cis* and *s-trans* conformers of AcrSA. That their formation in the jet is favorable is consistent with the low calculated activation barrier for conversion of the van der Waals complex to the anhydride, as well as with our experience with the formic and acetic acid analogues.

Table 2.4 Comparison between Observed and Theoretical H/D Isotope Shifts

s-cis	**Observed Isotope Shift[a]**	**Calculated Isotope Shift[b]**	**(Obs. – Calc.)**
A [MHz]	–82.109	–86.759	4.650
B [MHz]	–1.040	–1.321	0.281
C [MHz]	–4.319	–4.660	0.341
s-trans			
A [MHz]	–51.145	–53.518	2.372
B [MHz]	–2.455	–2.911	0.456
C [MHz]	–5.896	–6.262	0.365

(a) Value of the rotational constant for the OD species minus that for the OH species.
(b) Determined from M06-2X/6-311++G(3df,3pd) optimized geometries.

The reaction of SO_3 + acrylic acid is energetically favorable. Specifically, relative to SO_3 + acrylic acid, the anhydrides are 19 kcal/mol more stable than the isolated monomers. Note that in free acrylic acid, the *s-cis* conformer is lower in energy than the *s-trans* conformer by 0.25 kcal/mol while in the anhydride, the energies are essentially the same (at the level of theory used).

The definitive observation of acrylic sulfuric anhydride provides the third experimental demonstration that carboxylic acids readily react with SO_3 in the gas phase to form a corresponding carboxylic sulfuric anhydride. In all cases, supporting theoretical calculations indicate a cycloaddition mechanism with a small or negative activation barrier. With HCOOH, the reaction is straightforward. With CH_3COOH, the mechanism is essentially the same, though internal rotation of the methyl group introduces some complications that have been discussed.[124] In the case of acrylic acid, the new feature is the existence of a pair of conformers derived from the two conformations of the parent acid. As noted above, the *s-cis* form of the acid gives rise to the *s-trans* form of the anhydride and vice versa. However, this does not arise from an internal rotation about the C5-C9 bond. Rather, it is because the carbon-oxygen double bond migrates from O6 to O7 and because the *s-cis* and *s-trans* conformers are named according to the dihedral angle between the two double bonds separated by the C5-C9 single bond (See Figure 2.4.).

A variety of carboxylic acids with concentrations ranging from a few hundredths to a few tens of parts per billion[131,133,134] have been detected in the atmosphere, and their potential to enhance atmospheric nucleation has been discussed.[29,139-141] Although we are unaware of any specific observations of acrylic acid, the generality of the cycloaddition mechanism for the RCOOH + SO_3 reaction and the absence of any significant activation barrier suggest that carboxylic sulfuric anhydrides could also play a role in atmospheric chemistry. As we have noted previously, one such role may be serving as a vehicle to incorporate small organic molecules into atmospheric aerosol via hydrolysis in clusters or pre-existing aqueous droplets.

Conclusion

The *s-cis* and *s-trans* conformers of acrylic sulfuric anhydride have been formed in a supersonic jet and observed by microwave spectroscopy. M06-2X/6-311++G(3df,3pd) calculations indicate that their formation proceeds via a $\pi_2 + \pi_2 + \sigma_2$ cycloaddition reaction within the acrylic acid – SO_3 complex and that the zero-point corrected activation barrier is less than zero. CCSD(T)/CBS calculations at the optimized M06-2X geometries indicate that *s-cis*-AcrSA and *s-trans*-AcrSA are lower in energy than their corresponding free monomer precursors by 19.0 kcal/mol and 18.8 kcal/mol, respectively. Because the carbon-oxygen double bond migrates from the C=O oxygen of the COOH group to the OH oxygen during the cycloaddition, the *s-cis* conformer of acrylic acid produces the *s-trans* conformer of the anhydride and vice versa. This system provides a third experimental example of the facile reaction between SO_3 and a carboxylic acid, suggesting that the cycloaddition reaction occurs for a variety of acids. Given the aggregate concentration of these organic acids in the atmosphere, carboxylic sulfuric anhydrides may play a role in atmospheric chemistry.

Acknowledgements

This work was supported by the National Science Foundation (Grant Nos. CHE–1266320 and CHE 1563324) and the Minnesota Supercomputing Institute.

Chapter 3: Hydration of an Acid Anhydride: The Water Complex of Acetic Sulfuric Anhydride

Adapted with permission from C. J. Smith, Anna K. Huff, Rebecca B. Mackenzie, Kenneth R. Leopold, *J. Phys. Chem A.*, **122**, 4549-4554, (2018).

Overview

The complex formed from acetic sulfuric anhydride (CH_3COOSO_2OH, ASA) and water has been observed by pulsed nozzle Fourier transform microwave spectroscopy. ASA was formed *in situ* in the supersonic jet via the reaction of SO_3 and CH_3COOH, and subsequently complexed with water using a concentric, dual injection needle that allows reagents to be introduced at different points along the expansion axis. Spectroscopic constants for the parent, fully deuterated, and $CH_3{}^{13}COOSO_2OH$ species are reported. Both A and E internal rotor states have been observed and analyzed. The fitted internal rotation barrier of the methyl group is 219.598(21) cm^{-1} for the parent species, indicating that complexation with water lowers the internal rotation barrier of the methyl group by 9% relative to that of the free ASA. M06-2X/6-311++G(3df,3pd) calculations predict at least two distinct isomeric forms of ASA···H_2O. Spectroscopic constants for the observed species agree with those for the lowest energy isomer in which the water inserts into the intramolecular hydrogen bond of the ASA monomer. CCSD(T)/CBS(D-T) calculations place the binding energy of this isomer at 13.3 kcal/mol below that of the isolated ASA and H_2O monomers. The calculations further indicate that the doubly hydrogen bonded complex CH_3COOH···H_2SO_4, which contains the hydrolysis products of ASA, lies even lower in energy, but this species was not observed in this study. This system represents the first stage of microsolvation of an acid anhydride, and the results indicate that a single water molecule does not induce spontaneous hydrolysis in a cold molecular cluster.

Introduction

Recent work in our laboratory has established that carboxylic acids readily react with sulfur trioxide under supersonic jet conditions to form carboxylic sulfuric anhydrides.[31-32,122] Microwave spectra of the species derived from HCOOH,[31] CH_3COOH,[122] and $H_2C{=}CHCOOH$[32] have been reported, and M06-2X/6-311++G(3df,3pd) calculations indicate that these reactions proceed through a cyclic transition state corresponding to a $\pi_2 + \pi_2 + \sigma_2$ cycloaddition, as shown in Equation 3.1 below.

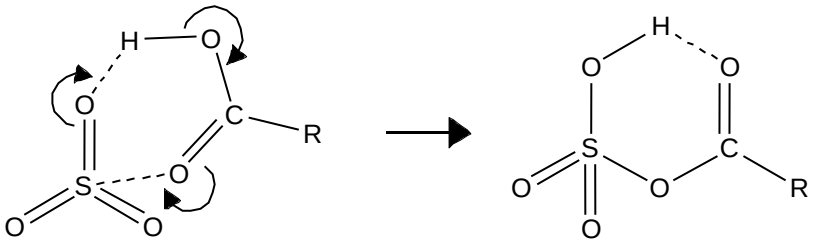

(3.1)

RCOOH–SO_3 Complex

Carboxylic Sulfuric Anhydride

Additional calculations at the CCSD(T)/CBS(D-T) level of theory indicate that the zero point corrected activation energy is small for the HCOOH reaction (0.2 kcal/mol) and near zero or slightly negative for the reactions with CH_3COOH and $H_2C{=}CHCOOH$. Additional calculations on pinic and benzoic acids[31] have yielded similar results, though no experimental observations have been attempted. The virtually barrierless nature of the reactions is consistent with the strong signals observed in experimental studies when SO_3 and the corresponding carboxylic acid are co-expanded in a supersonic jet.

Carboxylic acids are abundant atmospheric trace gases,[133,142] and we have previously speculated that their reaction with SO_3 to produce $RCOOSO_2OH$ could play a role in the formation of atmospheric aerosol.[31-32,122] Moreover, because products of these reactions are the anhydrides, they are subject to hydrolysis to produce RCOOH + H_2SO_4 and, as such, could provide a pathway for incorporating volatile organic matter into pre-existing aqueous droplets.

The possibility of a reaction between an acid anhydride with water raises interesting questions as to whether hydrolysis can occur in a hydrated molecular cluster and if so, how many water molecules are required. This is analogous to the much more thoroughly studied question of how many water molecules are needed to ionize a simple protic acid.[9] In the case of acid ionization, however, the products are charged species, while for the hydrolysis of an acid anhydride, they are neutral species. Thus the "solvation" requirements for stabilizing the reaction products may differ. In this work, we use microwave spectroscopy and computational chemistry to investigate the complex formed from water and acetic sulfuric anhydride (ASA). This system represents the first stage of hydration of an acid anhydride, and the results establish that a cold molecular complex containing ASA and a single water molecule can exist without spontaneous conversion to acetic and sulfuric acids.

Experimental and Results

All rotational spectra reported here were recorded on our conventional cavity Fourier transform microwave spectrometer, details of which have been given elsewhere.[54,143] Spectra were observed between 5.7 and 12.7 GHz, and transition frequencies were typically measured with an accuracy of ~4 kHz. In all experiments, SO_3 was introduced into the expansion through a 0.8 mm nozzle orifice by passing argon over solid polymerized SO_3 at a stagnation pressure of 2.0 atm. The expansion was immediately guided through a 0.5 in. stainless steel cone, which terminates in a 0.19 in. diameter orifice. The design of this source, which is very similar to that previously described in our studies of H_3N-$SO_3\cdots H_2O$,[144] is shown in Figure 3.1. This configuration allowed SO_3 to react with CH_3COOH and then subsequently complex with H_2O several millimeters downstream of the nozzle orifice. The inner needle had a 0.006 in. inner diameter (ID) and an outer diameter (OD) of 0.012 in., while the outer needle had an ID of 0.020 in. and an OD of 0.032 in. The best conditions for generating the $ASA\cdots H_2O$ complex were obtained when water and acetic acid vapors were flowed through the inner and outer needles, respectively, with the inner needle extending 0.09 in. beyond the outer needle. Although this configuration was successful at locating spectra and was used to obtain the majority of the

transitions reported here, we note that once the spectra were identified, a single-needle source design[135] was also found to be adequate for observing the ASA···H_2O complex. Nonetheless, the use of the dual-injection source provided the ability to quickly test the dependence of signals on the presence of water, and allowed for independent control of acetic acid and water concentrations in the jet.

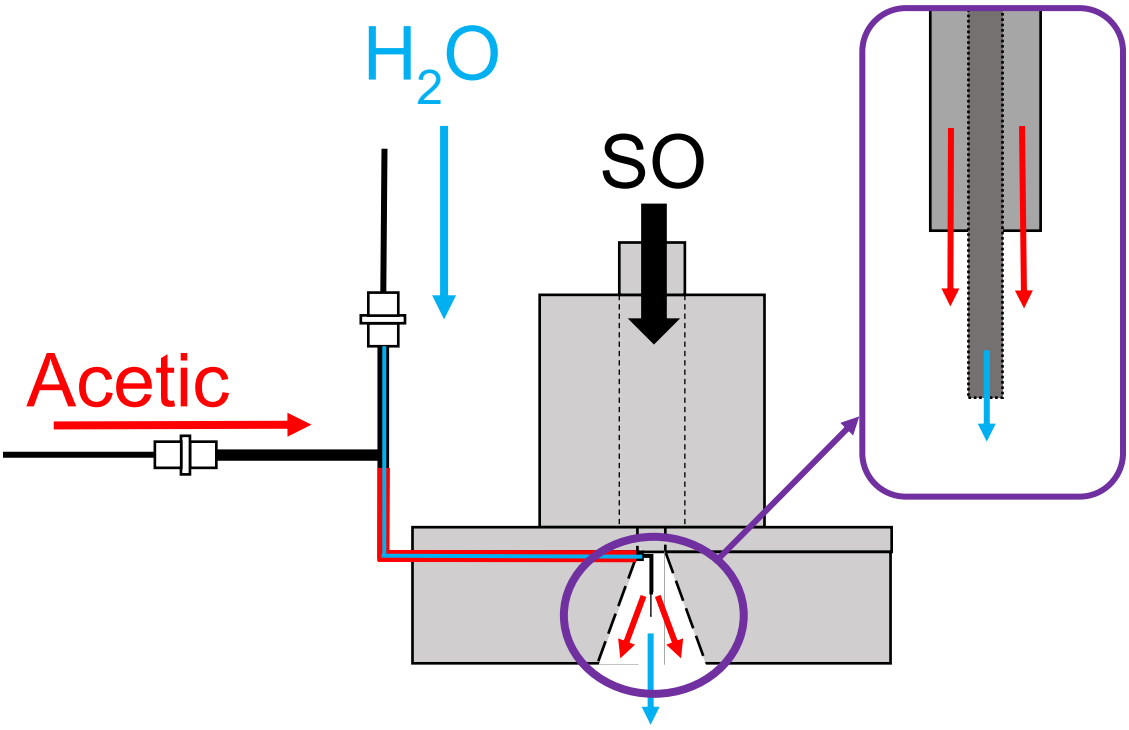

Figure 3.1 Schematic of the concentric dual-injection nozzle used to obtain most of the spectra recorded in this work. Acetic acid vapor enters through the outer sheath of the concentric needle. H_2O vapor is admitted though the inner needle.

Spectra were recorded for the parent species and two isotopologues, $CD_3COOSO_2OD\cdots D_2O$ and $CH_3{}^{13}COOSO_2OH\cdots H_2O$. The $CD_3COOSO_2OD\cdots D_2O$ isotopologue was generated by using isotopically enriched samples of d_4-Acetic Acid (99%) from Sigma-Aldrich and D_2O (99% D_2O) from Cambridge Isotope Laboratories, Inc. Spectra of $CH_3{}^{13}COOSO_2OH–H_2O$ were obtained using a sample of $CH_3{}^{13}COOH$ (50% ^{13}C) from Sigma-Aldrich.

Consistent with the predicted dipole moment components (see next section), *a*-type transitions were the strongest observed. Several weaker *b*-type lines were also predicted and recorded, but no *c*-type transitions were observed. Rotational transitions from $J = 3 \leftarrow 2$ to $J = 7 \leftarrow 6$ were obtained for the parent, while transitions from $J = 4 \leftarrow 3$ to $J = 7 \leftarrow 6$ and $J = 4 \leftarrow 3$ to $J = 6 \leftarrow 5$ were observed for the fully deuterated and ^{13}C isotopologues, respectively. For the parent species, transitions involving $K_{-1} = 0–3$ were assigned at two J levels whereas, for the two isotopologues, assigned transitions involved mostly $K_{-1} = 0$ and 1, although one transition with $K_{-1} = 2$ was observed and assigned for the fully deuterated species. For all three species, both A and E internal rotor states of the methyl rotor were observed. Figure 3.2 shows a spectrum containing A and E state transitions of the parent species, which fortuitously lie within the span of a single data collection window. No spectral doubling, such as would be expected in the presence of water tunneling motions, was observed, and the nuclear hyperfine structure in the CD_3COOSO_2OD species was not resolved. Full lists of transitions for all species studied are given in Appendix C.

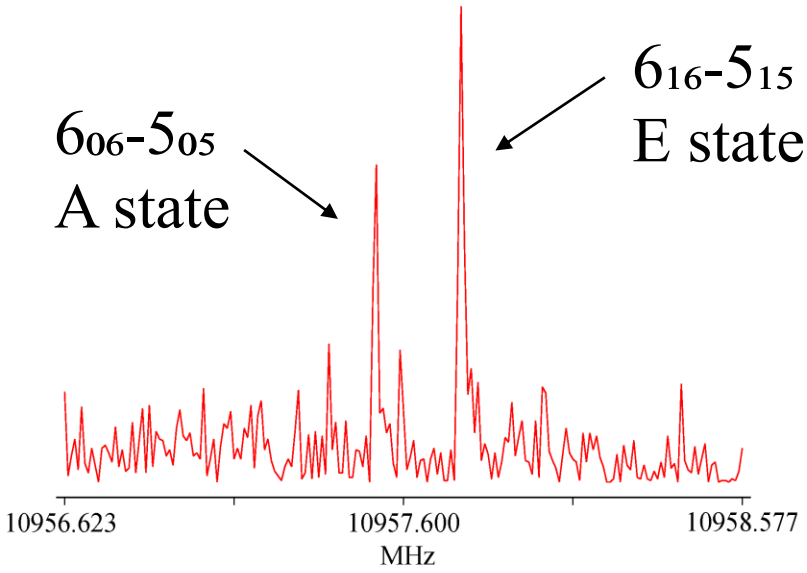

Figure 3.2 A portion of the ASA···H_2O spectrum showing rotational transitions from the A and E internal rotor states. This spectrum was the average of 4000 free induction decay signals.

Spectra were fit using the XIAM program of Hartwig,[37] which implements the extended internal axis method introduced by Woods.[57] The program utilizes the Hamiltonian of equation 3.2,

$$\mathbf{H} = \mathbf{H}_{rot} + \mathbf{H}_{cd} + \mathbf{H}_{ir} \tag{3.2}$$

where $\mathbf{H}_{rot}$ is the rigid rotor Hamiltonian, $\mathbf{H}_{cd}$ is the Watson A-reduced centrifugal distortion Hamiltonian, and $\mathbf{H}_{ir}$ treats the internal rotation of the methyl rotor. Contained in $\mathbf{H}_{ir}$ are the rotational constant of the methyl group about its symmetry axis (F_o), the three-fold internal rotation barrier (V_3), and δ and ε, which are the polar angles that define the orientation of the internal rotor axis in the principal axis system of the molecule. δ is the angle between the internal rotation axis and the *a*-axis of the molecule, and ε specifies the angle between the *b*-axis and the projection of the internal rotation axis on the *b*-*c* plane.

Several details regarding spectral analysis are noteworthy. As previously observed for ASA,[122] F_o and V_3 were found to be highly correlated. Therefore, the value of F_o for the parent and ^{13}C species was held fixed at the computationally derived values of 158.86 GHz. For the fully deuterated species, a computed value of F_o = 79.50 GHz was used. The fitted values of ε and δ for the parent form were 9.3 deg and 20.7 deg, respectively, and were in good agreement with their predictions described in the next section (6.6 deg and 22.7 deg, respectively). Similar results were obtained for the ^{13}C derivative. For the fully deuterated sample, however, ε could not be fit and, consequently, was fixed at 11.0 deg. This value was obtained by adding the average value of ($\varepsilon_{obs} - \varepsilon_{calc}$) = 3.2 deg for the parent and ^{13}C species to the calculated value for the perdeuterated species. Attempts to include a V_6 term in the potential did not give a statistically significant result and hence only the V_3 term was retained in the analysis. Values of V_3 for the parent and ^{13}C species are in reasonable agreement, while the value for the perdeuterated isotopologue is seen to be 2.3% lower than that of the parent form. A similar trend was observed for free ASA, where the fitted value of V_3 for the deuterated species was 2.7% lower than that of the parent form.[122]

Computational Methods and Results

In order to be consistent with prior calculations on formic,[31] acetic,[122] and acrylic[32] sulfuric anhydrides, all optimizations and frequency calculations were done at the M06-2X/6-311++G(3df,3pd) level of theory[138] using the Gaussian suite of programs.[88] Initial calculations on the ASA···H_2O dimer yielded the two structures shown in Figure 3.3, both of which were confirmed by frequency calculations to correspond to true minima on the potential energy surface. In the minimum energy structure (I), the water inserts into the intramolecular hydrogen bond of the ASA, creating an 8-membered ring. In a second structure, (II), which lies 10.6 kcal/mol higher in energy (9.7 kcal/mole with zero-point corrections), the water is hydrogen bonded to the sulfuric acid end of the ASA. The dipole moment components, in Debye, are (μ_a, μ_b, μ_c) = (3.47, 2.07, 0.40) and (5.74, 0.75, 0.07) for the lower and higher energy structures, respectively. Chemically significant results are given in Table 3.2. Additional interatomic distances and angles, as well as full sets of Cartesian coordinates for both structures, are provided in Appendix C.

The internal rotation barrier for structure I was calculated by rotating the methyl group 60° from its equilibrium position and optimizing a transition state. The resulting energy was 238 cm^{-1} above that of the minimum energy configuration and this energy difference represents the peak-to-peak difference in the 3-fold periodic potential for internal rotation of the methyl group. Therefore, it is directly comparable to the fitted value of V_3 and is seen to be in good agreement with the experimental value of 219.6 cm^{-1} for the parent species (Table 3.1). For structure II, a similar procedure yielded an internal rotation barrier of 266 cm^{-1}.

Table 3.1 Spectroscopic Constants of the ASA···H_2O Isotopologues[a]

	$CH_3COOSO_2OH\cdots H_2O$	$CD_3COOSO_2OD\cdots D_2O$	$CH_3{}^{13}COOSO_2OH\cdots H_2O$
A [MHz]	1670.0420(12)	1566.7629(89)	1670.070(16)
B [MHz]	1311.26529(29)	1181.5894(27)	1301.7339(44)
C [MHz]	862.85050(20)	786.31270(56)	858.71107(38)
Δ_J [kHz]	0.0453(29)	0.0239(91)	0.024(12)
Δ_{JK} [kHz]	0.411(31)	0.56(17)	0.79(26)
V_3 [cm^{-1}]	219.598(21)	214.6(12)	221.14(26)
ε [deg]	9.31(2)	11.0[e]	10.3(2)
δ [deg]	20.71(4)	16.4(5)	19.1(4)
F_o [GHz][b]	158.86	79.50	158.86
N[c]	53	25	16
σ [kHz][d]	3.1	3.0	2.0

(a) Numbers in parentheses are one standard error in the least squares fit.
(b) Fixed to the value derived from the M06-2X/6-311++G(3df,3pd) structure.
(c) Number of lines included in the fit.
(d) Standard deviation of the residuals.
(e) Parameter fixed at computed value, corrected for the average (ε_{obs} - ε_{calc}) = 3.2 deg for the parent and ^{13}C species, i.e., 7.8° + 3.2° = 11.0°.

Table 3.2 Computational Results for ASA···H_2O and Comparison with Experiment[a]

	M06-2X/6-311++G(3df,3pd)			Experimental Value
	Structure I	Structure II	$CH_3COOH\cdots H_2SO_4$	
A [MHz]	1732	3358	3531	1670.0420(12)
B [MHz]	1317	806	677	1311.26529(29)
C [MHz]	880	757	643	862.85050(20)
V_3 [cm^{-1}]	238	266		219.598(21)
δ [deg]	22.7	28.2		20.71(4)
ε [deg]	6.6	19.0		9.31(2)
μ_a [D]	3.47	5.74		-
μ_b [D]	2.07	0.75		-
μ_c [D]	0.40	0.07		-
Binding Energy (Relative to ASA + H_2O)[b]	13.3 (11.1)	4.3 (3.1)		
Selected Ring Parameters				
R(O3-H8) [Å]	1.030	0.975		-
∠(S1-O6-C5) [deg]	122	120		-
O-H and Hydrogen Bond Distances				
R(H8-O13) [Å]	1.509	(d)		-
R(H14···O7) [Å]	1.953	(d)		-
R(H8···O7) [Å]	(c)	2.062		-
R(H14···O2) [Å]	(c)	2.434		-
R(H15···O4) [Å]	(c)	2.416		-
Hydrogen Bond Angles				
∠(O3-H8···O13) [deg]	171	(d)		-
∠(O13-H14···O7) [deg]	142	(d)		-
∠(O3-H8···O7) [deg]	(c)	122		-
∠(O13-H14···O2) [deg]	(c)	124		-
∠(O13-H15···O4) [deg]	(c)	124		-

(a) Values are for the parent isotopologue.
(b) From CCSD(T)/CBS(D-T) calculations. Value in parentheses is corrected for zero-point energy using the M06-2X frequencies.
(c) This parameter is not chemically relevant in structure I.
(d) This parameter is not chemically relevant in structure II.

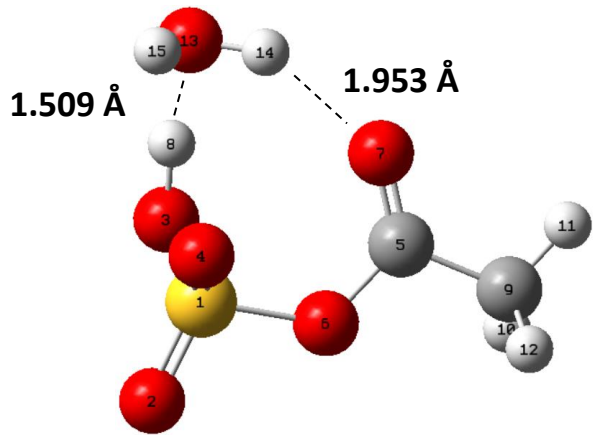

(I)

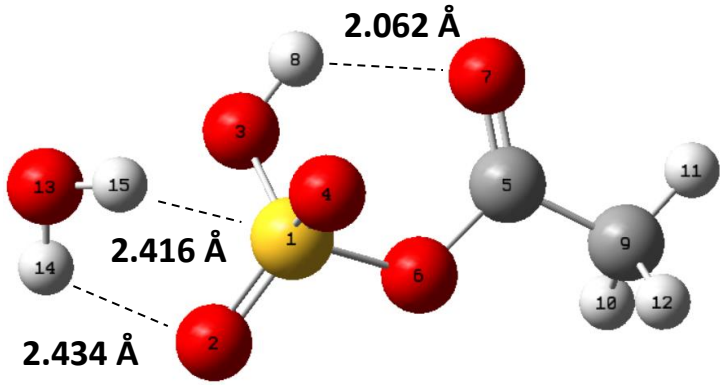

(II)

Figure 3.3 Structures at two minima on the potential energy surface of ASA···H_2O calculated using the M06-2X/6-311++G(3df,3pd) level of theory. Structure I is lower in energy by 10.6 kcal/mol (9.7 kcal/mol with zero-point energy corrections).

In order to obtain more accurate energies, single-point calculations were performed at the M06-2X geometries using CCSD(T) with the complete basis set [(CBS(D-T)] extrapolation of Neese and Valeev between the ANO-pVDZ and ANO-pVTZ basis sets.[138] At this level of theory, without zero-point corrections, structures I and II lie 13.3 and 3.3 kcal/mol below the sum of the free ASA and H_2O monomer energies. With zero-point corrections using the M06-2X frequencies, the minimum energy structure (I) and the higher

energy isomer (II) lie 11.1 and 2.1 kcal/mol, respectively, lower in energy than the sum of the ASA and H_2O monomer energies. For comparison, counterpoise corrected binding energies from the M06-2X calculations were 14.1 and 3.8 kcal/mol for structures I and II, respectively. Note that although these structures represent local minima on the potential energy surface for the system, they are not the global minimum. The doubly hydrogen bonded complex $CH_3COOH\cdots H_2SO_4$, which is formed from hydrolysis products of the anhydride and is shown in Figure 3.4, was found to lie 11.0 kcal/mol lower in energy than structure I. It is interesting to note that the two hydrogen bond lengths, 1.696 Å and 1.499 Å are exceptionally short. The calculated rotational constants are included in Table 3.2 and atomic Cartesian coordinates for this structure are also provided in Appendix C.

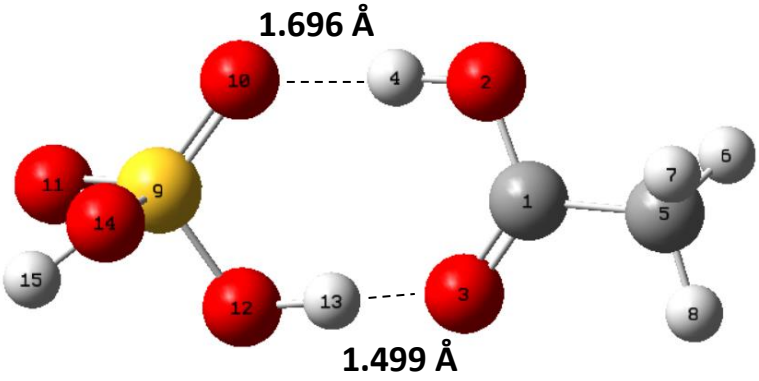

Figure 3.4 Structure of the doubly hydrogen bonded dimer $CH_3COOH\cdots H_2SO_4$ calculated at the M06-2X/6-311++G(3df,3pd) level of theory.

Discussion

Table 3.2 compares the experimentally observed results for the parent form of the complex with those calculated results for structures I and II, as well as those for $CH_3COOH\cdots H_2SO_4$. The predicted constants for $CH_3COOH\cdots H_2SO_4$ are clearly inconsistent with the experimental values and moreover, it is clear that the observed values of A, B, C, V_3, δ, and ε are all in much better agreement with the predicted values for structure I than for structure II, suggesting it is, indeed, the species observed. Table 3.3 further compares the observed shifts in the rotational constants upon isotopic substitution with those calculated for structures I and II, and unequivocally supports the same assignment. It is sensible that the

structure with the lower calculated energy is the one observed in the supersonic jet. Spectra of the higher energy form, II, are likely below detection limits due to reduced population. Note also, that, while not indicated in Table 3.2, the calculated values of *A*, *B*, and *C* for the $SO_3\cdots CH_3COOH\cdots H_2O$ complex are 3345.8, 740.5, and 693.6 MHz, respectively, clearly ruling out this trimer as the carrier of the observed spectra.

Table 3.3 Comparison of Theoretical and Experimental Isotopic Shifts[a]

	Observed Shift	Calculated, Structure I	Calculated, Structure II
$CD_3COOSO_2OD\cdots D_2O$			
A	–103.279	–103.6	–193.1
B	–129.676	–130.1	–77.1
C	–76.538	–77.2	–69.8
$CH_3{}^{13}COOSO_2OH\cdots H_2O$			
A	0.028	0.0[b]	–0.8
B	–9.531	–9.7	–5.3
C	–4.139	–4.3	–4.7

(a) All values in MHz. Isotopic shifts are the value for the isotopologue minus the value for the parent species.
(b) This value is not identically zero. The calculated value is –0.022 MHz.

In its lowest energy configuration, the $ASA\cdots H_2O$ dimer adopts a cyclic structure in which the water moiety inserts into the internal hydrogen bond of ASA. This results in the formation of two new hydrogen bonds. The first, a "primary" hydrogen bond formed between H8 and O13, is calculated to be quite short (1.509 Å) and nearly linear, with ∠(O3-H8···O13) equal to 171 deg. The second is a ring-closing hydrogen bond between H14 and O7, which is somewhat longer (1.953 Å) and less linear, with ∠(O13-H14···O7) equal to 142 deg. The exceptionally short primary hydrogen bond suggests that the ASA proton may be strongly acidic. The cyclic motif exhibited by this complex is reminiscent of the "homodromic rings"[145] commonly observed in the hydration of other strong protic acids (e.g., HNO_3, H_2SO_4).[9]

It is interesting to compare the calculated structures of complexes I and II. Unlike structure I, structure II leaves the internal hydrogen bond of ASA intact, with an H8···O7 distance of 2.062 Å and an O3-H8···O7 angle of 122 deg. These values are similar to the 2.01 Å

and 125 deg values previously determined for free ASA.[124] The interaction with the water in structure II involves H···O non-bonded interactions which are long and far from linear. The two shortest intermolecular hydrogen – oxygen distances in structure II are H15···O4 (2.416 Å) and H14···O2 (2.434 Å), with corresponding hydrogen bond angles, ∠(O13-H15···O4) and ∠(O13-H14···O2), which are both 124 deg. Thus, they would appear to be weak and it is not surprising that structure I is the lower energy form. Note that in both structures, the O3-H8 distance is a typical O-H covalent bond length (1.030 Å for structure I and 0.975 Å for structure II), confirming H8 has been transferred to one of the SO_3 oxygens during the formation of the complex from $SO_3 + CH_3COOH + H_2O$. Also, the S1-O6-C5 angle is virtually the same in both systems (122 deg in structure I and 120 deg in structure II).

To the best of our knowledge, there have been no other studies of a gas phase hydrate of an acid anhydride. The existence of a hydrated form of an acid anhydride is, in a sense, analogous to the existence of hydrated forms of strong protic acids. Although strong acids dissociate in bulk aqueous solution, the stability of hydrogen bonded (i.e., non-proton transferred) complexes for small acid hydrates is well known. Indeed, the minimum number of water molecules needed to enable proton transfer is typically in the 4-7 range[9] and this may be thought to arise from the need for a sufficient number of "solvent" molecules to stabilize the charge separation arising from the proton transfer. In the case of an acid anhydride, however, the hydrolysis products (here, H_2SO_4 and CH_3COOH) are neutral species and do not involve the kind of charge separation associated with proton transfer. Thus, the energetic requirements for stabilizing the products are not necessarily the same, and an interesting question is how large a water cluster can be formed without spontaneous conversion to hydrolysis products. One significant difference between the hydration of a protic acid and an acid anhydride, however, is that in the case of protic acids with small hydration numbers, only the complexes with the undissociated acid correspond to potential energy minima. The hydrated ionic products do not emerge until larger hydration numbers. In contrast, in the case of ASA, with even one water molecule, both the hydrated form and the hydrolyzed form correspond to potential energy minima, with

the latter being lower in energy. The structural rearrangements and activation energy necessary to accomplish hydrolysis within the cluster are, at this point, unclear, but this study verifies that in a complex with only one water molecule, the un-hydrolyzed form represents a minimum on the system's potential energy surface and can exist without spontaneously reverting to the parent acids.

Finally, it is of interest to compare the methyl group internal rotation barrier with those determined for free ASA,[122] free acetic acid,[91] and the mono- dihydrates of acetic acid.[146] The comparison is given in Table 3.4, where it is readily seen that the value of V_3 in ASA decreases by ~9% upon complexation with water. This trend is similar to that previously observed for sequential hydration of acetic acid, for which the internal rotation barrier decreases by 18% upon complexation with one water molecule and another 14% upon complexation with a second water molecule. The values for both ASA and ASA$\cdots H_2O$, however, are both significantly larger than for free acetic acid and its hydrates, but similar to the 254.711(38) cm^{-1} barrier reported for formic acetic anhydride.[147] These trends are interesting, but we caution against over-interpretation insofar as internal rotation barriers have been shown to be complex combinations of competing terms and are difficult to rationalize on simple steric grounds.[44]

Table 3.4 Internal Rotation Barriers for ASA$\cdots H_2O$ and Related Species

	V_3 (cm^{-1})
CH_3COOSO_2OH (ASA)[a]	241.093(30)
$CH_3COOSO_2OH\cdots H_2O$ (ASA$\cdots H_2O$)[b]	219.60(2)
CH_3COOH[c]	168.16(10)
$CH_3COOH\cdots H_2O$[d]	138.396(5)
$CH_3COOH\cdots (H_2O)_2$[d]	118.482(2)
$CH_3COOCHO$[e]	254.711(38)

(a) Reference 122.
(b) This work, Structure I.
(c) Reference 91.
(d) Reference 146.
(e) Reference 147.

Conclusion

The microwave spectrum of the ASA···H_2O complex has been observed in a supersonic jet containing SO_3, acetic acid, and H_2O. A and E states arising from the internal rotation of the methyl group were observed, and the barrier obtained, 219.598(21) cm^{-1} for the parent isotopologue, is 9% smaller than that of free ASA. Density functional theory has identified two isomers of the ASA···H_2O complex. In the lower energy form, observed in this study, the water inserts into the intramolecular hydrogen bond of ASA, creating an 8-membered ring. CCSD(T)/CBS(D-T) calculations at the optimized M06-2X geometries indicate that the ASA···H_2O complex is lower in energy than its corresponding monomers (ASA + H_2O) by 13.3 kcal/mol (11.1 kcal/mol with zero point corrections). The doubly hydrogen bonded complex CH_3COOH···H_2SO_4 lies even lower in energy, but was not observed in this work. While any possible role of anhydrides in atmospheric processes remains to be seen, the barrierless reaction of SO_3 + RCOOH and the possibility of subsequent hydrolysis in small clusters or aqueous droplets raise the question as to whether such species could play a role in determining atmospheric aerosol composition. The ASA···H_2O complex is the first step in understanding its interaction with water and shows that a stable complex with one water molecule can exist without hydrolysis. Future work should focus on the di- and trihydrate complexes and the role of microsolvation in promoting hydrolysis.

Acknowledgements

This work was supported by the National Science Foundation (Grant Nos. CHE–1266320 and CHE 1563324) and the Minnesota Supercomputing Institute. Anna Huff was supported by a Lester C. and Joan M. Krogh Fellowship, administered through the University of Minnesota.

Chapter 4: Observation of Propiolic Sulfuric Anhydride by Microwave Spectroscopy and the Determination of Equilibrium Constants for Previously Studied Carboxylic Sulfuric Anhydrides Using Statistical Thermodynamics

From C. J. Smith, Anna K. Huff, Rebecca B. Mackenzie, Kenneth R. Leopold

Overview

Carboxylic acids react with sulfur trioxide to form carboxylic sulfuric anhydrides, $RCOOSO_2OH$. In this article, new supersonic jet microwave spectra are presented for the anhydride derived from propiolic acid (HCCCOOH), and recent work on a series of carboxylic sulfuric anhydrides is reviewed. For the propiolic acid derivative, computed minimum-energy structures are reported for both the anhydride ($HCCCOOSO_2OH$) and its precursor complex ($HCCCOOH–SO_3$), and additional CCSD(T)/CBS(D–T)//M06-2X/6-311++G(3df,3pd) calculations indicate that, after zero-point energy corrections, the barrier to anhydride formation is effectively zero. These results are similar to those for other carboxylic sulfuric anhydrides studied and are consistent with their rapid production under supersonic jet conditions. Carboxylic sulfuric anhydrides, as a class, have not been widely characterized in the chemical literature and thus their study represents a new feature of the chemistry of sulfur oxides and oxyacids. As such, structural and energetic features of the carboxylic sulfuric anhydrides derived from formic, acetic, acrylic, trifluoroacetic, propiolic, pinic, and benzoic acids are compared. Computed vibrational frequencies are provided as Supporting Information and should be useful for possible future observation by infrared and/or Raman spectroscopy. Statistical thermodynamics is used to estimate the equilibrium constants for the formation reactions at a series of temperatures, and the results indicate values ranging from ~10^4 atm^{-1} for formic acid at 288 K to over 10^{11} atm^{-1} for benzoic acid at 217 K. We speculate that carboxylic sulfuric anhydrides could be active species in the Earth's atmosphere and atmospheric concentrations have, therefore, been estimated assuming an equilibrium state. These estimates are subject to significant uncertainties in the atmospheric SO_3 and carboxylic acid concentrations, but may be as high as 10^7 molecules/cm^3 in some locations. Related calculations suggest that equilibrium anhydride concentrations may exceed those of the sulfuric acid precursors $SO_3–H_2O$ and $SO_3–(H_2O)_2$ by several orders of magnitude. Kinetic modeling will ultimately be necessary to fully assess the role, if any, of carboxylic sulfuric anhydrides in atmospheric processes.

Introduction and Overview

Sulfur forms a wide variety of oxyacids, whose structures and properties may be found in any comprehensive book on inorganic chemistry.[148] Members of this class of compounds range from exotic species such as peroxymonosulfuric and polythionic acids to the more common sulfuric acid, which is a mainstay of the chemical industry. In the atmosphere, sulfuric acid is a constituent of polar stratospheric clouds and is widely recognized as a key molecule in the early stages of aerosol nucleation.

Recent work in our laboratory has demonstrated the existence of a largely unreported type of sulfur oxyacid in the gas phase, which forms via a cycloaddition reaction of a carboxylic acid with sulfur trioxide.[31,32,122,149] The reaction product, a carboxylic sulfuric anhydride, has been observed in a supersonic jet and characterized for a variety of acid precursors by microwave spectroscopy and computational chemistry. The proposed mechanism is shown below.

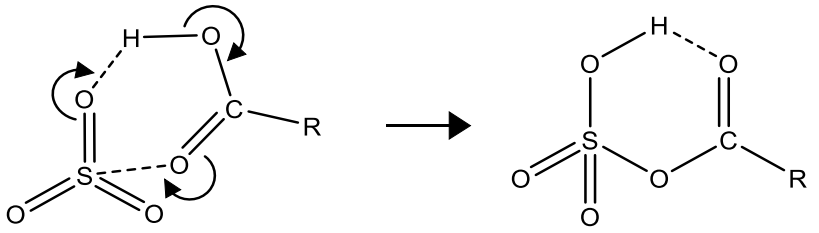

K_1 (4.1)

$RCOOH{-}SO_3$ Complex

$RCOOSO_2OH$ (Carboxylic Sulfuric Anhydride)

To date, we have reported the microwave spectroscopic observation of these anhydrides with R = H,[31] CH_3,[122] CH_2=CH,[32] and CF_3.[149] Calculations at the CCSD(T)/CBS(D-T)//M06-2X/6-311++G(3df,3pd) level/basis set indicate that, after zero-point energy corrections, the barrier to reaction (4.1) appears to be either very small or slightly negative for hydrocarbon R groups, consistent with the facile product formation during the collisional phase of the supersonic expansion. For the CF_3 derivative, the activation barrier relative to the $CF_3COOH{-}SO_3$ precursor complex is somewhat larger, approximately 1.2

kcal/mol at the same level of theory. Additional calculations on benzoic and pinic acids[31] indicate that the same reaction should take place with slightly negative activation energies, though no experimental observations have been attempted.

To our surprise, relatively little appears to have been reported about these species in the literature. The sodium salt of the methyl derivative, $Na^+CH_3COOSO_3^-$, was first prepared in 1921,[150] and kinetic studies involving the parent acid, CH_3COOSO_2OH, have indicated that it is unstable with respect to rearrangement or decomposition in solution.[151,152] An infrared study of 1:1 mixtures of cyclohexanecarboxylic anhydride and SO_3 in liquid SO_2 reports a related compound, dicyclohexanecarbonylsulphate (RCOO-SO_2-OCOR) as the predominant species,[153] and keto-enol equilibria involving acetic sulfuric anhydride in liquid SO_2 has been studied.[154] A number of related systems have also been mentioned briefly in other works,[155-157] but to the best of our knowledge, little or no additional spectroscopic characterization of any gas phase carboxylic sulfuric anhydride beyond the microwave work noted above has been reported. Interestingly, more recent theoretical work has investigated the vapor pressure of clusters of the anhydride derivative formed from 3-methyl-1,2,3-butanetricarboxylic acid,[158] and a Born-Oppenheimer molecular dynamic study indicates the formation of a carboxylic sulfuric anhydride – hydronium ion pair at the air-water interface.[159]

Aside from their intrinsic interest as sulfur oxyacids, carboxylic sulfuric anhydrides are of possible importance in connection with mechanisms for the formation of atmospheric aerosols. SO_3 is an active atmospheric species, widely understood to be the primary precursor to sulfuric acid, whose role in aerosol nucleation is well documented.[160-162] Carboxylic acids are also prevalent, as they are derived largely from the atmospheric photo-oxidation of vehicular exhaust, biogenic emissions, and the combustion of biomass.[131,133,163-167] They are found both in the gas phase and in aerosol particles, and their complexes with other atmospheric species may stabilize pre-nucleation clusters.[139,141,168-171] Moreover, their interaction with SO_3 is of particular interest, as Hazra and Sinha have shown, through computational methods, that formic acid provides an effective catalyst for

the reaction $SO_3 + H_2O \rightarrow H_2SO_4$.[30] In this general context, therefore, the near-zero or even slightly negative activation barriers calculated for reaction (4.1) raises the questions, "Can carboxylic sulfuric anhydrides attain significant concentrations in the atmosphere?" and "If they do, what role(s) might they play?". One possible answer to the latter question involves their hydrolysis in preexisting aqueous droplets, thus leading to the deposition of both organic matter and H_2SO_4 into atmospheric aerosol particles. Another is that the anhydrides themselves could serve as seed molecules for homogeneous nucleation. While neither of these roles, nor even the presence of these species in the atmosphere, has yet been established, further investigation of these species seems warranted.

In this article, we first report new experimental and computational results for propiolic sulfuric anhydride, $HC{\equiv}CCOOSO_2OH$ (PSA). We then provide a collective summary and comparison of carboxylic sulfuric anhydrides studied to date. Finally, we begin the investigation of their possible atmospheric significance by reporting statistical thermodynamic calculations of the equilibrium constant for their formation from SO_3 and the parent carboxylic acids in the gas phase.

Propiolic Sulfuric Anhydride

A. Experimental Methods and Results: The methods used to observe propiolic sulfuric anhydride were similar to those used in our studies of other carboxylic sulfuric anhydrides. Spectra were taken using a Fourier transform microwave spectrometer with combined chirped-pulse[14] and Fabry-Perot cavity[13] capabilities. The instrument has been described previously.[15,54] SO_3 vapor was seeded in argon by passing the latter over a polymerized sample prior to expansion through the 0.8 mm orifice of a commercial pulsed solenoid valve. Propiolic acid vapor was seeded in argon and injected into the early part of the expansion using a 0.012 in. inner diameter hypodermic needle, as previously described.[135] Because the vapor pressure of propiolic acid is somewhat lower than that of other carboxylic acids we have used, a special bubbler was made to fit in the vacuum chamber immediately adjacent to the pulsed valve in order to minimize the distance to the nozzle

and hence reduce the need for passivation of the gas line. A diagram of the molecular source for these experiments is shown in Figure 4.1. For $HC{\equiv}CCOOSO_2OD$, a 20:3 propiolic acid/D_2O mixture was used to collect rotational spectra with the same apparatus. Spectra of the ^{34}S isotopologue were observed in natural abundance. Propiolic acid and SO_3 were obtained from Sigma-Aldrich and D_2O was obtained from Cambridge Isotope Laboratories, Inc.

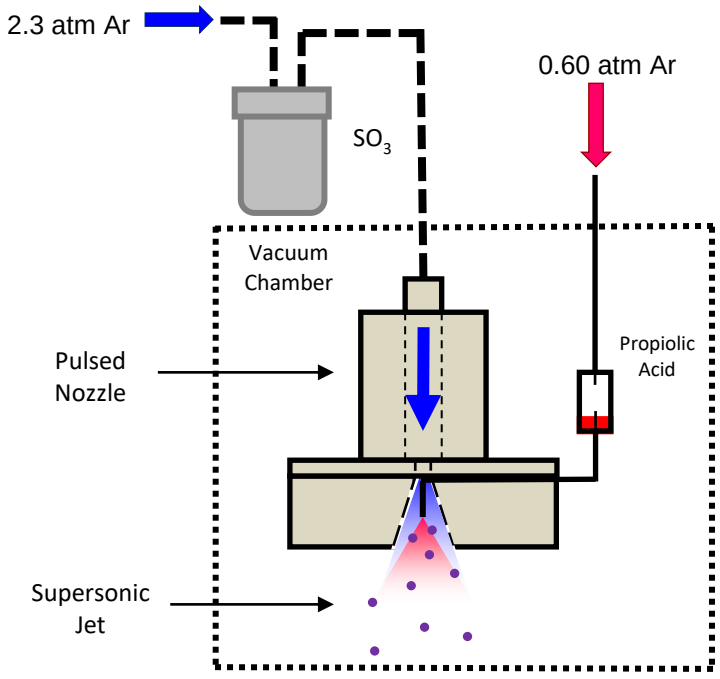

Figure 4.1 Molecular Source Used to Produce Propiolic Sulfuric Anhydride in a Supersonic Jet.

Initially, spectra were collected from 6 to 18 GHz in 3 GHz segments using our broadband chirped-pulse system, which provided frequencies with a typical accuracy of about 30 kHz. For each segment, 10,000 free induction decay signals were averaged, each with a 90 μs collection time. A portion of the chirped pulse spectrum is shown in Figure 4.2. A strong *a*-type spectrum was identified based on a predicted structure and was fit to the A-reduced Watson Hamiltonian[10] using the SPFIT program of Pickett.[136] Preliminary fits utilized only these *a*-type transitions, but *b*- and *c*-type transitions were also anticipated since non-zero dipole moment components were predicted along all three inertial axes. After switching to

our narrowband cavity spectrometer, several weaker *b*- and *c*-type transitions were observed, and higher resolution measurements of a number of the *a*-type transitions were also obtained. Spectra of both the deuterated and ^{34}S isotopologues were readily recorded with the cavity system, with transitions measured between 5.3 and 11.1 GHz. In the monodeuterated isotopologue, deuterium hyperfine structure was not resolved and, therefore, no nuclear quadrupole coupling constants were obtained. For all measurements using the cavity mode of the spectrometer, the sample was pulsed at a rate of 4 Hz and four free induction decay signals were collected per pulse, each with a collection time of 140.8 μs. Transition frequencies were accurate to ~4 kHz. A trace of the $4_{14} \leftarrow 3_{03}$ transition of the parent complex is shown in the inset of Figure 4.2. Spectroscopic constants for all three isotopologues are given in Table 4.1 and observed frequencies, assignments, and residuals from the least squares fits are given in Appendix D.

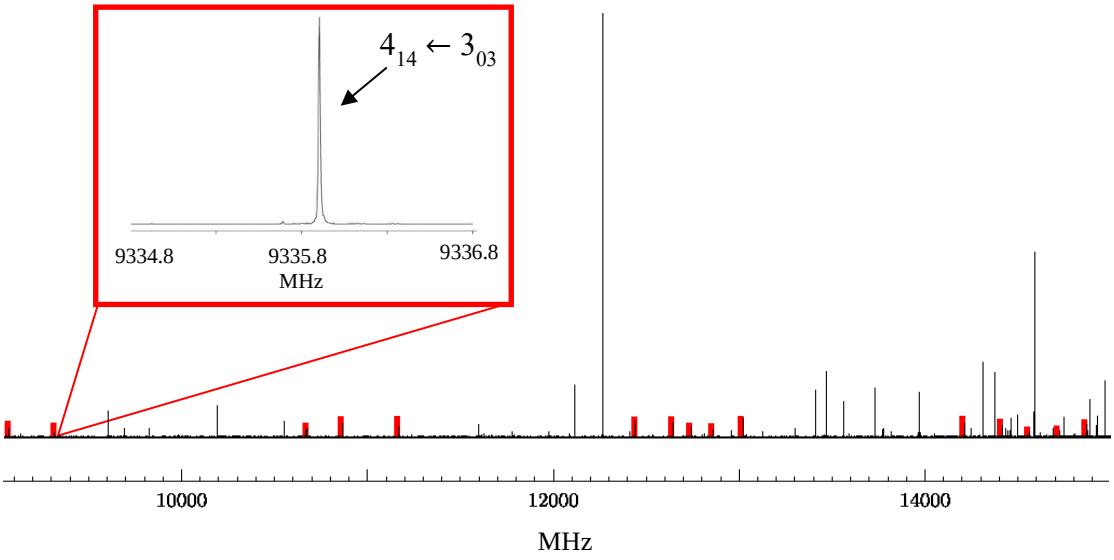

Figure 4.2 9-15 GHz Chirped-Pulse Spectrum of SO_3 and Propiolic Acid in Ar. The spectrum is an average of 10,000 free induction decays signals. PSA signals are highlighted in red and known instrumental artifacts have been removed from the spectrum. A trace of the $4_{14} \leftarrow 3_{03}$ transition recorded on the cavity spectrometer is shown in the inset.

Table 4.1 Spectroscopic Constants of Propiolic Sulfuric Anhydride[a]

Constant	$HCCCOOSO_2OH$	$HCCCOOSO_2OD$	$HCCCOO^{34}SO_2OH$
A [MHz]	3371.85309(45)	3300.0064(31)	3369.936(93)
B [MHz]	952.68843(12)	950.79390(15)	947.10604(17)
C [MHz]	869.16994(11)	863.94576(17)	864.43126(16)
Δ_J [kHz]	0.0603(29)	0.0430(27)	0.0439(37)
Δ_{JK} [kHz]	0.213(38)	0.286(28)	0.389(71)
δ_J [kHz]	0.0145(22)	-	-
N[b]	30	17	13
RMS [kHz][c]	5.4	1.5	1.5

(a) Number in parentheses represent the uncertainty in the last digit.
(b) Number of transitions in the fit.
(c) Root-mean-square of the residuals (from the least-squares fit)

B. Theoretical Methods and Results: As in our previous studies, structures and dipole moment components of both the anhydride ($HCCCOOSO_2OH$) and the putative precursor complex ($HCCCOOH–SO_3$) were calculated using the M06-2X/6-311++G(3df,3pd) level/basis and the Gaussian 09 suite of programs.[88] The equilibrium structures are shown in Figure 4.3 and Cartesian coordinates are provided in Appendix D. Table 4.2 compares the calculated rotational constants for the anhydride and the precursor complex with the observed values for the parent isotopologue. The results for the anhydride are clearly in much better agreement with experiment (within 0.6%), providing strong evidence for assignment of the observed spectra to that species. The table also compares the computed isotope shifts for the ^{34}S and deuterated isotopologues with the observed values. While less definitive than the rotational constants themselves, these comparisons also favor assignment of the observed spectra to the anhydride. Finally, the dipole moment components, μ_a, μ_b, and μ_c, of the anhydride are 4.16, 0.52, and 0.93 D, respectively, whereas for the precursor complex, they are 5.54, 0.60, and 0.06 D respectively. The very small value of μ_c for the precursor complex would be expected to preclude the observation of *c*-type transitions and thus, the observation of such transitions provides further evidence that the recorded spectra arise from the anhydride. Overall, based on the body of

experimental and computational results, we conclude that the observed species is propiolic sulfuric anhydride. Selected structural parameters and harmonic vibrational frequencies for the anhydride are given in Table 4.3.

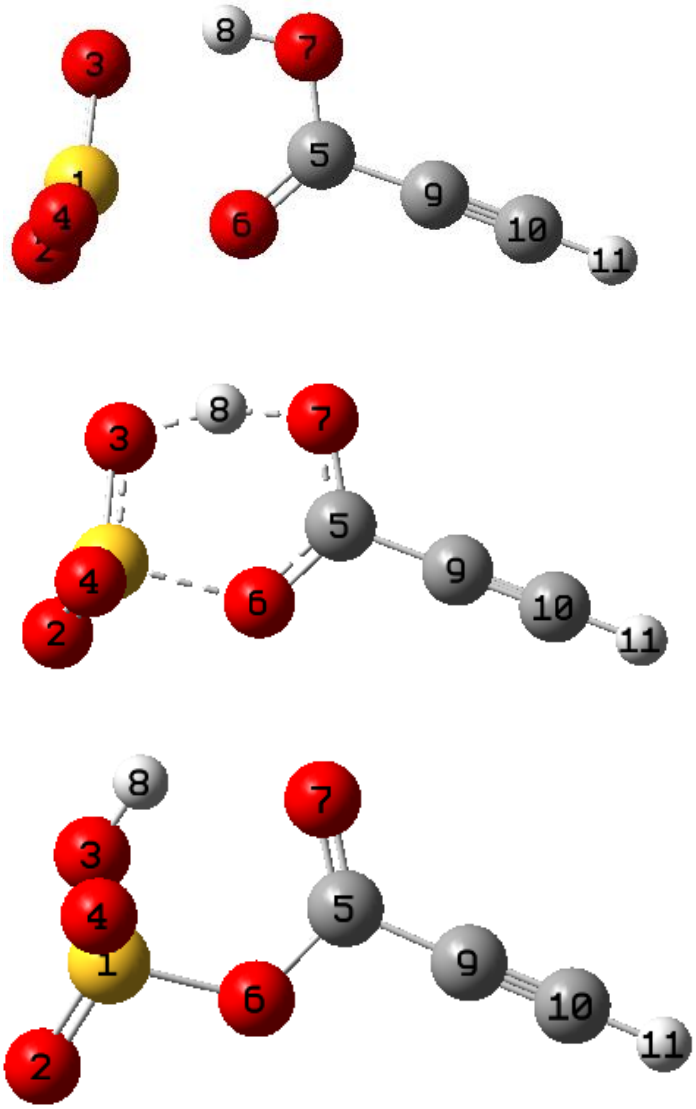

Figure 4.3 Calculated Equilibrium Structures.
(a) The propiolic acid – SO_3 precursor complex
(b) The transition state leading to propiolic sulfuric and anhydride
(c) Propiolic sulfuric anhydride.

Table 4.2 Computational Results and Comparison with Experiment

Constant	$HCCCOOSO_2OH$		
	Obs.	**Calc.[a] Anhydride**	**Calc.[a] Precursor**
A [MHz]	3371.85309(45)	3390	3473
B [MHz]	952.68843(12)	957	854
C [MHz]	869.16994(11)	873	788
μ_a [D]	$\neq 0$[b]	4.16	5.54
μ_b [D]	$\neq 0$[b]	0.52	0.60
μ_c [D]	$\neq 0$[b]	0.93	0.06

Isotope Shifts Relative to Parent Species

	D			**^{34}S**		
	Obs.	**Calc.[a] Anhydride**	**Calc.[a] Precursor**	**Obs.**	**Calc.[a] Anhydride**	**Calc.[a] Precursor**
A [MHz]	−71.84669	−75	−68	−1.91709	−2	−1
B [MHz]	−1.89453	−2	0	−5.58239	−6	−7
C [MHz]	−5.22418	−5	−3	−4.73868	−5	−5

(a) Calculated using M06-2X/6-311++G(3df,3pd) Cartesian coordinates.
(b) From the observation of *a*-, *b*-, and *c*-type rotational transitions.

Table 4.3 Selected Structural and Vibrational Properties of Carboxylic Sulfuric Anhydrides and their Precursor Complexes[a,b]

	***R*(S1-06) [Å]**		***R*(O7–H8) [Å]**		***R*(O3-H8) [Å]**		***R*(C5-O7) [Å]**		**ν(C5-O7) (cm^{-1})**	
R Group	Anhydride	Precursor Complex	Anhydride	Precursor Complex	Anhydride	Precursor Complex	Anhydride	Precursor Complex	Anhydride	Precursor Complex
CF_3[c]	1.648	2.148	2.153	0.987	0.974	1.724	1.186	1.290	1917	1540
H[d]	1.635	2.013	2.081	0.995	0.975	1.655	1.189	1.285	1860	1471
HC≡C[e]	1.636	1.997	2.068	0.999	0.975	1.622	1.194	1.289	1851	1521
CH_3[f]	1.626	1.932	2.013	1.004	0.976	1.589	1.194	1.286	1877	1549
s-trans-H_2C=CH[g]	1.624	1.912	2.000	1.006	0.976	1.577	1.198	1.286	1849	1543
s-cis-H_2C=CH[g]	1.627	1.914	1.995	1.007	0.976	1.568	1.197	1.286	1848	1552
C_6H_5[d]	1.625	1.896	1.978	1.009	0.977	1.559	1.199	1.286	1837	1558

(a) Derived from optimized M06-2X/6-311++G(3df,3pd) geometries. (b) Atomic numbering of Figure 3. (c) Reference 149. (d) Reference 31. (e) This work. (f) Reference 122. (g) Reference 32.

In order to provide improved energies at various points on the potential energy surface for the system, additional single-point calculations at the M06-2X geometries were carried out at the CCSD(T) level with complete basis set extrapolation between the ANO-pVDZ and ANO-pVTZ basis sets.[138] Zero-point energy (ZPE) corrections were applied using harmonic frequencies from the M06-2X calculations. The binding energy of the HCCCOOH–SO_3 precursor complex is 12.9 kcal/mol relative to the free monomers, and the energy for PSA is 16.7 kcal/mol below the sum of the free-monomer energies, including ZPE corrections.

A computational search for the transition state connecting the HCCCOOH–SO_3 complex and PSA was also conducted at the M06-2X/6-311++G(3df,3pd) level of theory, and a single-point energy calculation was then performed at the CCSD(T)/CBS(D-T) level. A cyclic transition state (Figure 4.3 [b]) structure was identified, analogous to those found previously for the RCOOH–SO_3 → $RCOOSO_2OH$ reactions (where R = H, CH_3, CF_3, and H_2C=CH, see equation 4.1). Without zero-point energy corrections, the CCSD(T) transition state barrier relative to the complex is 2.1 kcal/mol. However, with the inclusion of ZPE, the calculations indicate a barrierless process, with a zero-point corrected activation energy of 0.01 kcal/mol. The imaginary frequency found at the transition state corresponds to the concerted $\pi_2 + \pi_2 + \sigma_2$ cycloaddition mechanism, as previously proposed.[31,32,122,149] A diagram summarizing the relative energies at key points on the potential energy surface is given in Figure 4.4.

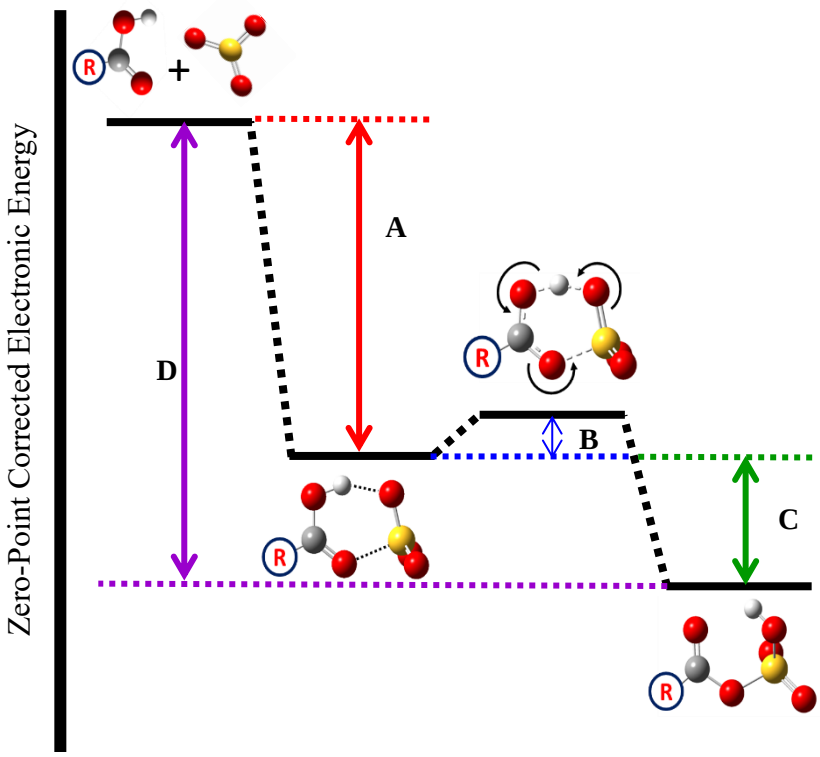

Figure 4.4 Generalized Energy Diagram. Energy diagram depicting key points on the intermolecular potential surface for the formation of carboxylic sulfuric anhydrides that do not involve internal rotation. For the reaction with CH_3COOH and CF_3COOH, see references 122 and 149, respectively, for a more complete representation including internal rotation. Electronic energies are calculated at the CCSD(T)/CBS(D-T)//M06-2X/6-311++G(3df,3pd) level of theory with zero-point corrections from M06-2X frequencies. The structure with three arrows shown has an imaginary frequency corresponding to the cycloaddition that forms the anhydride. The energy differences labeled by letters A−D are summarized in Table 4.4.

General Features of Carboxylic Sulfuric Anhydrides and Their Precursor Complexes

Selected interatomic distances and harmonic vibrational frequencies in the minimum energy structures for a series of carboxylic sulfuric anhydrides and their precursor complexes are summarized in Table 4.3, ordered according to the O7-H8 distance in the anhydride. The precursor complexes involve an interaction between the sulfur of the SO_3 and the carbonyl oxygen that evolves to become a chemical bond (S1-O6) in the anhydride.

Both species, the precursor complex and anhydride, adopt cyclic structures. It is interesting to note that in the precursor complexes, the S1-O6 distances range from approximately 1.9 to 2.1 Å, and are considerably shorter than a typical sulfur – oxygen van der Waals distance. For example, in the $SO_3 \cdots H_2O$ complex, the intermolecular S···O distance is 2.432(3) Å.[172] In the anhydride, the S1-O6 distances hover in tight range between 1.62 and 1.65 Å, which is very similar to the sum of the standard sulfur-oxygen covalent bond radii of ~1.7 Å.[173] Thus, the precursor complexes are best regarded as "partially bound" systems, whose structural features lie in the intermediate regime between chemical and non-covalent bonding.[174,175] The cycloaddition reaction of equation 4.1 transforms the partially bound system into a covalently bonded species and is relatively independent of the nature of the R group on the carboxylic acid.

Accompanying the cycloaddition reaction is the transfer of H8 from the OH site on the carboxylic acid to one of the SO_3 oxygens. The transfer is apparent in that the O7-H8 distances in the precursor complexes are 0.99 – 1.01 Å, but increase to 2.00 – 2.15 Å in the anhydrides. Concomitantly, the O3-H8 distance decreases from 1.6 – 1.7 Å in the precursor complexes to 0.97 – 0.98 Å in the anhydrides, indicating the formation of a new OH bond. The accompanying conversion of the C5-O7 bond from a single bond in the precursor complexes to a double bond in the anhydrides is also signaled by its contraction upon cycloaddition. Interestingly, the contraction is only about 0.1 Å, whereas standard values for C–O and C=O bonds differ by about 0.2 Å. The conversion from a single bond to a double bond is also reflected in the calculated carbonyl stretching frequencies, ν(C5-O7), which change from values near 1500 cm^{-1} in the precursor complex to values near 1850 cm^{-1} in the anhydrides.

Calculated energies relevant to the formation of the anhydrides are summarized in Table 4.4, which is largely taken from reference 149, but modified to include new values for the propiolic acid species as well as results for the benzoic acid species. The letter designations in the top row refer to the energy differences shown pictorially in Figure 4.4. The binding

energies of the precursor complexes range from 10.2 – 18.0 kcal/mol, and the anhydrides lie 14.4 – 20.7 kcal/mol lower in energy than the sum of the free SO_3 and RCOOH energies. The zero-point corrected activation barriers for the cycloaddition are all small and, in some cases, negative, consistent with the observation that the anhydrides are readily observed in a supersonic jet. Since the carboxylic acid vapor is injected directly into the early phase of the expansion, the observed signals indicate that the anhydrides readily form in a time comparable to the duration of the collisional phase of the supersonic expansion, which is only several tens of microseconds.

The magnitude of the energy change for the cycloaddition reaction can be understood in the context of bond energies. From reaction (4.1) it is apparent that, apart from the formation of the internal hydrogen bond, the net effect of the cycloaddition reaction is to convert one S=O double bond in SO_3 into two S–O single bonds. Thus, the energy change for the reaction should be approximately [BE(S=O) – 2BE(S–O)], where "BE" represents the bond energy. A value for the S=O double bond energy does not appear in many common tabulations, but Huheey[176] gives the sulfur – oxygen bond energy in SO_3 as 112 ± 2 kcal/mol. Using the commonly reported value of 63.3 kcal/mole for a sulfur – oxygen single bond[177] gives [BE(S=O) – 2BE(S–O)] = –15 kcal/mol. The reaction energies in Table 4.4 (column D) are, in most cases, slightly larger in magnitude and could reflect the extra stabilization of the internal hydrogen bond, though we note that bond energy calculations are inherently approximate. In any case, the result is of the right order of magnitude and supports this somewhat simplistic interpretation of the reaction energetics.

Table 4.4 Energetics Relevant to the Formation of Various Carboxylic Sulfuric Anhydrides[a,b]

	A	**B**	**C**	**D**
R Group	Binding energy of precursor complex	Barrier to anhydride formation relative to precursor complex	Energy relative to precursor complex	Energy relative to free monomers
CF_3[c]	10.2	1.17(1.21)[d]	–4.2	–14.4
H[e]	12.6	0.26	–3.9	–16.5
HC≡C[f]	12.9	–0.25	–4.1	–16.7
CH_3[g]	15.7	0.057(-0.12)[d]	–3.1	–18.9
s-trans-H_2C=CH[h]	16.1	–0.22	–2.7	–18.8
s-cis-H_2C=CH[h]	16.1	-0.33	–2.9	–19.0
C_6H_5[e]	17.0	–0.36	–2.5	–19.5

(a) All energies in kcal/mol calculated at CCSD(T)/CBS(D-T)//M06-2X/6-311++G(3df,3pd) with zero-point corrections from M06-2X/6-311++G(3df,3pd) frequencies.
(b) Letters in the first row refer to the energy differences as indicated in Figure 4.4.
(c) Reference 149.
(d) Value outside of parentheses corresponds to the barrier of the sequential pathway of the CF_3 or CH_3 transition state followed by the cycloaddition transition state. Value inside the parentheses corresponds to the barrier of the simultaneous pathway in which both CF_3 or CH_3 rotation and cycloaddition occur simultaneously via a second order saddle point.
(e) Reference 31.
(f) This work.
(g) Reference 122.
(h) Reference 32.

Statistical Thermodynamics of Anhydride Formation

We have noted above and elsewhere[31,32,122,149] that the reaction of SO_3 with carboxylic acids may have a role to play in atmospheric chemistry. Given the low concentrations of SO_3 and carboxylic acids, however, the viability of reaction (4.1) as an atmospherically significant process will depend, at least in part, on its thermodynamic favorability. Thus, a series of statistical thermodynamic calculations has been performed to estimate the equilibrium constant, K_p, for reaction (4.1) with a representative set of carboxylic acids. The method, which employs harmonic vibrational frequencies, is straightforward and has been described elsewhere,[178,179] but a full procedure of the calculation is provided in Appendix D.[88,178,179,180] While more accurate methods that account for anharmonicity and torsion are available to calculate partition functions[181,182] from first principles, the significant uncertainties and variability in the concentrations of SO_3 and carboxylic acids in the atmosphere (see below) do not prescribe their application at this time. The intent is only to provide estimates of the magnitude of these constants, with the ultimate aim of assessing possible importance at various altitudes. Note that the reactions considered here are homogeneous, gas phase processes.

Input data for the calculations, which include computed binding energies, vibrational frequencies, and rotational constants, are provided in Appendix D. Calculated harmonic vibrational frequencies were multiplied by a scaling factor of 0.97 to provide better estimates of the zero-point energy.[183] The resulting equilibrium constants are most sensitive to the calculated values of the binding energy and thus, two sets of calculations were performed. The first employed the single-point CCSD(T)/CBS(D-T) energies at the minimum energy structure obtained from the M06-2X/6-311++G(3df,3pd) calculations reported above. The second employed CCSD(T)/CBS(D-T) energies obtained at the optimized MP2/6-311++G(3df,3pd) geometries, and are included to provide some measure of the variation that may be expected due to computational methodology. (In these latter calculations, MP2 rotational constants and scaled vibrational frequencies were also used.) The results at a series of temperatures are given in Table 4.5, where the temperatures chosen correspond to those at 5 km intervals in the atmosphere.[183] Note that, for the present

purpose, the *s-cis* and *s-trans* forms of acrylic acid were treated as separate species and that the *s-cis* conformer of the anhydride forms from the *s-trans* conformer of the parent acid and vice versa.[32] The acetic acid reaction is not included due to the complications from methyl torsion. Such complications can be managed by more advanced approaches, but were not pursued in this work.

Two reactions form the primary basis for understanding the gas-phase formation of sulfuric acid in the atmosphere:[114-117,121,184]

$$SO_3 + (H_2O)_2 \rightarrow SO_3{-}(H_2O)_2 \rightarrow H_2SO_4 + H_2O \qquad K_2 \qquad (4.2)$$

$$SO_3{-}H_2O + H_2O \rightarrow SO_3{-}(H_2O)_2 \rightarrow H_2SO_4 + H_2O \qquad K_3 \qquad (4.3)$$

Thus, to provide a point of comparison with other significant players in the atmospheric chemistry of SO_3, similar calculations were performed for the formation of $SO_3{-}H_2O$ and $SO_3{-}(H_2O)_2$ viz.,

$$SO_3 + H_2O \rightarrow SO_3{-}H_2O \qquad K_4 \qquad (4.4)$$

$$SO_3{-}H_2O + H_2O \rightarrow SO_3{-}(H_2O)_2 \qquad K_5 \qquad (4.5)$$

where the equilibrium constants, K_4 and K_5 are indicated. Calculated values of the equilibrium constants for these reactions have been previously reported,[30,117,121] but have been repeated here to maintain consistency with the level of theory used throughout this work. The results are given in Table 4.6 and are in quite reasonable agreement with literature values.[30,117,185] Values of ΔH and ΔS were also calculated for reactions R1, R4, and R5 are given in Table 4.7. Because these quantities vary slightly with temperature, values are given at both the low and high ends of the temperature range studied (217 K and 288 K). Note that other studies indicate that complexes of SO_3 with higher hydration numbers may also contribute to sulfuric acid production,[121] but for the present purpose, we focus only on the formation of mono- and dihydrates.

Table 4.5 Calculated Equilibrium Constants for the Reaction RCOOH + SO_3 ⇌ $RCOOSO_2OH$ [(a)]

Altitude [km]	T [K]	R = H–		R = HCC–		R = CH_2=CH– *(s-cis)*[b]		R = CH_2=CH– *(s-trans)*[b]		R = CF_3–		R = C_6H_5–	
		M06-2X	MP2	M06-2X	MP2	M06-2X	MP2	M06-2X	MP2	M06-2X	MP2	M06-2X	MP2
0	288	$2.2x10^4$	$1.3x10^4$	$1.1x10^4$	$1.2x10^4$	$1.2x10^6$	$6.8x10^5$	$7.3x10^5$	$5.2 x 10^5$	$2.8 x 10^2$	$2.0 x 10^2$	$2.0 x 10^6$	$1.3x10^6$
5	256	$9.4x10^5$	$5.2x10^5$	$4.6x10^5$	$4.8x10^5$	$8.7x10^7$	$4.6x10^7$	$5.0x10^7$	$3.4 x 10^7$	$7.3 x 10^3$	$4.9 x 10^3$	$1.5 x 10^8$	$9.6x10^7$
10	223	$1.4x10^8$	$7.3x10^7$	$7.0x10^7$	$6.7x10^7$	$2.6x10^{10}$	$1.3x10^{10}$	$1.4x10^{10}$	$8.9 x 10^9$	$5.6 x 10^5$	$3.4 x 10^5$	$5.2 x 10^{10}$	$2.9x10^{10}$
15	217	$4.2x10^8$	$2.1x10^8$	$2.1x10^8$	$1.9x10^8$	$9.0x10^{10}$	$4.3x10^{10}$	$4.8x10^{10}$	$3.0 x 10^{10}$	$1.4 x 10^6$	$8.5 x 10^5$	$1.8 x 10^{11}$	$1.0x10^{11}$
20	217	$4.2x10^8$	$2.1x10^8$	$2.1x10^8$	$1.9x10^8$	$9.0x10^{10}$	$4.3x10^{10}$	$4.8x10^{10}$	$3.0 x 10^{10}$	$1.4 x 10^6$	$8.5 x 10^5$	$1.8 x 10^{11}$	$1.0x10^{11}$
25	222	$1.7x10^8$	$8.6x10^7$	$8.3x10^7$	$8.0x10^7$	$3.2x10^{10}$	$1.6x10^{10}$	$1.7x10^{10}$	$1.1 x 10^{10}$	$6.5 x 10^5$	$4.0 x 10^5$	$6.3 x 10^{10}$	$3.6x10^{10}$
30	227	$7.2x10^7$	$3.7x10^7$	$3.5x10^7$	$3.4x10^7$	$1.2x10^{10}$	$5.9x10^9$	$6.6x10^9$	$4.2 x 10^9$	$3.1 x 10^5$	$1.9 x 10^5$	$2.3 x 10^{10}$	$1.3x10^{10}$
35	237	$1.4x10^7$	$7.5x10^6$	$7.0x10^6$	$7.0x10^6$	$1.9x10^9$	$9.7x10^8$	$1.1x10^9$	$6.9 x 10^8$	$7.6 x 10^4$	$4.9 x 10^4$	$3.6 x 10^9$	$2.1x10^9$
40	250	$2.1x10^6$	$1.2x10^6$	$1.1x10^6$	$1.1x10^6$	$2.2x10^8$	$1.2x10^8$	$1.3x10^8$	$8.4 x 10^7$	$1.5 x 10^4$	$9.7 x 10^3$	$4.0 x 10^8$	$2.4x10^8$
45	264	$3.3x10^5$	$1.9x10^5$	$1.7x10^5$	$1.8x10^5$	$2.7x10^7$	$1.5x10^7$	$1.6x10^7$	$1.1x10^7$	$3.0x10^3$	$2.1x10^3$	$4.7x10^7$	$3.0x10^7$
50	271	$1.4x10^5$	$8.2x10^4$	$7.2x10^4$	$7.7x10^4$	$1.0x10^7$	$5.7x10^6$	$6.1x10^6$	$4.2x10^6$	$1.4x10^3$	$1.0x10^2$	$1.8x10^7$	$1.1x10^7$

(a) Values in the table were obtained using energies determined at the CCSD(T) level of theory at either the M06-2X/6-311++G(3df,3pd) or MP2/6-311++G(3df,3pd) geometries. Rotational constants and vibrational frequencies were obtained from the M06-2X or MP2 calculations with vibrational frequencies multiplied by 0.97 to obtain improved zero-point energies.
(b) "*s-cis*" refers to the formation of the *s-cis* anhydride from the *s-trans* acid. "*s-trans*" refers to the formation of the *s-trans* anhydride from the *s-cis* acid. See text for discussion.

Table 4.6 Calculated Equilibrium Constants for the Formation of SO_3–H_2O and SO_3–$(H_2O)_2$[a]

Altitude [km]	T [K]	$SO_3 + H_2O \rightarrow SO_3$–$H_2O$		SO_3–$H_2O + H_2O \rightarrow SO_3$–$(H_2O)_2$	
		M06-2X	MP2	M06-2X	MP2
0	288	1.8	3.1	7.5	2.5
5	256	1.0×10^1	1.8×10^1	9.1×10^1	2.6×10^1
10	223	1.1×10^2	1.9×10^2	2.5×10^3	5.6×10^2
15	217	1.7×10^2	3.2×10^2	5.2×10^3	1.1×10^3
20	217	1.7×10^2	3.2×10^2	5.2×10^3	1.1×10^3
25	222	1.2×10^2	2.1×10^2	2.8×10^3	6.2×10^2
30	227	7.7×10^1	1.4×10^2	1.6×10^3	3.7×10^2
35	237	3.6×10^1	6.5×10^1	5.5×10^2	1.4×10^2
40	250	1.5×10^1	2.7×10^1	1.6×10^2	4.2×10^1
45	264	6.5	1.1×10^1	4.6×10^1	1.4×10^1
50	271	4.4	7.5	2.6×10^1	8.1

(a) Values in the table were obtained using energies determined at the CCSD(T) level of theory at either the M06-2X/6-311++G(3df,3pd) or MP2/6-311++G(3df,3pd) geometries. Rotational constants and vibrational frequencies were obtained from the M06-2X or MP2 calculations, with vibrational frequencies multiplied by 0.97 to obtain improved zero-point energies.

Table 4.7 Computed Thermodynamic Data for the Formation of Carboxylic Sulfuric Anhydrides, SO_3–H_2O, and SO_3–$(H_2O)_2$ [a]

	***ΔH* (kcal/mol)**				***ΔS* (J mol^{-1} K^{-1})**			
	M06-2X		MP2		M06-2X		MP2	
RCOOH + SO_3 → RCOOSO_2OH	217 K	288 K	217 K	288 K	217 K	288 K	217 K	288 K
R = H–	–17.3	–17.2	–17.0	–16.9	–169	–167	–168	–167
R = HCC–	–17.3	–17.2	–17.0	–16.9	–174	–172	–169	–167
R = CH_2–CH– (*s-cis*)[b]	–19.7	–19.6	–19.4	–19.2	–170	–168	–170	–168
R = CH_2–CH– (*s-trans*)[c]	–19.5	–19.4	–19.2	–19.1	–171	–169	–170	–168
R = CF_3–	–15.0	–14.9	–14.6	–14.5	–171	–169	–169	–167
R = C_6H_5–	–20.0	–19.9	–19.7	–19.6	–170	–169	–169	–168
SO_3 + H_2O → SO_3–H_2O	–8.0	–7.9	–8.2	–8.1	–111	–110	–110	–108
SO_3–H_2O + H_2O → SO_3–$(H_2O)_2$	–11.4	–11.5	–10.6	–10.6	–148	–150	–146	–147

(a) Values in the table were obtained using energies determined at the CCSD(T) level of theory at either the M06-2X/6-311++G(3df,3pd) or MP2/6-311++G(3df,3pd) geometries. Rotational constants and vibrational frequencies were obtained from the M06-2X or MP2 calculations. Frequencies were scaled by a factor of 0.97.
(b) Refers to the formation of *s-cis* acrylic sulfuric anhydride from *s-trans* acrylic acid.
(c) Refers to the formation of *s-trans* acrylic sulfuric anhydride from *s-cis* acrylic acid.

Discussion

It may be seen from Table 4.5 that, at the surface of the Earth (288K), the equilibrium constants for anhydride formation are in the 10^2 to 10^6 atm^{-1} range, depending on the parent acid. Since the reaction is exothermic, the equilibrium constants increase as the temperature decreases, reaching maximum values in the 10^6 to 10^{11} range at a temperature corresponding to an altitude of 15-20 km. The CF_3 derivative consistently defines the low end of the range, with most of the hydrocarbon derivatives significantly higher. The results

based on MP2 energies, geometries, and vibrational frequencies are systematically smaller than those using the M06-2X results, but the differences do not alter the overall picture. The calculated values of K_p as a function of altitude are presented graphically for the formic and benzoic acid derivatives in Figure 4.5.

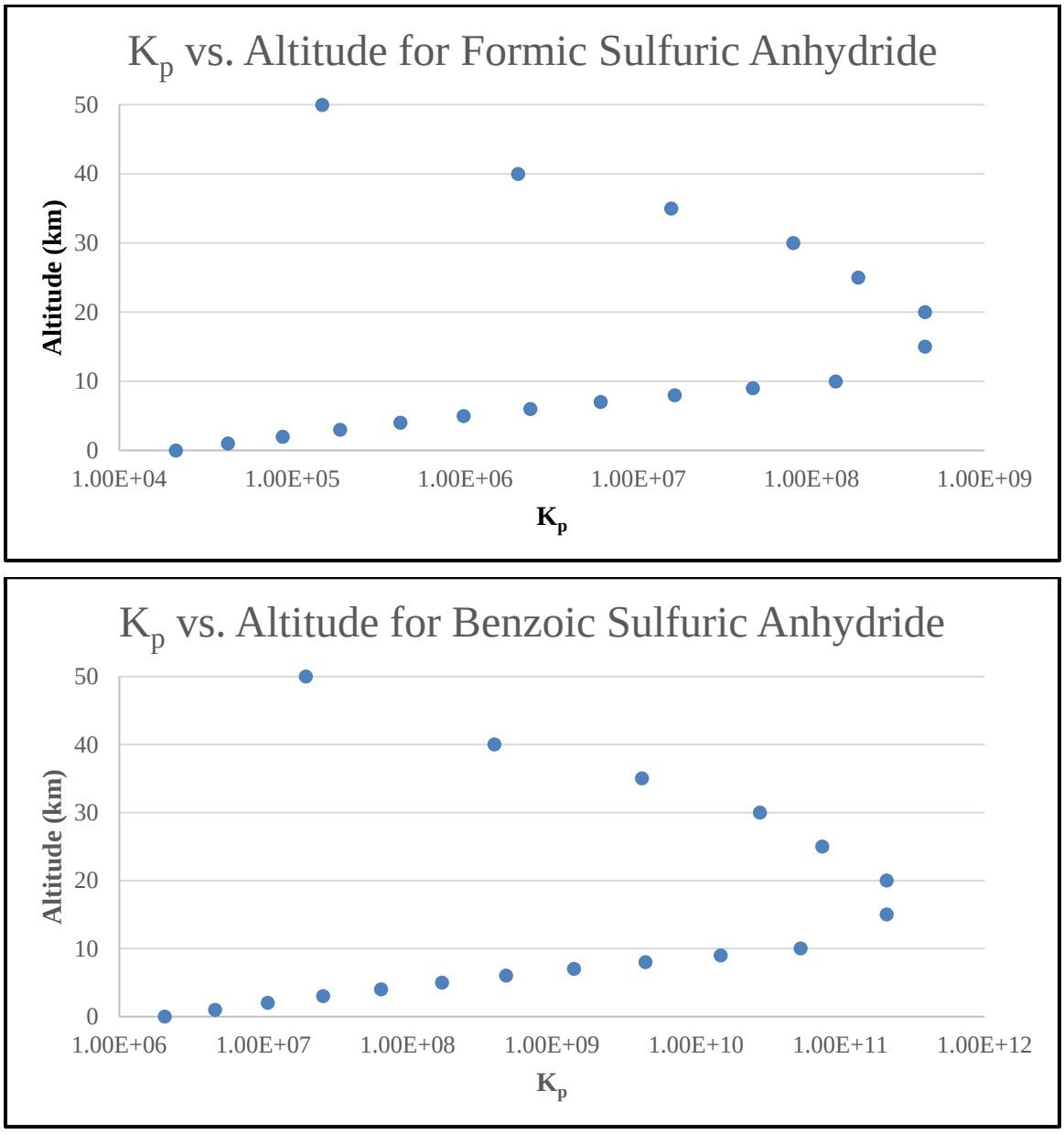

Figure 4.5 Calculated Values of K_p vs. Altitude for Formic and Benzoic Sulfuric Anhydrides.

The equilibrium constants are large at all altitudes considered, indicating that reaction (4.1) is thermodynamically favorable. However, the concentrations of SO_3 and carboxylic acids are low in the atmosphere and it is not immediately obvious that the large K_p values imply atmospherically significant concentrations of the anhydrides. Moreover, there is no guarantee that, in a kinetically dynamic system, steady state concentrations will equal equilibrium concentrations. Indeed, a full accounting of the possible role of carboxylic sulfuric anhydrides in the atmosphere will also require the determination of rate constants, which is beyond the scope of this work. Nevertheless, it is of some interest to estimate the implications of the calculated equilibrium constants for concentrations in a hypothetical equilibrium state.

Carboxylic acids are abundant trace gases in the atmosphere and appear to play a role in aerosol nucleation through their interactions with other species such as sulfuric acid,[139,140] amines,[169] and oxidized organics.[161,162] Many reports place mixing ratios for formic and acetic acids at a few parts per billion by volume (ppbv), but concentrations vary with location, altitude, and time of measurement. Chebbi and Carlier,[186] for example, summarize the results of over twenty measured formic acid concentrations prior to 1996 with results ranging from as low as 0.03 ppbv to as high as 40 ppbv. A similar compilation by Khare et al. in 1999 gives formic and acetic acid concentrations as low as 0.03 and 0.05 ppbv, respectively, in marine sites and as high as 19.8 and 17.8 ppbv, respectively, in urban sites.[187] Montero, et al. report formic and acetic acid concentrations as high as 19.0 and 10.6 ppbv, respectively.[188] Many other carboxylic acids have been observed, albeit at generally lower mixing ratios.[132,189,190] For SO_3, far fewer estimates of atmospheric abundance are available. One report estimates 10^5 molecules/cm^3 at an altitude of 30 km,[116] but only 0.1 molecules/cm^3 at 0 km. A negligible concentration of 0.2 molecules/cm^3 in the troposphere is also estimated by Lovejoy, et al.[117] Concentrations may be much higher, however, in sulfur-rich regions such as those arising from aircraft exhaust[191] and those near volcanic activity.[192] Overall, it appears that there are little or no data that would allow knowledge of both SO_3 and carboxylic acid concentrations in the same region at the same time.

Despite the above uncertainties, a few rough estimates of the implications of the K_p values in Table 4.5 can be made for a systems near the equilibrium state. Using the 10^5 molecules/cm^3 value of the SO_3 concentration at 30 km (where the temperature is 227 K) and a nominal formic acid concentration of 10 ppbv, the M06-2X value of K_p in Table 4.5 implies a concentration of formic sulfuric anhydride, $HCOOSO_2OH$, of only 900 molecules/cm^3. At 15 km, where K_p is larger, the value is $5x10^4$ molecules/cm^3, assuming the same SO_3 and HCOOH mixing ratios. Compared with the CSAs listed in Table 4.5, however, the equilibrium constants for the reaction of SO_3 with HCOOH are rather small. Repeating the above calculations for the benzoic acid analog (which represents the high end of the range of CSAs studied) gives equilibrium concentrations of benzoic sulfuric anhydride (BzSA) of 2×10^7, and 3×10^5 molecules/cm^3 at 15, and 30 km, respectively.

The effect of the large uncertainty in the partial pressure of SO_3 can be removed if concentration *ratios* are calculated, rather than absolute concentrations. Since H_2SO_4 is an important aerosol precursor, and since SO_3–H_2O and SO_3–$(H_2O)_2$ are key precursors to H_2SO_4, it is of some interest to compare their concentrations with that of a typical carboxylic sulfuric anhydride. From reactions (4.1), (4.4), and (4.5) we have

$$\frac{P_{RCOOSO_2OH}}{P_{SO_3-H_2O}} = \left(\frac{K_1}{K_4}\right)\frac{P_{RCOOH}}{P_{H_2O}} \tag{4.6}$$

$$\frac{P_{RCOOSO_2OH}}{P_{SO_3-(H_2O)_2}} = \left(\frac{K_1}{K_4K_5}\right)\frac{P_{RCOOH}}{P_{H_2O}^2} \tag{4.7}$$

where K_p is the equilibrium constant for reaction (4.1) with the free monomers as reactants, as calculated in the previous section. Again, using formic acid as an example, assuming a 10 ppbv concentration and water mixing ratios of 1.4×10^{-2}, 2.9×10^{-6}, and 4.4×10^{-6} at 0 km, 15 km, and 30 km, respectively,[185] the ratio of $P_{HCOOSO_2OH}/P_{SO_3-H_2O}$ is $8x10^{-3}$, $8x10^3$, and $2x10^3$ at these altitudes. The ratios are favored at increasing altitude by both the increase in equilibrium constant (up to 15 km) and the decreasing water vapor

concentration. This means that, assuming the monomer concentrations are correct, the equilibrium partial pressure of the formic sulfuric anhydride may exceed that of SO_3–H_2O by factors as high as several thousand. Similarly, if we compare the pressures of $HCOOSO_2OH$ and SO_3–$(H_2O)_2$, we obtain values of $\frac{P_{HCOOSO_2OH}}{P_{SO_3-(H_2O)_2}}$ equal to $8x10^{-2}$, $5x10^6$, and $2x10^7$ at 0, 15, and 30 km, respectively, indicating a large excess of $HCOOSO_2OH$ over SO_3–$(H_2O)_2$ at 15 and 30 km. These results are summarized in Table 4.8. For the benzoic acid analog, the ratios of BSA to SO_3–H_2O are 0.8, $4x10^6$, and $7x10^5$ and the ratios of BSA to SO_3–$(H_2O)_2$ are $7x10^0$, $2x10^9$, and $8x10^9$ at these same altitudes. These results are also included in Table 4.8. Even if benzoic acid concentrations are three orders of magnitude smaller than the 10 ppbv assumed here, the ratio of the anhydride concentration to the SO_3–$(H_2O)_2$ concentration is quite large.

Table 4.8 Calculated Concentrations and Concentration Ratios at an Equilibrium State[a]

Altitude [km]	Temperature [K]	[RCOOSO$_2$OH] [molecules/cm^3]		$\frac{P_{RCOOSO_2OH}}{P_{SO_3-H_2O}}$		$\frac{P_{RCOOSO_2OH}}{P_{SO_3-(H_2O)_2}}$	
		R = H	R = C_6H_5	R = H	R = C_6H_5	R = H	R = C_6H_5
0	288	$2x10^1$	$2x10^3$	$8x10^{-3}$	$8x10^{-1}$	$8x10^{-2}$	$7x10^0$
15	217	$5x10^4$	$2x10^7$	$8x10^3$	$4x10^6$	$5x10^6$	$2x10^9$
30	227	$9x10^2$	$3x10^5$	$2x10^3$	$7x10^5$	$2x10^7$	$8x10^9$

(a) Values are based on M06-2X/6-311++G(3df,3pd) equilibrium constants from Tables 4.5 and 4.6, assuming a 10 ppbv concentration of the parent carboxylic acid and an SO_3 concentration of 10^5 molecules/cm^3. Water concentrations are taken from Reference 185.

Sulfuric acid has long been recognized for its role in initiating homogeneous aerosol nucleation in the atmosphere[160-162] and concentrations as low as 10^6 - 10^7 molecules/cm^3 appear to be atmospherically significant from the point of view of initiating new particle formation.[162,193-195] While the concentrations of carboxylic sulfuric anhydrides given in Table 4.8 are, in most cases, are not quite in this range, some are close enough that their

role could be important if the volatility of their complexes is especially low. Recent calculations have indicated that this may indeed be the case.[158] Moreover, even modest increases in the SO_3 and carboxylic acid concentrations over those used in the above calculations could bring anhydride concentrations into or above the 10^6 - 10^7 molecule/cm^3 range, making them potentially able to seed new particle formation. Such could be the case in select locations, e.g., jet plumes or polluted environments. Another possible role of these anhydrides involves a scenario in which their formation temporarily reduces the volatility of small organic acids, allowing them to be incorporated into pre-existing droplets prior to their regeneration via hydrolysis. Of course, both of these roles are speculative at this point. It is clear that more information about SO_3 and carboxylic acid concentrations is needed, as are reliable estimates of reaction rate constants pertinent to establishing steady-state rather than equilibrium concentrations.

Conclusion

Sulfur trioxide reacts readily with carboxylic acids in the gas phase to produce carboxylic sulfuric anhydrides. New microwave spectra have been presented on the reaction product formed from propiolic acid and SO_3 in a supersonic jet, and supporting calculations indicate that the zero-point corrected overall formation energy for the corresponding anhydride at the CCSD(T)/CBS(D-T)//M06-2X/6-311++G(3df,3pd) level is −16.7 kcal/mol. CCSD(T) calculations, with zero-point vibrational corrections obtained from M06-2X/6-311++G(3df,3pd) frequencies, indicate that the activation energy relative to a putative SO_3–HCCCOOH complex is essentially zero. These results are consistent with the observation that the anhydride is rapidly formed during the early, collisional stages of the supersonic expansion, and are similar to those previously obtained for related systems. A series of structural and energetic comparisons has been made among a set of anhydrides derived from a representative set of carboxylic acids, and statistical thermodynamic calculations have been used to compute equilibrium constants for their formation. The thermodynamic results provide additional confirmation that the formation of these carboxylic sulfuric anhydrides is a favorable process. The calculated vibrational frequencies used in these calculations are provided as Supporting Information, and should

aid in the observation infrared and/or Raman spectra. Carboxylic sulfuric anhydrides appear to be largely uncharacterized in the literature and thus, these results offer an interesting new addition to the chemistry of sulfur oxides and oxyacids.

Because SO_3 is the primary precursor to sulfuric acid in the atmosphere, carboxylic sulfuric anhydrides may have implications for atmospheric chemistry. The calculated equilibrium constants for their formation are large, ranging from ~10^4 atm^{-1} for the HCOOH system at 0 km (288K) to over 10^{11} atm^{-1} for the benzoic acid system at an altitude of 15 km (217 K). The concentrations of reacting species are small, but using rough estimates of the atmospheric concentrations of SO_3 and carboxylic acids, equilibrium concentrations of the carboxylic sulfuric anhydrides are in the range from $2x10^1$ to $2x10^7$ molecules/cm^3, depending on altitude and parent acid of the anhydride. The high end of this range overlaps the range of number densities of H_2SO_4 that appear to be relevant to aerosol nucleation in the atmosphere. In most cases, the calculated concentrations are highest near 15 – 20 km where the temperature in the atmosphere is lowest, but this will depend, also, on the altitude dependence of the concentrations of RCOOH and SO_3. Calculated equilibrium concentrations of carboxylic sulfuric anhydrides at some altitudes exceed those of the sulfuric acid precursors SO_3–H_2O and SO_3–$(H_2O)_2$ by several orders of magnitude. These results suggest that carboxylic sulfuric anhydrides could also participate in atmospheric processes, especially in polluted environments or during episodes of high RCOOH or SO_3 concentrations. However, significant uncertainties in the atmospheric concentrations of the reacting species require further investigation, and kinetic modeling is ultimately needed to assess the effects of competition with other viable processes.

Acknowledgments

This work was supported by the National Science Foundation (Grant Nos. CHE–1266320 and CHE 1563324) and the Minnesota Supercomputing Institute. A.K.H. was supported by a Lester C. and Joan M. Krogh Fellowship, administered through the University of Minnesota. We are grateful to Professor Chris Hogan for a helpful correspondence.

References

1. T. Haber, U. Schmitt, M. A. Suhm,, *Phys. Chem. Chem. Phys.*, **1**, 5573, (1999).

2. A. Campargue, L. Biennier, A. Kachanov, R. Jost, B. Bussery-Honvault, V. Veyret, S. Churassy, R. Bacis, *Chem. Phys. Lett.*, **288**, 734, (1998).

3. M. Kulmala, T. Petäjä, M. Ehn, J. Thornton, M. Sipilä, D. R. Worsnop, V. M. Kerminen, *Annu. Rev. Phys. Chem.*, **65**, 21, (2014).

4. S. M. Casey, D. G. Leopold, *Chem. Phys. Lett.*, **201**, 205, (1993).

5. S. R. Miller, T. P. Marcy, E. L. Millam, D. G. Leopold, *J. Am. Chem. Soc.*, **129**, 3482, (2007).

6. S. W. Reeve, W. A. Burns, F. J. Lovas, R. D. Suenram, K. R. Leopold, *J. Phys. Chem.*, **97**, 10630, (1993).

7. Y. Xu, J. Van Wijngaarden, W. Jager, *Int. Rev. Phys. Chem.*, **24**, 301, (2005).

8. Y. Kawashima, A. Sato, Y. Orita, *J. Phys. Chem. A*, **116**, 1224, (2012).

9. K. R. Leopold, *Annu. Rev. Phys. Chem.*, **62**, 327, (2011).

10. W. Gordy, R. L. Cook, *Microwave Molecular Spectra*, 3rd edition, (John Wiley & Son: New York) 1984.

11. Y. Kawashima, H. Takeo, C. Matsumura, *Chem. Phys. Lett.*, **57**, 145-147, (1978).

12. C. M. Western, P. R. R. Langridge-Smith, B. J. Howard, S. E. Novick, *Mol. Phys.*, **44**, 145, (1981).

13. T. J. Balle, W. H. Flygare, *Rev. Sci. Instrum.*, **52**, 33, (1981).

14. G. G. Brown, B. C. Dian, K. O. Douglas, S. M. Geyer, S. T. Shipman, B. H. Bate, *Rev. Sci. Instrum.*, **79**, 053103, (2008).

15. C. T. Dewberry, R. B. Mackenzie, S. Green, K. R. Leopold, *Rev. Sci. Instrum.*, **86**, 065107, (2015).

16. E. G. Robertson, J. P. Simons, *Phys. Chem. Chem. Phys.*, **3**, 1, (2001).

17. G. G. Hammes, S. J. Benkovic, S. Hammes-Schiffer, *Biochemistry*, **50**, 10422, (2011).

18. L. Ferres, W. Stahl, and H. V. L Nguyen, *J. Chem. Phys*., **148**, 124304, (2018).

19. K. Eibl, W. Stahl, I. Kliener, and H. V. L. Nguyen, *J. Chem. Phys.*, **149**, 144306, (2018).

20. R. Hakiri, N. Derbel, H. V. L Nguyen, H. Mouhib, *Phys. Chem. Chem. Phys.*, **20**, 25577, (2018).

21. R. B. Mackenzie, C. T. Dewberry, R. D. Cornelius, C. J. Smith, K. R. Leopold, *J. Phys. Chem. A*, **121**, 855, (2017).

22. C. J. Smith, A. Huff, H. Zhang, Y. Mo, K. R. Leopold, *J. Chem. Phys.*, **150**, 134302, (2019).

23. M. Kulmala, *Science*, **302**, 1000, (2003).

24. F. Yu, R. P. Turco, *J. Geophys. Res*., **106**, 4797, (2001).

25. S.-H. Lee, J. M. Reeves, J. C. Wilson, D. E. Hunton, A. A. Viggiano, T. M. Miller, J. O. Ballenthin, L. R. Rait, *Science*, **301,** 1886, (2003).

26. M. Kulmala, L. Pirjola, J. Mäkelä, *Nature*, **404**, 66, (2000).

27. S. M. Kathmann, G. K. Schenter, B. C. Garrett, *Adv. Quant. Chem.,* **55**, 429, (2008).

28. S. M. Ball, D. R. Hanson, F. L. Eisele, P. H. McMurry, *J. Geophys. Res*., **104**, 23709, (1999).

29. Y. Xu, A. B. Nadykto, F. Yu, J. Herb, W. Wang, *J. Phys. Chem. A*, **114**, 387, (2010).

30. M. K. Hazra, A. Sinha; *J. Am. Chem. Soc.*, **133**, 17444, (2011).

31. R. B. Mackenzie, C. T. Dewberry, K. R. Leopold, *Science*, **349**, 58, (2015).

32. C. J. Smith, Anna, K. Huff, R. B. Mackenzie, Kenneth R. Leopold, *J. Phys. Chem. A*, **121**, 9074, (2017).

33. C. J. Smith, A. K. Huff, R. B. Mackenzie, K. R. Leopold, *J. Phys. Chem. A*, **122**, 4549, (2018).

34. C. J. Smith, A. K. Huff, R. B. Mackenzie, K. R. Leopold, *Thesis: Chapter 4*, (2019).

35. E. B. Wilson, Jr., *Proc. Natl. Acad. Sci. U. S. A.*, **43**, 816, (1957).

36. C. C. Lin, J. D. Swalen, *Rev. Mod. Phys.*, **31**, 841, (1959).

37. H. Hartwig, H. Dreizler, *Z. Naturforsch A Phys. Sci.*, **51**, 923, (1996).
38. P. Groner, *J. Chem. Phys.*, **107**, 4483, (1997).

39. P. Groner, *J. Mol. Spectrosc*., **278**, 52, (2012).

40. I. Kleiner, *J. Mol. Spectrosc*., **260**, 1, (2010).

41. J. T. Hougen, I. Kleiner, M. Godefroid, *J. Mol. Spectrosc.*, **163**, 559, (1994).

42. V. V. Ilyushin, Z. Kisiel, L. Pszczółkowski, H. Mäder, J.T. Hougen, *J. Mol. Spectrosc.*, **259**, 26, (2010).

43. L. H. Spangler, *Annu. Rev. Phys. Chem*., **48**, 481, (1997).

44. L. Goodman, V. Pophristic, F. Weinhold, *Acc. Chem. Res.*, **32**, 983, (1999).

45. T. Kundu, B. Pradhan, B. P. Singh, *Proc. Indian Acad. Sci. (Chem. Sci.),* **114**, 623, (2002).

46. S. Liu, N. Govind, L. G. Pedersen, *J. Chem. Phys*., **129**, 094104, (2008).

47. S. Liu, N. Govind, *J. Phys. Chem. A*, **112**, 6690, (2008).

48. Y. Mo, J. Gao, *Acc. Chem. Res.*, **40**, 113, (2007).

49. T. Naito, O. Ohashi, I. Yamaguchi, *J. Mol. Spectrosc.*, **68,** 32, (1977).

50. H. S. Randhawa, W. Walter, C. O. Meese, *J. Mol. Struct*., **37**, 187, (1977).

51. R. M. Romano, C.O. Della Védova, A. J. Downs, *J. Phys. Chem. A*, **106**, 7235, (2002).

52. W. Gordy, *J. Chem. Phys*., **14**, 560, (1946).

53. E. A. Noe, *J. Am. Chem. Soc*., **99**, 2803, (1977).

54. J. A. Phillips, M. Canagaratna, H. Goodfriend, A. Grushow, J. Almlöf, K. R. Leopold, *J. Am. Chem. Soc.*, **117,** 12549, (1995).

55. G. M. Plummer, E. Herbst, F. C. De Lucia, *Ap. J.*, **318**, 873, (1987).

56. J. C. Pearson, K. V. L. Sastry, M. Winnewisser, E. Herbst, F. C. De Lucia, *J. Phys. Chem. Ref. Data*, **24**, 1, (1995).

57. R. C. Woods, *J. Mol. Spectrosc.*, **21,** 4, (1966).

58. R.C. Woods, *J. Mol. Spectrosc*., **22**, 49, (1967).
59. J. M. Vacherand, B. P. van Eijck, J. Burie, J. Demaison, *J. Mol. Spectrosc.*, **118**, 355, (1986).

60. D. Jelisavac, D. C. Cortés Gómez, H. V. L. Nguyen, L. W. Sutikdja, W. Stahl, I. Kleiner, *J. Mol. Spectrosc.*, **257**, 111, (2009).

61. H. V. L. Nguyen, H. Mouhib, W. Stahl, I. Kleiner, *Mol. Phys*., **108**, 763, (2010).

62. H. V. L. Nguyen, A. Jabri, V. Van, W. Stahl, *J. Phys. Chem. A*, **118,** 12130, (2014).

63. K. Eibl, R. Kannengießer, W. Stahl, H. V. L. Nguyen, I. Kleiner, *Mol. Phys*., **23**, 3483, (2016).

64. B. Kirtman, *J. Chem. Phys.*, **37,** 2516, (1962).

65. R. M. Lees, J. G. Baker, *J. Chem. Phys.*, **48,** 5299, (1968).

66. E. Herbst, J. K. Messer, F. C. De Lucia, P. Helminger, *J. Mol. Spectrosc.*, **108,** 42, (1984).

67. H. V. L. Nguyen, W. Stahl, I. Kleiner, *Mol. Phys.*, **110,** 2035, (2012).

68. V. Ilyushin, E. Alekseev, J. Demaison, I. Kleiner, *J. Mol. Spectrosc.*, **240**, 127, (2006.)

69. A "global" fit of our data for the parent *syn* conformer, together with the frequencies from reference 51 was also performed. The rms residual from this fit was somewhat larger (143 kHz) and likely arises from the inclusion of a few higher J transitions, and the lower resolution of the previous work. The *V3* value obtained was 76.289(29) cm−1, in good agreement with the values in Tables 1.1, 1.2.A, 1.2.B, and 1.3. Frequencies and residuals from that fit are included in Appendix A.

70. P. W. Payne, L. C. Allen, *Modern Theoretical Chemistry*, edited by H. F. Schaefer, III, (Plenum Press: New York 1977), Vol. 4, p. 29.

71. K. B. Wiberg, *Encyclopedia of Computational Chemistry*, edited by P. v. R. Schleyer (John Wiley & Sons: Berlin 1998), p. 2518.

72. P. R. Schreiner, *Angew. Chem. Int. Ed.,* **41**, 3579, (2002)**.**

73. N. D.Epiotis, W. R. Cherry, S. Shaik, R. L.Yates, F. Bernardi, *Topics in Current Chemistry: Structural Theory of Organic Chemistry*., Vol. 70, (1977).

74. T. K. Brunck, F. Weinhold, *J. Am. Chem. Soc.,* **101**, 1700, (1979).

75. J. K. Badenhoop, F. Weinhold, *Int. J. Quantum Chem.,* **72**, 269, (1999).
76. V. Pophristic, L. Goodman, *Nature,* **411**, 565, (2001).

77. F. Weinhold, *Angew. Chem. Int. Ed.,* **42**, 4188, (2003).

78. F. M. Bickelhaupt, E. J. Baerends, *Angew. Chem. Int. Ed.,* **42**, 4183, (2003).

79. Y. Mo, W. Wu, L. Song, M. Lin, Q. Zhang, J. Gao, *Angew. Chem. Int. Ed.,* **43**, 1986, (2004).

80. Y. Mo, *Nat. Chem.,* **2**, 666, (2010).

81. Y. Mo, S. D. Peyerimhoff, *J. Chem. Phys.,* **109**, 1687, (1998).

82. Y. Mo, L. Song, Y. Lin, *J. Phys. Chem. A,* **111**, 8291, (2007).

83. Y. Mo, *The Chemical Bond: Fundamental Aspects of Chemical Bonding*, G. Frenking, S. Shaik, Eds. (Wiley-VCH, 2014), pp 199.

84. D. L. Cooper, *Valence Bond Theory*., (Elsevier: Amsterdam, 2002.)

85. S. S. Shaik, P. C. Hiberty, *A Chemist's Guide to Valence Bond Theory*., Wiley-Interscience: New York, **2007**.

86. W. Wu, P. Su, S. Shaik, P. C. Hiberty, *Chem. Rev.,* **111**, 7557, (2011).

87. L. Song, Z. Chen, F. Ying, L. Song, X. Chen, P. Su, Y. Mo, Q. Zhang, W. Wu, XMVB 2.1: An ab initio Non-orthogonal Valence Bond Program, Xiamen University: Xiamen 361005, China, (2015).

88. M. J. Frisch, G. W. Trucks, H. B. Schlegel, G. E. Scuseria, M. A. Robb, J. R. Cheeseman, G. Scalmani, V. Barone, B. Mennucci, G. A. Petersson, H. Nakatsuji, M. Caricato, X. Li, H. P. Hratchian, A. F. Izmaylov, J. Bloino, G. Zheng, J. L. Sonnenberg, M. Hada, M. Ehara, K. Toyota, R. Fukuda, J. Hasegawa, M. Ishida, T. Nakajima, Y. Honda, O. Kitao, H. Nakai, T. Vreven, J. A. Montgomery Jr., J. E. Peralta, F. Ogliaro, M. Bearpark, J. J. Heyd, E. Brothers, K. N. Kudin, V. N. Staroverov, R. Kobayashi, J. Normand, K. Raghavachari, A. Rendell, J. C. Burant,

S. S. Iyengar, J. Tomasi, M. Cossi, N. Rega, J. M. Millam, M. Klene, J. E. Knox, J. B. Cross, V. Bakken, C. Adamo, J. Jaramillo, R. Gomperts, R. E. Stratmann, O. Yazyev, A. J. Austin, R. Cammi, C. Pomelli, J. W. Ochterski, R. L. Martin, K. Morokuma, V. G. Zakrzewski, G. A. Voth, P. Salvador, J. J. Dannenberg, S. Dapprich, A. D. Daniels, Ö. Farkas, J. B. Foresman, J. V. Ortiz, J. Cioslowski, D. J. Fox, Gaussian 09, Revision E.01, Gaussian Inc., Wallingford, CT, (2009).

89. N. Kuze, A. Ishikawa, M. Kono, T. Kobayashi, N. Fuchisawa, T. Tsuji, H. Takeuchi, *J. Phys. Chem. A*, **119**, 1774, (2015).

90. W. Caminati, F. Scappini, G. Corbelli, *J. Mol. Spectrosc*., **75**, 327, (1979).

91. B. P. van Eijck, J. van Opheusden, M. M. M. van Schaik, E. van Zoeren, *J. Mol. Spectrosc*., **86**, 465, (1981).

92. V. V. Ilyushin, E. A. Alekseev, S. F. Dyubko, S. V. Podnos, I. Kleiner, L. Margulès, G. Wlodarczak, J. Demaison, J. Cosléou, B. Maté, E.N. Karyakin, G. Yu. Golubiatnikov, G. T. Fraser, R. D. Suenram, J. T. Hougen, *J. Mol. Spectrosc*., **205**, 286, (2001).

93. V. V. Ilyushin, E. A. Alekseev, S. F. Dyubka, I. Kleiner, *J. Mol. Spectrosc*., **220**, 170, (2003).

94. J. L. Derissen, *J. Mol. Struct*., **7**, 67, (1971).

95. S. J. Atkinson, R. Noble-Eddy, S. L. Masters, *J. Phys. Chem. A*, **120**, 2041, (2016).

96. E. M. S. Maçôas, L. Khriachtchev, M. Pettersson, R. Fausto, M. Räsänen, *J. Am. Chem. Soc.*, **125**, 16188, (2003).

97. S. Lopes, A. V. Domanskaya, R. Fausto, M. Räsänen, L. Khriachtchev, *J. Chem. Phys*., **133**, 144507, (2010).

98. E. M. S. Maçôas, L. Kriachtchev, R. Fausto, M. Räsänen, *J. Phys. Chem. A*, **108**, 3380, (2004).

99.. M. L. Senent, *Mol. Phys.*, **99,** 1311, (2001).

100. C. E. Kolb, D. R. Worsnop, *Annu. Rev. Phys. Chem*., **63**, 471, (2012).

101. W. Gong, C. Stroud, L. Zhang, *Atmosphere,* **2**, 567, (2011).

102. D. A. Hegg, M. B. Baker, *Rep. Prog. Phys*., **72**, 056801, (2009).

103. IPCC, 2013: Climate Change 2013: The Physical Science Basis. Contribution of Working Group I to the Fifth Assessment Report of the Intergovernmental Panel on Climate Change, T. F. Stocker, D. D Qin, G.-K. Plattner, M. Tignor, S. K. Allen, J. Boschung, A. Nauels, Y. Xia, V. Bex, P. M. Midgley, Editors, Cambridge University Press, Cambridge, United Kingdom and New York, NY, USA, pp. 1535 doi:10.1017/CBO9781107415324.

104. R. J. Weber, P. H. McMurry, L. Mauldin, D. J. Tanner, F. L. Eisele, F. J. Brechtel, S. M. Kreidenweis, G. L. Kok, R. D. Schillawski, D. Baumgardner, *J. Geophys. Res.*, **103**, 16385, (1998).

105. R. Zhang, A. Khalizov, L. Wang, M. Hu, W. Xu, *Chem. Rev.*, **112**, 1957, (2012).
106. M. Chen, M. Titcombe, J. Jiang, C. Jen, C. Kuang, M. L. Fischer, F. L. Eisele, J. I. Siepmann, D. R. Hanson, J. Zhao, P. H. McMurry, *Proc. Nat. Acad. Sci. U.S.A.*, **109**, 18713, (2012).

107. T. Yli-Juuti, K. Barsanti, L. H. Ruiz, A.-J. Kieloaho, U. Makkonen, T. Petäjä, T. Ruuskanen, M. Kulmala, I. Riipinen, *Atmos. Chem. Phys.*, **13**, 12507, (2013).

108. P. Paasonen, T. Nieminen, E. Asmi, H. E. Manninen, T. Petäjä, C. Plass-Dülmer, H. Flentije, W. Birmili, A. Wiedensohler, U. Hõrrak, et al., *Atmos. Chem. Phys*., **10**, 11223, (2010).

109. N. M. Donahue, I. K. Ortega, W. Chuang, I. Riipinen, F. Riccobono, S. Schobesberger, J. Dommen, U. Baltensperger, M. Kulmala, D. R. Worsnop, *Faraday Discuss*., **165**, 91, (2013).

110. R. Hofmann-Sievert, A. W. Castleman, Jr., *J. Phys. Chem*., **88**, 3329, (1984).

111. P. M. Holland, A. W. Castleman, Jr., *Chem. Phys. Lett.*, **56**, 511, (1978).

112. T. S. Chen, P. L. Moore Plummer, *J. Phys. Chem.*, **89**, 3689, (1985).

113. M. Hofmann, P. v. R. Schleyer, *J. Am. Chem. Soc.*, **116**, 4947, (1994).

114. K. Morokuma, C. Muguruma, *J. Am. Chem. Soc.*, **116**, 10316, (1994).

115. C. E. Kolb, J. T. Jayne, D. R. Worsnop, M. J. Molina, R. F. Meads, A. A. Viggiano, *J. Am. Chem. Soc*., **116**, 10314, (1994).

116. J. T. Jayne, U. Pöschl, Y.-M. Chen, D. Dai, L. T. Molina, D. R. Worsnop, C. E. Kolb, M. J. Molina, *J. Phys. Chem. A*, **101**, 10000, (1997).

117. E. R. Lovejoy, D. R. Hanson, L. G. Huey, *J. Phys. Chem*., **100**, 19911, (1996).

118. M. Torrent-Sucarrat, J. S. Francisco, J. M. Anglada, *J. Am. Chem. Soc.*, **134**, 20632, (2012).

119. J. Gonzalez, M. Torrent-Sucarrat, J. M. Anglada, *Phys.Chem.Chem.Phys*., **12**, 2116, (2010).

120. B. Long, Z.-W. Long, Y.-B. Wang, X.-F. Tan, Y.-H. Han, C.-Y. Long, S.-J. Qin, W.-J. Zhang, *Chem.Phys.Chem.*, **13**, 323, (2012).

121. T. Loerting, K. R. Liedl, *Proc. Nat. Acad. Sci. U.S.A.*, **97**, 8874, (2000).

122. A. K. Huff, R. B. Mackenzie, C. J. Smith, K. R. Leopold, *J. Phys. Chem.*, **121**, 5659, (2017).

123. G. P. Moss, *Pure and Appl. Chem*., **68**, 2193, (1996).

124. K. Bolton, D. G. Lister, J. Sheridan, *J. Chem. Soc., Faraday Trans. 2*, **70**, 113, (1974).

125. A. Kulbida, M. N. Ramos, M. Rasanen, J. Nieminen, O. Schrems, R. Fausto, *J. Chem.* Soc. *Faraday Trans.*, **91**, 1571, (1995).

126. R. J. Loncharich, T. R. Schwartz, K. N. Houk, *J. Am. Chem. Soc.*, **109**, 14, (1987).

127. W.-H. Fang, *Chem. Phys. Lett*., **325**, 683, (2000).

128.https://iaspub.epa.gov/triexplorer/release_fac?p_view=USFA&trilib=TRIQ1&sort=_VIEW_&sort_fmt=1&state=All+states&county=All+counties&zipcode=&epa_region=&chemical=000079107&industry=ALL&YEAR=2015&tab_rpt=1&FLD=RELLBY&FLD=TSFDSP

129. See also http://www.toxipedia.org/display/toxipedia/Acrylic+Acid.

130. M. A. Teruel, M. B. Blanco, G. R. Luque, *Atmos. Environ.*, **41**, 5769, (2007).

131. P. R. Veres, J. M. Roberts, A. K. Cochran, J. B. Gilman, W. C. Kuster, J. S. Holloway, M. Graus, J. Flynn, B. Lefer, C. Warneke, J. de Gouw, *Geophys. Res. Lett*., **38**, L17807, (2011).

132. M. Vaïtilingom, T. Charbouillot, L. Deguillaume, R. Maisonobe, M. Parazols, P. Amato, M. Sancelme, A.-M. Delort, *Atmos. Chem. Phys*., **11**, 8721, (2011).

133. H. A. Khwaja, *Atmos. Environ*., **29**, 127, (1995).

134. B. J. Finlayson-Pitts, J. N. Pitts, Jr., *Chemistry of the Upper and Lower Atmosphere, Theory Experiments, and Applications*. Academic Press: San Diego **2000**, and references therein.

135. M. Canagaratna, J. A. Phillips, H. Goodfriend, K. R. Leopold, *J. Am. Chem. Soc*., **118**, 5290, (1996).

136. H. M. Pickett, *J. Mol. Spectrosc*., **148**, 371, (1991).

137. Y. Zhao, D. G. Truhlar, *Theor. Chem. Accts.*, **120**, 215, (2008).

138. F. Neese, E. F. Valeev, *J. Chem. Theory Comput*., **7**, 33, (2011).

139. R. Zhang, I. Suh, J. Zhao, D. Zhang, E. C. Fortner, X. Tie, L. T. Molina, M. J. Molina, *Science*, **304**, 1487, (2004).

140. R. Zhang, L. Wang, A. F. Khalizov, J. Zhao, J. Zheng, R. L. McGraw, L. T. Molina, *Proc. Nat. Acad. Sci. U.S.A.*, **106**, 17650, (2009).

141. J. Elm, T. Kurtén, M. Bilde, K. V. Mikkelsen, *J. Phys. Chem. A*, **118**, 7892, (2014).

142. S. R. Souza, P. C. Vasconcellos, L. R. F. Carvalho, *Atmos. Environm*., **33**, 2563, (1999).

143. J. A. Phillips, Ph.D. thesis, University of Minnesota, **1996**.

144. S. W. Hunt, C. S. Brauer, M. B. Craddock, K. J. Higgins, A. M. Nienow, K. R. Leopold, *Chem. Phys*., **305**, 155, (2004).

145. P. R. McCurdy, W. P. Hess, S. S. Xantheas, *J. Phys. Chem. A*, **106**, 7628, (2002).

146. B. Ouyang, B. J. Howard, *Phys.Chem.Chem.Phys*., **11**, 366, (2009).

147. A. Bauder, *Mol. Phys*., **111**, 1999, (2013).

148. N. N. Greenwood, A. Earnshaw, *Chemistry of the Elements*, Pergamon Press: Oxford, **1984**.

149. A. K. Huff, R. B. Mackenzie, C. J. Smith, K. R. Leopold, *J. Phys. Chem. A*, **123**, 2237, (2019).

150. A. J. van Peski, *Rec. Trav. Chim.*, **40**, 103, (1921).

151. J. Russell, A. E. Cameron, *J. Am. Chem. Soc.*, **60**, 1345, (1938).

152. S. J. Benkovic, R. C. Hevey, *J. Am. Chem. Soc.*, **92**, 4971, (1970).

153. E. Montoneri, L. Giuffré, M. Cassago, E. Tempesti, M. Fornaroli, *Can. J. Chem.*, **55**, 355, (1970).

154. E. Montoneri, E. Tempesti, L. Giuffré, A. Castoldi, *J. Chem. Soc. Perkin Trans. 2*, 662, (1980).

155. E. E. Gilbert, *Chem. Rev.*, **62**, 5449, (1962).

156. D. C. Burdick, Process for the Preparation of Isoflavones, World Intellectual Property Organization, International Bureau, International Publication Number WO 02/015881 A1, **2002**.

157. R. C. Paul, K. C. Malhotra, D. Singh, *J. Indian Chem. Soc.,* **46**, 819, (1969).

158. H. Zhang, W. Wang, S. Pi, L. Liu, H. Li, Y. Chen, Y. Zhang, X. Zhang, Z. Li, *Chemosphere*, **212**, 504, (2018).

159. J. Zhong, H. Li, M. Kumar, J. Liu, L. Liu, X. Zhang, X. C. Zheng, J. S. Francisco, *Angew Che. Int. Ed.*, **58**, 8351, (2019).

160. S. L. Sihto, M. Kulmala, V.-M. Kerminen, M. Dal Maso, T. Petäjä, I. Riipinen, H. Korhonen, F. Arnold, R. Janson, M. Boy, A. Laaksonen, K. E. J. Lehtinen, *Atoms. Chem. Phys.*, **6**, 4079, (2006).

161. I. Riipinen, S.-L. Sihto, M. Kulmala, F. Arnold, M. Dal Maso, W. Birmili, K. Saarnio, K. Teinilä, V.-M. Kerminen, A. Laaksonen, K. E. J. Lehtinen, *Atmos. Chem. Phys.*, **7**, 1899, (2007).

162. C. Kuang, P. H. McMurray, A. V. McCormick, F. L. Eisele, *J. Geophys. Res.*, **113**, D 10209-1-9, (2008).

163. P. Veres, J. M. Roberts, I. R. Burling, C. Warneke, J. de Gouw, R. J. Yokelson, *J. Geophys. Res.*, **115**, D 23302-1-15, (2010).

164. K. F. Ho, S. C. Lee, S. S. H. Ho, K. Kawamura, E. Tachibana, Y. Cheng, T. Zhu, *J. Geophys. Res.*, **115**, D 19312-1-14, (2010).

165. K. Kawamura, S. Steinberg, I. R. Kaplan, *Atmos. Environ.*, **34**, 4175, (2000).

166. P. Khare, N. Kumar, K. M Kumari, *Rev. Geophys.*, **37**, 227, (1999).

167. G. Helas, H. Bingemer, M. O. Andreae, *J. Geophys. Res.*, **97**, 6187, (1992).

168. T. Hoffman, R. Bandur, U. Marggraf, M. Linscheid, *J. Geophys. Res.*, **103**, 25569, (1998).

169. P. M. Winkler, J. Orgeta, T. Karl, L. Cappellin, H. R. Friedli, K. Barsanti, P. H. McMurry, J. N. Smith, *Geophys. Res. Lett.*, **39**, L20815-1-6, (2012).

170. W. Xu, R. Zhang, *J. Chem. Phys.*, **139**, 064312-1-11, (2013).

171. J. Elm, N. Myllys, T. Olenius, R. Halonen, T. Kurtén, H. Vehkamäki, *Phys. Chem. Chem. Phys.*, **19**, 4877, (2017).

172. J. A. Phillips, M. Canagratna, H. Goodfriend, K. R. Leopold, *J. Phys. Chem.*, **99**, 501, (1995).

173. F. A. Cotton, G. Wilkinson, *Advanced Inorganic Chemistry. A Comprehensive Text*, 3rd Ed. John Wiley and Sons, New York, **1972**.

174. K. R. Leopold, M. Canagaratna, J. A. Phillips, *Acc. Chem. Res.*, **30**, 57, (1997).

175. K. R. Leopold, Partially Bonded Molecules and Their Transition to the Crystalline State, in *Advances in Molecular Structure Research*; M. Hargittai, I. Hargittai, Eds.; JAI Press: Greenwich, CT, **1996**; Vol. 2, p. 103.

176. J. E. Huheey, *Inorganic Chemistry, Third Edition. Principles of Structure and Reactivity, Harper and Row*: New York (1983).

177. M. S. Silberberg, P. G. Amateis, *Chemistry. The Molecular Nature of Matter and Change*, 8th Ed.: McGraw Hill Education, New York, 2018.

178. D. A. McQuarrie, *Statistical Mechanics*, Harper& Row: New York, 1976.

179. V. Vaida, J. E. Headrick, *J. Phys. Chem. A*, **104**, 5401, (2000).

180. G. Brasseur, S. Solomon, *Aeronomy of the Middle Atmosphere: Chemistry and Physics of the Stratosphere and Mesosphere*, D. Reidel Publishing: Dordrecht, **1986**.

181. E. Kamarchik, A. W. Jasper, *J. Chem. Phys.*, **138**, 194109-1-8, (2013), and references therein.

182. J. Zheng, T. Yu, E. Papajak, I. M. Alecu, S. L. Mielke, D. G. Truhlar, *Phys. Chem. Chem. Phys.*, **13**, 10885, (2011), and references therein.

183. The value of 0.97 was estimated from the following tabulation based on the value reported for the M06-2X level with basis sets similar to those used in this work: S. Kanchanakungwankul, J. L. Bao, J. Zheng, I. M. Alecu, B. J. Lynch, Y. Zhao, D. G. Truhlar, Database of Frequency Scal Factors for Electronic Model Chemistries – Version 4: http://comp.chem.umn.edu/freqscale/190107_Database_of_Freq_Scale_Factors_V4.pdf, 2018.

184. T. Reiner, F. Arnold, *J. Chem. Phys.*, **101**, 7399, (1994).

185. H. Fliegl, A. Glöß, Ó. Wlez, M. Olzmann, W. Klopper, *J. Chem. Phys.*, **125**, 054312-1-7, (2006).

186. R. Zhang, L. Wang, A. F. Khalizov, J. Zhao, J. Zheng, R. L. McGraw, L. T. Molina, *Proc. Nat. Acad. Sci.*, **106**, 17650, (2009).

187. A. Chebbi, P. Carlier, *Atmos. Environ.*, **30**, 4233, (1996).

188. P. Khare, N. Kumar, K. M. Kumari, S. S. Srivastava, *Rev. Geophys.*, **37**, 227, (1999).

189. L. Montero, P. C. Vasconcellos, S. R. Souza, M. A. F. Pires, O. R. Sanchez-Ccoyllo, M. F. Andrade, L. R. F. Carvalho, *Environ. Sci. Technol.*, **35**, 3071, (2001).

190. C. G. Nolte, M. P. Fraser, G. R. Cass, *Environ. Sci. Technol.*, **33**, 540, (1999).

191. R. C. Brown, M. R. Anderson, R. C. Miake-Lye, C. E. Kolb, A. A. Sorokin, Y. Y. Buriko, *Geophys. Lett.*, **23**, 3603, (1996).

192. D. S. Sevenson, C. E. Johnson, W. J. Collins, R. G. Derwent, The Tropospheric Sulphur Cycle and the Role of Volcanic SO_2 in *Volcanic Degassing*, C. Oppenheimer, D. M. Pyle, J. Barclay, Eds. *Geophys. Soc. London*, Special Publication, **2013**, pp. 295.

193. M. Sipilä, T. Berndt, T. Petäjä, D. Brus, J. Vanhanen, F. Stratmann, J. Patokoski, R. L. Mauldin III, A.-P. Hyvärinen, H. Lihavainen, M. Kulmala, *Science*, **327**, 1243, (2010).

194. W. Birmili, A. Wiedensohler, C. Plass-Dülmer, H. Berresheim, *Geophys. Res. Lett.*, **27**, 2205, (2000).

195. R. J. Weber, P. H. McMurry, R. L. Mauldin III, D. J. Tanner, F. L. Eisele, A. D. Clarke, V. N. Kapustin, *Geophys. Res. Lett.*, **26**, 307, (1999).

Appendices

Appendix A: Supplemental Material for Chapter 1

Table A.1. Cartesian coordinates from M06-2X/6-311+G(d,p) calculations of minimum energy structures of *syn*- and *anti*-thioacetic acid

Syn-Thioacetic Acid			
Atom Number	x	y	z
C1	-0.51377	-0.13405	0.001361
O2	-0.99273	-1.22891	-0.0001
C3	-1.30523	1.14994	-0.00021
H4	-2.3657	0.909884	0.03932
H5	-1.02407	1.762352	0.858228
H6	-1.08273	1.716199	-0.90663
S7	1.271345	0.132344	0.000172
H8	1.554344	-1.17909	-0.00847

Anti-Thioacetic Acid			
Atom Number	x	y	z
C1	-0.51188	-0.13009	0.000821
O2	-0.97771	-1.2295	0.000185
C3	-1.33031	1.139907	-0.00044
H4	-2.38504	0.871723	0.008471
H5	-1.09004	1.740793	0.878303
H6	-1.10238	1.728115	-0.8911
S7	1.283833	0.055207	-0.00044
H8	1.300978	1.397355	0.010889

Table A.2 Observed transitions for the parent isotopologue of *syn*-thioacetic acid and Obs.-Calc. based on BELGI-Cs fit (CH_3COSH)

J'	Ka'	Kc'	J''	Ka''	Kc''	Sym	Observed Frequency [MHz]	Obs.-Calc. [MHz]
4	2	3	3	3	0	A	3650.186	0.000
2	1	2	2	0	2	E	3883.203	-0.005
1	1	1	1	0	1	E	4115.366	-0.001
4	1	4	3	2	1	A	5428.893	0.002
3	1	3	2	2	1	E	6081.233	0.002
5	1	5	4	2	2	A	6208.164	0.000
1	1	0	1	0	1	A	6636.826	-0.002
2	0	2	1	1	0	E	6787.629	-0.006
2	1	1	2	1	2	E	6870.088	0.000
3	1	2	2	2	0	E	7654.400	0.003
1	0	1	0	0	0	E	7737.340	0.006
4	2	2	3	3	1	A	7961.254	0.001
1	0	1	0	0	0	A	8323.192	-0.001
2	1	1	2	0	2	A	8580.060	-0.002
4	2	3	4	1	3	E	8749.105	0.002
1	1	0	1	0	1	E	8933.266	0.005
3	2	2	3	1	2	E	9070.136	-0.003
2	2	1	2	1	1	E	9451.359	0.001
5	2	4	4	3	1	A	10441.365	-0.003
2	1	1	2	0	2	E	10753.290	-0.006
2	0	2	1	1	1	A	11292.674	0.001
2	0	2	1	1	1	E	11605.530	0.000
1	1	1	0	0	0	E	11852.707	0.006
3	1	2	3	0	3	A	12005.807	0.000
3	1	2	2	2	1	A	12086.477	0.002
3	0	3	2	1	1	E	12681.317	-0.006
7	3	5	7	2	5	E	13122.018	0.000
1	1	1	0	0	0	A	13346.689	0.001
3	1	2	3	0	3	E	13390.333	-0.002
3	2	1	3	1	2	A	14450.089	0.003
4	2	2	4	1	3	A	14465.720	0.000
5	2	3	4	3	1	E	14540.360	0.000
2	1	2	1	1	1	A	15032.843	-0.003
2	2	0	2	1	1	A	15400.239	0.001
2	1	2	1	1	1	E	15488.732	-0.006
3	1	3	2	1	1	E	15532.594	0.005
2	0	2	1	0	1	E	15720.896	0.000

Table A.2 Observed transitions for the parent isotopologue of *syn*-thioacetic acid and Obs.-Calc. based on BELGI-Cs fit (CH_3COSH) cont…

J'	K_a'	K_c'	J''	K_a''	K_c''	Sym	Observed Frequency [MHz]	Obs.-Calc. [MHz]
6	2	5	5	3	2	A	15739.517	0.001
5	2	3	5	1	4	A	16006.515	-0.001
2	0	2	1	0	1	A	16316.167	-0.001
2	2	1	2	1	2	E	16321.446	0.001
4	1	3	4	0	4	E	17117.789	0.002
4	1	3	4	0	4	A	17133.674	0.001

Table A.3 Observed transitions for the parent isotopologue of *syn*-thioacetic acid and Obs.-Calc. based on XIAM fit (CH_3COSH)

J'	K_a'	K_c'	J''	K_a''	K_c''	Sym	Observed Frequency [MHz]	Obs.-Calc. [MHz]
4	2	3	3	3	0	A	3650.186	0.116
2	1	2	2	0	2	E	3883.203	0.009
1	1	1	1	0	1	E	4115.366	-0.108
4	1	4	3	2	1	A	5428.893	-0.078
3	1	3	2	2	1	E	6081.233	0.012
5	1	5	4	2	2	A	6208.164	0.023
1	1	0	1	0	1	A	6636.826	0.026
2	0	2	1	1	0	E	6787.629	-0.069
2	1	1	2	1	2	E	6870.088	-0.070
3	1	2	2	2	0	E	7654.400	0.040
1	0	1	0	0	0	E	7737.340	0.016
4	2	2	3	3	1	A	7961.254	-0.065
1	0	1	0	0	0	A	8323.192	0.014
2	1	1	2	0	2	A	8580.060	0.050
4	2	3	4	1	3	E	8749.105	0.049
1	1	0	1	0	1	E	8933.266	0.031
3	2	2	3	1	2	E	9070.136	0.078
2	2	1	2	1	1	E	9451.359	0.031
5	2	4	4	3	1	A	10441.365	0.020
2	1	1	2	0	2	E	10753.290	-0.063
2	0	2	1	1	1	A	11292.674	0.001
2	0	2	1	1	1	E	11605.530	0.071
1	1	1	0	0	0	E	11852.707	-0.091
3	1	2	3	0	3	A	12005.807	0.046
3	1	2	2	2	1	A	12086.477	-0.022
3	0	3	2	1	1	E	12681.317	-0.075
7	3	5	7	2	5	E	13122.018	-0.068
1	1	1	0	0	0	A	13346.689	0.019
3	1	2	3	0	3	E	13390.333	0.089
3	2	1	3	1	2	A	14450.089	0.009
4	2	2	4	1	3	A	14465.720	-0.012
5	2	3	4	3	1	E	14540.360	-0.041
2	1	2	1	1	1	A	15032.843	0.000
2	2	0	2	1	1	A	15400.239	-0.017
2	1	2	1	1	1	E	15488.732	0.079
3	1	3	2	1	1	E	15532.594	0.045
2	0	2	1	0	1	E	15720.896	-0.037

Table A.3 Observed transitions for the parent isotopologue of *syn*-thioacetic acid and Obs.-Calc. based on XIAM fit (CH_3COSH) cont…

J'	K_a'	K_c'	J''	K_a''	K_c''	Sym	Observed Frequency [MHz]	Obs.-Calc. [MHz]
6	2	5	5	3	2	A	15739.518	0.076
5	2	3	5	1	4	A	16006.515	-0.195
2	0	2	1	0	1	A	16316.167	0.003
2	2	1	2	1	2	E	16321.446	-0.041
4	1	3	4	0	4	E	17117.789	0.390
4	1	3	4	0	4	A	17133.674	-0.057

Table A.4 Observed transitions for the S^{34} isotopologue of *syn*-thioacetic acid and Obs.-Calc. based on BELGI-Cs fit ($CH_3COS^{34}H$)

J'	K_a'	K_c'	J"	K_a"	K_c"	Sym	Observed Frequency [MHz]	Obs.-Calc. [MHz]
2	0	2	1	1	0	E	6380.744	0.001
3	1	2	2	2	0	E	6669.291	0.000
1	1	0	1	0	1	A	6698.699	-0.001
1	0	1	0	0	0	E	7556.163	0.000
1	0	1	0	0	0	A	8106.007	-0.001
2	1	1	2	0	2	A	8526.631	0.001
1	1	0	1	0	1	E	8953.825	0.000
4	2	3	4	1	3	E	9063.301	0.000
3	2	2	3	1	2	E	9393.665	0.000
2	2	1	2	1	1	E	9849.793	0.002
2	1	2	1	1	0	E	10393.588	-0.002
2	1	1	2	0	2	E	10682.743	0.002
2	0	2	1	1	1	A	10753.489	0.000
3	1	2	2	2	1	A	10920.442	0.000
2	0	2	1	1	1	E	11133.545	0.000
3	1	2	3	0	3	A	11733.334	0.000
1	1	1	0	0	0	E	11757.187	0.000
3	1	2	3	0	3	E	13213.433	0.000
1	1	1	0	0	0	A	13270.509	0.001
4	2	2	4	1	3	A	14660.679	0.001
3	2	1	3	1	2	A	14800.912	-0.001
2	2	0	2	1	1	A	15787.089	0.000
5	2	3	5	1	4	A	15905.258	0.000
1	1	0	0	0	0	E	16509.989	0.000
2	2	1	2	1	2	E	16519.684	-0.002
4	1	3	4	0	4	A	16552.489	0.000
4	1	3	4	0	4	E	16730.362	0.000

Table A.5 Observed transitions for the S^{34} isotopologue of *syn*-thioacetic acid and Obs.-Calc. based on XIAM fit ($CH_3COS^{34}H$)

J'	K_a'	K_c'	J''	K_a''	K_c''	Sym	Observed Frequency [MHz]	Obs.-Calc. [MHz]
2	0	2	1	1	0	E	6380.744	-0.026
3	1	2	2	2	0	E	6669.291	-0.027
1	1	0	1	0	1	A	6698.699	0.046
1	0	1	0	0	0	E	7556.163	-0.009
1	0	1	0	0	0	A	8106.007	-0.008
2	1	1	2	0	2	A	8526.631	0.044
1	1	0	1	0	1	E	8953.825	0.005
4	2	3	4	1	3	E	9063.301	0.009
3	2	2	3	1	2	E	9393.665	0.023
2	2	1	2	1	1	E	9849.793	-0.015
2	1	2	1	1	0	E	10393.588	0.049
2	1	1	2	0	2	E	10682.743	-0.042
2	0	2	1	1	1	A	10753.489	-0.037
3	1	2	2	2	1	A	10920.442	-0.035
2	0	2	1	1	1	E	11133.545	0.017
3	1	2	3	0	3	A	11733.334	0.000
1	1	1	0	0	0	E	11757.187	-0.048
3	1	2	3	0	3	E	13213.433	0.039
1	1	1	0	0	0	A	13270.509	0.021
4	2	2	4	1	3	A	14660.679	-0.180
3	2	1	3	1	2	A	14800.912	-0.068
2	2	0	2	1	1	A	15787.089	-0.003
5	2	3	5	1	4	A	15905.258	-0.410
1	1	0	0	0	0	E	16509.989	-0.004
2	2	1	2	1	2	E	16519.684	-0.141
4	1	3	4	0	4	A	16552.489	-0.138
4	1	3	4	0	4	E	16730.362	0.154

Table A.6 Observed transitions for the ^{13}C isotopologue of *syn*-thioacetic acid and Obs.-Calc. based on BELGI-Cs fit ($CH_3{}^{13}COSH$)

J'	K_a'	K_c'	J''	K_a''	K_c''	Sym	Observed Frequency [MHz]	Obs.-Calc. [MHz]
1	1	0	1	0	1	A	6639.802	-0.002
1	0	1	0	0	0	E	7721.889	-0.002
1	0	1	0	0	0	A	8305.539	-0.001
2	1	1	2	0	2	A	8574.073	0.003
1	1	0	1	0	1	E	8931.515	0.002
2	2	1	2	1	1	E	9485.475	-0.001
2	1	1	2	0	2	E	10745.984	-0.004
2	0	2	1	1	1	A	11251.045	0.000
2	0	2	1	1	1	E	11564.705	0.000
1	1	1	0	0	0	E	11845.855	0.002
3	1	2	3	0	3	A	11982.857	-0.001
3	1	2	2	2	1	A	11999.019	0.000
1	1	1	0	0	0	A	13338.158	0.000
3	1	2	3	0	3	E	13374.956	0.001
3	2	1	3	1	2	A	14471.926	0.000
2	2	0	2	1	1	A	15424.821	0.000

Table A.7 Observed transitions for the ^{13}C isotopologue of *syn*-thioacetic acid and Obs.-Calc. based on XIAM fit ($CH_3{}^{13}COSH$)

J'	K_a'	K_c'	J''	K_a''	K_c''	Sym	Observed Frequency [MHz]	Obs.-Calc. [MHz]
1	1	0	1	0	1	A	6639.802	0.083
1	0	1	0	0	0	E	7721.889	0.018
1	0	1	0	0	0	A	8305.539	-0.005
2	1	1	2	0	2	A	8574.073	0.061
1	1	0	1	0	1	E	8931.515	-0.012
2	2	1	2	1	1	E	9485.475	0.018
2	1	1	2	0	2	E	10745.984	0.086
2	0	2	1	1	1	A	11251.045	-0.041
2	0	2	1	1	1	E	11564.705	-0.001
1	1	1	0	0	0	E	11845.855	-0.016
3	1	2	3	0	3	A	11982.857	0.011
3	1	2	2	2	1	A	11999.019	-0.007
1	1	1	0	0	0	A	13338.158	0.055
3	1	2	3	0	3	E	13374.956	-0.008
3	2	1	3	1	2	A	14471.926	-0.085
2	2	0	2	1	1	A	15424.821	0.053

Table A.8 Observed transitions for the parent isotopologue of *anti*-thioacetic acid and Obs.-Calc. based on BELGI-Cs fit (CH_3COSH)

J'	K_a'	K_c'	J''	K_a''	K_c''	Sym	Observed Frequency [MHz]	Obs.-Calc. [MHz]
1	1	0	1	0	1	E	6630.917	0.002
1	1	0	1	0	1	A	6632.296	-0.002
5	1	5	4	2	2	A	6659.577	-0.007
5	1	5	4	2	2	E	6669.899	0.007
4	2	2	3	3	0	E	7020.204	0.002
1	0	1	0	0	0	E	8229.052	-0.004
1	0	1	0	0	0	A	8229.975	0.002
2	1	1	2	0	2	E	8469.917	0.003
2	1	1	2	0	2	A	8472.714	-0.005
5	2	4	4	3	1	E	9987.963	0.000
5	2	4	4	3	1	A	10008.816	-0.002
2	0	2	1	1	1	A	11068.407	0.007
2	0	2	1	1	1	E	11068.533	-0.004
3	1	2	2	2	1	A	11516.193	-0.004
3	1	2	2	2	1	E	11526.814	0.001
3	1	2	3	0	3	E	11700.239	0.004
3	1	2	3	0	3	A	11705.220	-0.004
1	1	1	0	0	0	E	13319.067	-0.004
1	1	1	0	0	0	A	13321.654	0.005
4	2	2	4	1	3	E	14497.887	0.004
4	2	2	4	1	3	A	14501.080	-0.004
3	2	1	3	1	2	E	14603.082	-0.001
3	2	1	3	1	2	A	14604.436	0.004
2	2	1	2	1	1	E	15260.458	-0.004
6	2	5	5	3	2	E	15502.640	-0.005
6	2	5	5	3	2	A	15503.146	0.006
2	2	0	2	1	1	A	15574.763	0.004
2	2	0	2	1	1	E	15581.536	-0.002
5	2	3	5	1	4	E	15799.326	0.007
5	2	3	5	1	4	A	15804.470	-0.009
4	1	3	4	0	4	A	16559.193	0.002

Table A.9 Observed transitions for the parent isotopologue of *anti*-thioacetic acid and Obs.-Calc. based on XIAM fit (CH_3COSH)

J'	K_a'	K_c'	J''	K_a''	K_c''	Sym	Observed Frequency [MHz]	Obs.-Calc. [MHz]
1	1	0	1	0	1	E	6630.917	-0.001
1	1	0	1	0	1	A	6632.296	-0.001
5	1	5	4	2	2	A	6659.577	-0.006
5	1	5	4	2	2	E	6669.899	0.001
4	2	2	3	3	0	E	7020.204	0.001
1	0	1	0	0	0	E	8229.052	-0.001
1	0	1	0	0	0	A	8229.975	0.000
2	1	1	2	0	2	E	8469.917	-0.002
2	1	1	2	0	2	A	8472.714	-0.002
5	2	4	4	3	1	E	9987.963	0.001
5	2	4	4	3	1	A	10008.816	-0.001
2	0	2	1	1	1	A	11068.407	0.004
2	0	2	1	1	1	E	11068.533	-0.002
3	1	2	2	2	1	A	11516.193	-0.002
3	1	2	2	2	1	E	11526.814	-0.001
3	1	2	3	0	3	E	11700.239	0.004
3	1	2	3	0	3	A	11705.220	-0.001
1	1	1	0	0	0	E	13319.067	-0.002
1	1	1	0	0	0	A	13321.654	0.003
4	2	2	4	1	3	E	14497.887	0.000
4	2	2	4	1	3	A	14501.080	-0.002
3	2	1	3	1	2	E	14603.082	-0.001
3	2	1	3	1	2	A	14604.436	0.000
2	2	1	2	1	1	E	15260.458	-0.001
6	2	5	5	3	2	E	15502.640	-0.024
6	2	5	5	3	2	A	15503.146	-0.011
2	2	0	2	1	1	A	15574.763	-0.003
2	2	0	2	1	1	E	15581.536	0.003
5	2	3	5	1	4	E	15799.326	0.007
5	2	3	5	1	4	A	15804.470	-0.001
4	1	3	4	0	4	A	16559.193	-0.002

Table A.10 Observed transitions for the S^{34} isotopologue of *anti*-thioacetic acid and Obs.-Calc. based on BELGI-Cs fit ($CH_3COS^{34}H$)

J'	K_a'	K_c'	J''	K_a''	K_c''	Sym	Observed Frequency [MHz]	Obs.-Calc. [MHz]
1	1	0	1	0	1	E	6698.933	0.001
1	1	0	1	0	1	A	6700.281	0.000
2	1	1	2	0	2	E	8427.802	0.004
2	1	1	2	0	2	A	8430.495	-0.002
3	1	2	2	2	1	A	10346.834	-0.004
3	1	2	2	2	1	E	10358.843	0.004
2	0	2	1	1	1	A	10527.097	0.006
2	0	2	1	1	1	E	10527.351	-0.005
3	1	2	3	0	3	E	11448.745	0.001
3	1	2	3	0	3	A	11453.456	-0.003
1	1	1	0	0	0	E	13248.687	-0.001
1	1	1	0	0	0	A	13251.264	0.000
4	2	2	4	1	3	E	14726.273	0.005
4	2	2	4	1	3	A	14729.297	-0.005
3	2	1	3	1	2	E	14974.531	0.001
3	2	1	3	1	2	A	14975.673	-0.001
2	2	0	2	1	1	A	15975.309	0.004
2	2	0	2	1	1	E	15983.084	-0.004
4	1	3	4	0	4	E	15999.274	-0.003
4	1	3	4	0	4	A	16006.955	0.003

Table A.11 Observed transitions for the S^{34} isotopologue of *anti*-thioacetic acid and Obs.-Calc. based on XIAM fit ($CH_3COS^{34}H$)

J'	K_a'	K_c'	J''	K_a''	K_c''	Sym	Observed Frequency [MHz]	Obs.-Calc. [MHz]
1	1	0	1	0	1	E	6698.933	-0.006
1	1	0	1	0	1	A	6700.281	-0.002
2	1	1	2	0	2	E	8427.802	-0.001
2	1	1	2	0	2	A	8430.495	0.001
3	1	2	2	2	1	A	10346.834	-0.001
3	1	2	2	2	1	E	10358.843	0.000
2	0	2	1	1	1	A	10527.097	0.005
2	0	2	1	1	1	E	10527.351	-0.001
3	1	2	3	0	3	E	11448.745	0.001
3	1	2	3	0	3	A	11453.456	-0.001
1	1	1	0	0	0	E	13248.687	0.000
1	1	1	0	0	0	A	13251.264	0.000
4	2	2	4	1	3	E	14726.273	0.002
4	2	2	4	1	3	A	14729.297	0.001
3	2	1	3	1	2	E	14974.531	0.001
3	2	1	3	1	2	A	14975.673	-0.001
2	2	0	2	1	1	A	15975.309	-0.021
2	2	0	2	1	1	E	15983.084	-0.026
4	1	3	4	0	4	E	15999.274	-0.004
4	1	3	4	0	4	A	16006.955	-0.013

Table A.12 Observed transitions for the ^{13}C isotopologue of *anti*-thioacetic acid and Obs.-Calc. based on BELGI-Cs fit ($CH_3{}^{13}COSH$)

J'	K_a'	K_c'	J''	K_a''	K_c''	Sym	Observed Frequency [MHz]	Obs.-Calc. [MHz]
1	1	0	1	0	1	E	6668.504	-0.014
1	1	0	1	0	1	A	6669.693	0.014
2	1	1	2	0	2	E	8442.243	0.025
2	1	1	2	0	2	A	8444.990	-0.025
5	2	4	4	3	1	A	9224.449	0.000
3	1	2	3	0	3	E	11548.717	-0.008
3	1	2	3	0	3	A	11553.815	0.008
1	1	1	0	0	0	E	13279.487	-0.004
1	1	1	0	0	0	A	13282.056	0.004
4	2	2	4	1	3	A	14626.184	0.000

Table A.13 Observed transitions for the ^{13}C isotopologue of *anti*-thioacetic acid and Obs.-Calc. based on XIAM fit ($CH_3{}^{13}COSH$)

J'	K_a'	K_c'	J''	K_a''	K_c''	Sym	Observed Frequency [MHz]	Obs.-Calc. [MHz]
1	1	0	1	0	1	E	6668.504	0.024
1	1	0	1	0	1	A	6669.693	0.013
2	1	1	2	0	2	E	8442.243	-0.026
2	1	1	2	0	2	A	8444.990	-0.008
5	2	4	4	3	1	A	9224.449	0.000
3	1	2	3	0	3	E	11548.717	0.008
3	1	2	3	0	3	A	11553.815	0.003
1	1	1	0	0	0	E	13279.487	-0.015
1	1	1	0	0	0	A	13282.056	0.023
4	2	2	4	1	3	A	14626.184	0.000

Table A.14 Spectroscopic Constants for the Observed Isotopologues of *syn*-Thioacetic Acid based on XIAM least squares fit[a]

Constant	CH_3COSH	$CH_3CO^{34}SH$	$CH_3C^{13}OSH$
A [MHz]	9913.196(12)	9907.555(28)	9910.702(29)
B [MHz]	4923.132(10)	4777.292(13)	4911.381(21)
C [MHz]	3354.778(10)	3285.775(12)	3349.035(19)
Δ_J [kHz]	0.41(27)	1.5(13)	2.8(15)
Δ_{JK} [kHz]	10.97(87)	5.3(17)	10.97[f]
Δ_{iJ} [MHz]	6.1(12)	6.14(98)	18.7(99)
Δ_{iK} [MHz]	-2.633(12)	-2.541(15)	-2.66(11)
Δ_{i-} [kHz]	93.8(47)	84.8(64)	62(54)
Δ_{cJ} [GHz]	-0.067(14)	-0.068(11)	-0.21(12)
V_3 [cm^{-1}]	77.819(1)	77.723(1)	77.793(5)
ε [deg][b]	0	0	0
δ [deg]	57.13018(37)	57.45241(44)	57.2055(39)
F_o[GHz][c]	158.029	158.029	158.029
N[d]	20, 23	12, 15	9, 7
σ [kHz][e]	68.3	44.3	68.7

[a]Numbers in parentheses are one standard error in the least squares fit.
[b]Fixed at zero degrees.
[c]Fixed to the value derived from the M06-2X/6-311+G(d,p) structure.
[d]Number of A and E state lines, respectively, included in the fit.
[e]Standard deviation of the residuals.
[f]Parameter fixed at the parent value.

Table A.15 Spectroscopic Constants for the Observed Isotopologues of *anti*-Thioacetic Acid based on XIAM least squares fit[a]

Constant	CH_3COSH	$CH_3CO^{34}SH$	$CH_3C^{13}OSH$
A [MHz]	9975.6935(98)	9974.5095(11)	9974.574(46)
B [MHz]	4884.8551(56)	4738.98574(70)	4801.096(27)
C [MHz]	3344.53002(89)	3275.36077(53)	3306.049(22)
Δ_J [kHz]	1.564(39)	0.904(59)	1.75(49)
Δ_{JK} [kHz]	3.94(17)	7.307(66)	1.08(86)
Δ_K [kHz]	4.48(26)	-	-
δ_J [kHz]	0.549(16)	0.450(17)	-
δ_K [kHz]	4.00(19)	-	-
Δ_{iJ} [MHz]	0.354(84)	0.354[f]	-
Δ_{iK} [MHz]	-2.54(26)	-2.54[f]	-
Δ_{i-} [MHz]	0.160(81)	0.160[f]	-
V_3 [cm^{-1}]	354.56(35)	354.58(2)	349.34(56)
ε [deg][b]	0	0	0
δ [deg]	54.17(17)	54.3300(65)	55.51(37)
F_o[GHz][c]	158.901	158.901	158.901
N[d]	15, 16	10, 10	6, 4
σ [kHz][e]	2.7	1.6	18.2

[a]Numbers in parentheses are one standard error in the least squares fit.
[b]Fixed at zero degrees.
[c]Fixed to the value derived from the M06-2X/6-311+G(d,p) structure.
[d]Number of A and E state lines, respectively, included in the fit.
[e]Standard deviation of the residuals.
[f]Parameter fixed at the parent value.

Table A.16 Transitions included in the Global fit for the parent isotopologue of *syn*-thioacetic acid and Obs.-Calc. based on BELGI-Cs (CH_3COSH)

J'	K_a'	K_c'	J"	K_a"	K_c"	Sym	Obs. Frequency [MHz]	Obs.-Calc. [MHz]
4	2	3	3	3	0	A	3650.186	0.003
4	1	4	3	2	1	A	5428.893	0.001
5	1	5	4	2	2	A	6208.164	0.001
1	1	0	1	0	1	A	6636.826	-0.001
4	2	2	3	3	1	A	7961.254	0.002
1	0	1	0	0	0	A	8323.192	-0.001
2	1	1	2	0	2	A	8580.06	-0.001
5	2	4	4	3	1	A	10441.365	-0.005
2	0	2	1	1	1	A	11292.674	0.001
3	1	2	3	0	3	A	12005.807	0.000
3	1	2	2	2	1	A	12086.477	0.001
1	1	1	0	0	0	A	13346.689	0.002
3	2	1	3	1	2	A	14450.089	0.003
4	2	2	4	1	3	A	14465.72	0.001
2	1	2	1	1	1	A	15032.843	-0.003
2	2	0	2	1	1	A	15400.239	0.002
5	2	3	5	1	4	A	16006.515	-0.001
2	0	2	1	0	1	A	16316.167	0.000
4	1	3	4	0	4	A	17133.674	-0.001
6	2	4	6	1	5	A	19436.52	0.163
3	0	3	2	1	2	A	19990.66	-0.039
2	1	2	1	0	1	A	20056.48	0.141
7	3	4	7	2	5	A	21690.18	-0.042
6	3	3	6	2	4	A	22296.29	-0.128
8	3	5	8	2	6	A	22919.06	-0.165
5	1	4	5	0	5	A	23710.15	0.085
5	3	2	5	2	3	A	24078.58	-0.117
7	2	5	7	1	6	A	24847.15	-0.018
3	1	3	2	0	2	A	26100.62	0.110
9	3	6	9	2	7	A	26355.75	-0.085
4	0	4	3	1	3	A	28217.79	0.052
6	1	5	6	0	6	A	31087.99	0.477
8	2	6	8	1	7	A	31880.04	-0.205
4	1	4	3	0	3	A	31884.77	-0.014
2	2	1	1	1	0	A	33329.28	-0.263
5	1	4	4	2	3	A	33549.39	-0.017

Table A.16 Transitions included in the Global fit for the parent isotopologue of *syn*-thioacetic acid and Obs.-Calc. based on BELGI-Cs (CH_3COSH) cont…

J'	K_a'	K_c'	J"	K_a"	K_c"	Sym	Obs. Frequency [MHz]	Obs.-Calc. [MHz]
2	1	2	2	0	2	E	3883.203	-0.006
1	1	1	1	0	1	E	4115.366	-0.012
3	1	3	2	2	1	E	6081.233	0.009
2	0	2	1	1	0	E	6787.629	0.000
2	1	1	2	1	2	E	6870.088	0.001
3	1	2	2	2	0	E	7654.4	0.000
1	0	1	0	0	0	E	7737.34	0.005
4	2	3	4	1	3	E	8749.105	0.013
1	1	0	1	0	1	E	8933.266	-0.015
3	2	2	3	1	2	E	9070.136	-0.023
2	2	1	2	1	1	E	9451.359	0.010
2	1	1	2	0	2	E	10753.29	-0.006
2	0	2	1	1	1	E	11605.53	-0.002
1	1	1	0	0	0	E	11852.707	-0.006
3	0	3	2	1	1	E	12681.317	-0.016
7	3	5	7	2	5	E	13122.018	-0.002
3	1	2	3	0	3	E	13390.333	0.019
5	2	3	4	3	1	E	14540.36	-0.001
2	1	2	1	1	1	E	15488.732	-0.008
3	1	3	2	1	1	E	15532.594	0.021
2	0	2	1	0	1	E	15720.896	-0.014
2	2	1	2	1	2	E	16321.446	0.010
4	1	3	4	0	4	E	17117.789	0.002
3	2	1	3	1	2	E	17819.56	0.121
4	2	2	4	1	3	E	18124.4	-0.154
5	2	3	5	1	4	E	19468.03	-0.274
3	0	3	2	1	2	E	19551.26	-0.160
6	2	4	6	1	5	E	21678.66	0.095
5	1	4	5	0	5	E	22430.19	-0.334
7	2	5	7	1	6	E	25104.42	0.361
3	1	3	2	0	2	E	26286.4	0.531
7	3	4	7	2	5	E	26371.46	-0.444
6	3	3	6	2	4	E	26571.27	-0.022
5	3	3	5	2	4	E	26942.18	0.310
8	3	5	8	2	6	E	27336.71	-0.109
4	0	4	3	1	3	E	27702.86	-0.010
5	3	2	5	2	3	E	27821.93	0.167

Appendix B: Supplemental Material for Chapter 2

Table B.1 Cartesian coordinates from M06-2X/6-311++G(3df,3pd) calculations of minimum energy and transition state structures related to the formation of cis-AcrSA and trans-AcrSA

Trans-Acrylic···SO_3			
Atomic Number	X	Y	Z
S1	-1.573560	-0.026797	0.019517
O2	-2.172831	-0.811770	-0.987716
O3	-1.252417	1.342393	-0.318630
O4	-1.812933	-0.303320	1.385327
C5	1.235062	-0.056863	-0.037481
O6	0.194394	-0.751613	-0.089873
O7	1.236820	1.228860	-0.009642
H8	0.285604	1.549694	-0.095077
C9	2.526527	-0.751584	-0.009041
H10	2.467716	-1.829306	-0.018136
C11	3.668774	-0.079982	0.026698
H12	3.680994	1.000884	0.034729
H13	4.616199	-0.598350	0.049432

TS Trans-Acrylic···SO_3			
Atomic Number	X	Y	Z
S1	1.304062	-0.180872	0.027510
O2	1.498795	-0.395665	1.410782
O3	1.312243	1.251699	-0.370664
O4	1.864697	-1.047782	-0.930663
C5	-1.289252	0.449871	-0.040966
O6	-0.408208	-0.498135	-0.151530
O7	-0.978675	1.655310	0.011093
H8	0.199650	1.676608	-0.149669
C9	-2.698240	0.050812	0.006397
H10	-3.399806	0.870801	0.045232
C11	-3.061845	-1.224145	0.009449
H12	-2.326013	-2.015197	-0.026255
H13	-4.104897	-1.502156	0.048789

Table B.1 Cartesian coordinates from M06-2X/6-311++G(3df,3pd) calculations continued…

Trans-AcrSA			
Atomic Number	X	Y	Z
S1	-1.206092	-0.218561	0.079363
O2	-1.855103	-1.367793	-0.401977
O3	-1.478295	0.936487	-0.924623
O4	-1.333944	0.23963	1.408732
C5	1.275226	0.524752	-0.042955
O6	0.373214	-0.499605	-0.175456
O7	0.939874	1.673919	0.001063
H8	-0.952776	1.711099	-0.647224
C9	2.668751	0.055123	0.008506
C10	3.005986	-1.226319	-0.00365
H11	2.259153	-2.005341	-0.056765
H12	4.043685	-1.52375	0.040426
H13	3.39422	0.853503	0.063747

Cis-Acrylic···SO_3			
Atomic Number	X	Y	Z
S1	-1.473305	-0.171389	0.015759
O2	-1.868042	-1.038458	-1.025175
O3	-1.472813	1.245025	-0.273221
O4	-1.654772	-0.544523	1.367454
C5	1.271913	0.439134	-0.028792
O6	0.412486	-0.469283	-0.091003
O7	0.988125	1.692914	0.005889
H8	-0.009897	1.797558	-0.067907
C9	2.699672	0.103212	0.005469
H10	3.375983	0.944629	0.032282
C11	3.100467	-1.160078	0.006362
H12	2.383670	-1.969240	-0.019400
H13	4.150942	-1.409728	0.033102

Table B.1 Cartesian coordinates from M06-2X/6-311++G(3df,3pd) calculations continued…

TS Cis-Acrylic···SO_3			
Atomic Number	X	Y	Z
S1	1.477420	-0.068304	0.031670
O2	1.714227	-0.215237	1.417029
O3	1.173508	1.325451	-0.387084
O4	2.210231	-0.807452	-0.916946
C5	-1.193615	-0.014248	-0.049100
O6	-0.130493	-0.753445	-0.132561
O7	-1.150158	1.230900	-0.007850
H8	-0.006290	1.502107	-0.168246
C9	-2.460841	-0.751503	-0.021096
H10	-2.383083	-1.827735	-0.047367
C11	-3.612333	-0.097488	0.037362
H12	-3.633821	0.983331	0.062986
H13	-4.553307	-0.627369	0.062211

Cis-AcrSA			
Atomic Number	X	Y	Z
S1	-1.326502	-0.109153	0.82585
O2	-2.217612	-1.086883	-0.389348
O3	-1.323831	1.06353	-0.938188
O4	-1.351197	0.384446	1.405093
C5	1.260613	0.054796	-0.05493
O6	0.152249	-0.744998	-0.156077
O7	1.194349	1.249683	-0.012983
H8	-0.6384	1.703097	-0.665814
C9	2.489012	-0.761188	-0.03492
C10	3.667529	-0.161617	0.041768
H11	3.73099	0.917252	0.086434
H12	4.585602	-0.730073	0.063436
H13	2.366999	-1.832813	-0.079248

Table B.2 Trans-AcrSA structural information from M06-2X/6-311++G(3df,3pd) calculations*†

	M06-2X/6-311++G(3df,3pd)
S1-O2	1.40486
S1-O3	1.55442
S1-O4	1.41192
S1-O6	1.62423
O3-H8	0.97629
C5-O6	1.37131
C5-O7	1.19791
C5-C9	1.47143
O7-H8	2.00095
C9-C10	1.32513
C9-H13	1.08017
C10-H11	1.08049
C10-H12	1.08038
∠(O2-S1-O3)	107.79825
∠(O2-S1-O4)	123.10861
∠(O2-S1-O6)	104.70824
∠(O4-S1-O3)	110.5566
∠(O4-S1-O6)	106.97252
∠(O3-S1-O6)	101.39176
∠(S1-O3-H8)	108.16713
∠(S1-O6-C5)	119.68085
∠(O6-C5-O7)	122.41216
∠(O6-C5-C9)	112.82473
∠(O7-C5-C9)	124.75156
∠(O7-H8-O3)	125.90638
∠(C5-C9-H13)	113.7002
∠(C5-C9-C10)	123.32168
∠(H13-C9-C10)	122.977
∠C9-C10-H11)	121.45082
∠(C9-C10-H12)	120.68305
∠(H11-C10-H12)	117.86611

*****All distances in Å.

†All angles in degrees.

Table B.3 Cis-AcrSA structural information from M06-2X/6-311++G(3df,3pd) calculations*†

	M06-2X/6-311++G(3df,3pd)
S1-O2	1.40455
S1-O3	1.55473
S1-O4	1.41183
S1-O6	1.62726
O3-H8	0.97624
C5-O6	1.37054
C5-O7	1.19746
C5-C9	1.47485
O7-H8	1.99768
C9-C10	1.32449
C9-H13	1.07946
C10-H11	1.08166
C10-H12	1.08003
∠(O2-S1-O3)	107.79087
∠(O2-S1-O4)	123.16285
∠(O2-S1-O6)	104.78901
∠(O4-S1-O3)	110.56971
∠(O4-S1-O6)	106.85149
∠(O3-S1-O6)	101.35414
∠(S1-O3-H8)	108.19006
∠(S1-O6-C5)	119.73934
∠(O6-C5-O7)	122.69339
∠(O6-C5-C9)	110.59169
∠(O7-C5-C9)	126.70472
∠(O7-H8-O3)	125.91782
∠(C5-C9-H13)	117.03587
∠(C5-C9-C10)	119.43498
∠(H13-C9-C10)	123.52825
∠C9-C10-H11)	120.40505
∠(C9-C10-H12)	121.28264
∠(H11-C10-H12)	118.31218

*****All distances in Å.

†All angles in degrees.

Table B.4 Observed transitions of Trans-Acrylic Sulfuric Anhydride

J'	K_a'	K_c'	J''	K_a''	K_c''	Obs. Frequency (MHz)	Calc. Frequency (MHz)	Obs. - Calc. (MHz)
3	1	2	2	1	1	6086.980*	6086.984	-0.004
4	1	4	3	1	3	7518.280	7518.286	-0.006
4	0	4	3	0	3	7744.199	7744.204	-0.005
4	2	3	3	2	2	7822.296	7822.299	-0.003
4	3	2	3	3	1	7845.432	7845.428	0.004
4	2	2	3	2	1	7907.135	7907.136	-0.001
4	1	3	3	1	2	8105.094	8105.098	-0.004
5	1	5	4	1	4	9383.658	9383.662	-0.004
5	0	5	4	0	4	9621.484*	9621.488	-0.004
5	2	4	4	2	3	9767.043	9767.049	-0.006
5	3	3	4	3	2	9812.825	9812.822	0.003
5	3	2	4	3	1	9819.481	9819.477	0.004
5	2	3	4	2	2	9931.785	9931.784	0.001
5	1	4	4	1	3	10112.905	10112.912	-0.007
4	1	3	3	0	3	10458.125*	10458.120	0.005
5	1	5	4	0	4	10627.997*	10627.998	-0.001
6	1	6	5	1	5	11241.144	11241.145	-0.001
3	2	1	2	1	1	11316.000*	11316.000	0.000
6	0	6	5	0	5	11468.763	11468.768	-0.005
6	2	5	5	2	4	11704.643	11704.652	-0.009
3	2	2	2	1	2	11714.438*	11714.442	-0.004
6	3	4	5	3	3	11782.676	11782.671	0.005
6	3	3	5	3	2	11800.262	11800.263	-0.001
6	2	4	5	2	3	11979.075	11979.077	-0.002
6	1	5	5	1	4	12106.622	12106.636	-0.014
7	1	7	6	1	6	13090.543	13090.539	0.004
7	0	7	6	0	6	13290.830	13290.832	-0.002
7	4	4	6	4	3	13743.361	13743.359	0.002
7	4	3	6	4	2	13744.534	13744.520	0.014
7	3	5	6	3	4	13754.077	13754.083	-0.006
7	3	4	6	3	3	13793.086	13793.087	-0.001
7	2	5	6	2	4	14042.575	14042.582	-0.007
7	1	6	6	1	5	14081.770	14081.786	-0.016
8	1	8	7	1	7	14932.175	14932.159	0.016
8	0	8	7	0	7	15096.015	15096.006	0.009
8	2	7	7	2	6	15553.310	15553.325	-0.015
8	3	6	7	3	5	15725.646	15725.656	-0.010
8	3	5	7	3	4	15801.873	15801.875	-0.002
8	1	7	7	1	6	16033.301	16033.327	-0.026
8	2	6	7	2	5	16112.124	16112.141	-0.017
9	1	9	8	1	8	16766.750	16766.721	0.029
9	0	9	8	0	8	16892.904	16892.875	0.029

*Transitions observed and measured on the cavity system.

Table B.5 Observed transitions of Cis-Acrylic Sulfuric Anhydride

J'	K_a'	K_c'	J"	K_a"	K_c"	Obs. Frequency (MHz)	Calc. Frequency (MHz)	Obs. - Calc. (MHz)
2	1	1	1	0	1	6328.066*	6328.066	0.000
4	1	4	3	1	3	6816.029	6816.029	0.000
4	0	4	3	0	3	6925.944*	6925.944	0.000
4	2	2	3	2	1	6943.807	6943.806	0.001
4	2	3	3	2	2	6934.507	6934.504	0.003
4	1	3	3	1	2	7050.727	7050.728	-0.001
3	1	2	2	0	2	8150.251*	8150.251	0.000
5	0	5	4	0	4	8650.491	8650.489	0.002
5	2	4	4	2	3	8666.957	8666.958	-0.001
5	3	3	4	3	2	8672.107	8672.106	0.001
5	3	2	4	3	1	8672.300	8672.299	0.001
5	2	3	4	2	2	8685.521	8685.521	0.000
5	1	5	4	1	4	8518.346	8518.344	0.002
5	1	4	4	1	3	8811.593	8811.594	-0.001
6	1	6	5	1	5	10219.583	10219.582	0.001
6	0	6	5	0	5	10370.501*	10370.500	0.001
6	2	5	5	2	4	10398.633	10398.633	0.000
6	3	4	5	3	3	10407.659	10407.658	0.001
6	3	3	5	3	2	10408.179	10408.175	0.004
6	2	4	5	2	3	10430.983	10430.983	0.000
6	1	5	5	1	4	10571.197	10571.197	0.000
5	1	4	4	0	4	11888.921*	11888.917	0.004
7	1	7	6	1	6	11919.578	11919.574	0.004
7	0	7	6	0	6	12085.229	12085.229	0.000
7	2	6	6	2	5	12129.369	12129.373	-0.004
7	3	5	6	3	4	12143.745	12143.746	-0.001
7	3	4	6	3	3	12144.906	12144.909	-0.003
7	2	5	6	2	4	12180.786	12180.785	0.001
7	1	6	6	1	5	12329.229	12329.234	-0.005
8	1	8	7	1	7	13618.184	13618.181	0.003
8	0	8	7	0	7	13794.077	13794.076	0.001
8	2	7	7	2	6	13859.018	13859.024	-0.006
8	1	7	7	1	6	14085.364	14085.369	-0.005
9	1	9	8	1	8	15315.292	15315.285	0.007
9	0	9	8	0	8	15496.668	15496.665	0.003
9	2	8	8	2	7	15587.431	15587.434	-0.003
9	2	7	8	2	6	15694.933	15694.932	0.001
9	1	8	8	1	7	15839.230	15839.237	-0.007
10	0	10	9	0	9	17192.905	17192.895	0.010
10	2	9	9	2	8	17314.451	17314.453	-0.002
10	1	9	9	1	8	17590.428	17590.434	-0.006

*****Transitions observed and measured on the cavity system.

Table B.6 Observed transitions of Trans-Acrylic-OD Sulfuric Anhydride*

J'	K_a'	K_c'	J"	K_a"	K_c"	Obs. Frequency (MHz)	Calc. Frequency (MHz)	Obs. - Calc. (MHz)
3	1	3	2	1	2	5615.162	5615.162	0.000
3	0	3	2	0	2	5809.771	5809.769	0.002
3	2	2	2	2	1	5846.739	5846.735	0.004
3	2	1	2	2	0	5883.716	5883.707	0.009
3	1	2	2	1	1	6066.660	6066.668	-0.008
4	1	4	3	1	3	7476.832	7476.832	0.000
4	0	4	3	0	3	7704.700	7704.697	0.003
4	2	3	3	2	2	7788.397	7788.399	-0.002
4	2	2	3	2	1	7879.341	7879.338	0.003
4	1	3	3	1	2	8077.167	8077.166	0.001
5	1	5	4	1	4	9330.900	9330.901	-0.001
5	0	5	4	0	4	9568.362	9568.361	0.001
5	2	4	4	2	3	9723.873	9723.878	-0.005
5	2	3	4	2	2	9899.973	9899.974	-0.001
5	1	4	4	1	3	10076.510	10076.512	-0.002

*All transitions were observed and measured with the cavity system.

Table B.7 Observed transitions of Cis-Acrylic-OD Sulfuric Anhydride*

J'	K_a'	K_c'	J"	K_a"	K_c"	Obs. Frequency (MHz)	Calc. Frequency (MHz)	Obs. - Calc. (MHz)
4	1	4	3	1	3	6787.770	6787.770	0.000
4	0	4	3	0	3	6903.140	6903.139	0.001
4	2	3	3	2	2	6912.959	6912.960	-0.001
4	2	2	3	2	1	6923.633	6923.634	-0.001
4	1	3	3	1	2	7035.568	7035.568	0.000
5	1	5	4	1	4	8482.779	8482.778	0.001
5	0	5	4	0	4	8620.970	8620.970	0.000
5	2	4	4	2	3	8639.862	8639.858	0.004
5	2	3	4	2	2	8661.149	8661.147	0.002
5	1	4	4	1	3	8792.369	8792.370	-0.001
6	1	6	5	1	5	10176.559	10176.560	-0.001
6	0	6	5	0	5	10333.626	10333.626	0.000
6	2	5	5	2	4	10365.862	10365.861	0.001
6	2	4	5	2	3	10402.937	10402.936	0.001
6	1	5	5	1	4	10547.715	10547.716	-0.001

*All transitions were observed and measured with the cavity system.

Appendix C: Supplemental Material for Chapter 3

Table C.1 Observed transitions of the $CH_3COOSO_2OH\cdots H_2O$ van der Waals Complex[*]

J'	K_a'	K_c'	J"	K_a"	K_c"	Sym	Observed Frequency (MHz)	Obs.-Calc. (MHz)
3	1	3	2	1	2	A	5726.890	0.000
3	1	3	2	1	2	E	5727.652	-0.001
3	0	3	2	0	2	E	5830.773	0.002
3	0	3	2	0	2	A	5831.834	0.000
3	1	2	2	1	1	E	6980.133	-0.007
3	1	2	2	1	1	A	6981.868	0.005
4	0	4	3	1	3	E	7478.745	-0.003
4	0	4	3	1	3	A	7481.836	-0.005
4	1	4	3	1	3	A	7491.177	-0.004
4	1	4	3	1	3	E	7493.268	0.002
4	0	4	3	0	3	E	7519.865	0.001
4	0	4	3	0	3	A	7522.572	0.001
4	1	4	3	0	3	A	7531.909	-0.002
4	1	4	3	0	3	E	7534.382	-0.001
4	2	3	3	2	2	A	8501.022	-0.002
4	2	3	3	2	2	E	8504.514	-0.001
4	1	3	3	1	2	E	8864.091	0.002
4	1	3	3	1	2	A	8865.933	-0.003
4	3	2	3	3	1	A	9005.145	-0.001
5	0	5	4	1	4	E	9216.873	0.000
5	0	5	4	1	4	A	9225.918	-0.004
5	1	5	4	1	4	A	9227.845	-0.003
5	1	5	4	1	4	E	9231.054	-0.002
5	0	5	4	0	4	E	9231.395	0.003
5	0	5	4	0	4	A	9235.263	0.001
5	1	5	4	0	4	A	9237.192	0.004
5	1	5	4	0	4	E	9245.571	-0.004
4	2	2	3	2	1	E	9641.582	0.001
4	2	2	3	2	1	A	9646.492	0.002
5	1	4	4	2	3	A	10283.959	0.003
5	1	4	4	2	3	E	10284.773	0.007
5	2	4	4	2	3	A	10361.749	0.000
5	2	4	4	2	3	E	10362.326	0.001
5	1	4	4	1	3	E	10535.369	0.002
5	1	4	4	1	3	A	10537.427	0.001
5	2	4	4	1	3	E	10612.920	-0.007
5	2	4	4	1	3	A	10615.213	-0.006

Table C.1 Observed transitions of the $CH_3COOSO_2OH\cdots H_2O$ van der Waals complex* cont…

J'	K_a'	K_c'	J"	K_a"	K_c"	Sym	Observed Frequency (MHz)	Obs.-Calc. (MHz)
6	0	6	5	0	5	E	10955.050	-0.004
6	0	6	5	1	5	A	10955.589	-0.008
6	1	6	5	1	5	A	10955.962	-0.007
6	0	6	5	0	5	A	10957.521	-0.002
6	1	6	5	1	5	E	10957.763	-0.001
6	1	6	5	0	5	A	10957.890	-0.005
5	3	3	4	3	2	A	11144.042	-0.002
5	2	3	4	2	2	A	11805.275	0.001
5	3	2	4	3	1	A	12068.623	-0.009
6	2	5	5	2	4	A	12142.143	0.002
6	1	5	5	1	4	E	12196.825	0.000
6	1	5	5	1	4	A	12199.959	-0.001
7	0	7	6	0	6	E	12680.430	0.002
7	1	7	6	1	6	A	12682.032	0.001
7	0	7	6	0	6	A	12682.327	-0.007
7	1	7	6	1	6	E	12683.257	0.002

*All transitions were measured on the cavity system

Table C.2 Observed transitions of the $CD_3COOSO_2OD\cdots D_2O$ van der Waals complex*

J'	Ka'	Kc'	J"	Ka"	Kc"	Sym	Observed Frequency (MHz)	Obs-Calc (MHz)
4	1	4	3	1	3	E	6827.591	-0.002
4	1	4	3	1	3	A	6827.617	0.001
4	0	4	3	0	3	E	6869.436	-0.001
4	0	4	3	0	3	A	6869.493	0.006
4	2	3	3	2	2	E	7718.559	-0.002
4	1	3	3	1	2	E	8101.140	0.004
5	1	5	4	1	4	A	8414.358	-0.001
5	1	5	4	1	4	E	8414.358	0.002
5	0	5	4	0	4	E	8425.809	0.000
5	0	5	4	0	4	A	8425.875	-0.004
5	1	5	4	0	4	A	8429.488	0.005
5	1	5	4	0	4	E	8429.488	0.005
5	1	4	4	1	3	E	9652.531	-0.009
5	1	4	4	1	3	A	9652.681	-0.001
6	0	6	5	1	5	E	9989.650	0.002
6	0	6	5	1	5	A	9989.912	-0.001
6	1	6	5	1	5	A	9990.718	0.001
6	1	6	5	1	5	E	9990.842	0.004
6	0	6	5	0	5	E	9993.322	-0.001
6	0	6	5	0	5	A	9993.515	-0.002
6	1	6	5	0	5	A	9994.320	0.000
6	1	6	5	0	5	E	9994.514	0.002
6	1	5	5	1	4	E	11158.875	-0.001
6	1	5	5	1	4	A	11159.024	0.013
7	0	7	6	0	6	A	11564.740	-0.001

*All transitions were measured on the cavity system

Table C.3 Observed transitions of the $CH_3{}^{13}COOSO_2OH\cdots H_2O$ van der Waals complex[*]

J'	K_a'	K_c'	J"	K_a"	K_c"	Sym	Observed Frequency (MHz)	Obs.-Calc. (MHz)
4	1	4	3	1	3	A	7454.922	0.001
4	1	4	3	1	3	E	7456.852	0.000
4	0	4	3	0	3	E	7486.087	0.000
4	0	4	3	0	3	A	7488.622	0.001
4	1	3	3	1	2	A	8826.813	0.000
5	1	5	4	1	4	A	9184.040	0.000
5	1	5	4	1	4	E	9187.305	-0.002
5	0	5	4	0	4	E	9188.329	-0.005
5	0	5	4	0	4	A	9192.247	0.004
5	1	4	4	0	4	A	9194.456	0.003
5	1	4	4	1	3	E	10493.161	0.001
5	1	4	4	1	3	A	10495.169	-0.001
6	0	6	5	0	5	E	10903.376	0.002
6	1	6	5	1	5	A	10904.137	-0.005
6	0	6	5	0	5	A	10905.912	0.000
6	1	6	5	1	5	E	10906.025	-0.002

[*]All transitions were measured on the cavity system

Table C.4 Cartesian coordinates from M06-2X/6-311++G(3df,3pd) calculations for the minimum energy structure of ASA···H_2O [I]

ASA-H_2O [I]			
Atom Number	x	y	z
S1	-0.84004	-0.642876	0.069656
O2	-1.411739	-1.903317	-0.182925
O3	-1.117916	0.301909	-1.098789
O4	-1.020267	0.032756	1.305887
C5	1.687581	0.061768	-0.002649
O6	0.759938	-0.931394	-0.091668
O7	1.411248	1.219523	0.103945
H8	-1.106254	1.280117	-0.776497
C9	3.066444	-0.511367	-0.068832
H10	3.17484	-1.081551	-0.989151
H11	3.792761	0.291412	-0.026703
H12	3.205693	-1.198902	0.763284
O13	-0.981257	2.628741	-0.111947
H14	-0.064422	2.496768	0.174313
H15	-1.503898	2.562767	0.694287

Table C.5 Cartesian coordinates from M06-2X/6-311++G(3df,3pd) calculations for ASA···H_2O [I] at the maximum energy along the CH_3 internal rotation coordinate

TS ASA-H2O (I.)			
Atom Number	x	y	z
S1	-0.833211	-0.741583	0.07165
O2	-1.299438	-2.045093	-0.178506
O3	-1.173926	0.172177	-1.104054
O4	-1.075213	-0.077042	1.303014
C5	1.630746	0.159384	0.006276
O6	0.788834	-0.904365	-0.075667
O7	1.26112	1.292189	0.107232
H8	-1.241223	1.150987	-0.787416
O9	-1.226111	2.506805	-0.133028
H10	-1.747474	2.407318	0.670574
H11	-0.303424	2.446677	0.159331
C12	3.064423	-0.269362	-0.059601
H13	3.524571	0.217934	-0.916517
H14	3.565562	0.090267	0.836447
H15	3.16024	-1.345346	-0.140803

Table C.6 Cartesian coordinates from M06-2X/6-311++G(3df,3pd) calculations for ASA···H_2O [II] at its local minimum of potential energy

ASA···H_2O [II]			
Atom Number	x	y	z
S1	-0.541212	-0.276296	-0.026409
O2	-1.262394	-1.412472	-0.438833
O3	-0.599996	0.7662	-1.171057
O4	-0.747963	0.338521	1.231087
C5	2.006927	0.212005	0.032322
O6	1.012058	-0.734896	-0.075548
O7	1.786301	1.380944	-0.050744
H8	-0.080312	1.548583	-0.910141
C9	3.329682	-0.444508	0.2405
H10	3.502163	-1.170675	-0.551046
H11	4.10697	0.310142	0.248999
H12	3.309775	-0.983413	1.186177
O13	-3.634269	0.422626	0.230747
H14	-3.477253	-0.482194	-0.050281
H15	-3.151503	0.505934	1.056685

Table C.7. Cartesian coordinates from M06-2X/6-311++G(3df,3pd) calculation for ASA···H_2O [II] at the maximum energy along the CH_3 internal rotation coordinate

TS ASA-H_2O [II]			
Atom Number	x	y	z
S1	0.546949	0.279212	-0.01755
O2	1.267195	1.417932	-0.424205
O3	0.592578	-0.751991	-1.172173
O4	0.758658	-0.346673	1.233254
C5	-2.003187	-0.199078	0.035555
O6	-1.008244	0.744777	-0.051307
O7	-1.783156	-1.368858	-0.051036
H8	0.06564	-1.531742	-0.916481
C9	-3.346636	0.430412	0.219183
H10	-3.965972	0.163017	-0.634528
H11	-3.800825	-0.001119	1.108356
H12	-3.277849	1.507536	0.311997
O13	3.632428	-0.437923	0.203762
H14	3.487325	0.473829	-0.06073
H15	3.163759	-0.525035	1.037388

Table C.8 Cartesian coordinates from M06-2X/6-311++G(3df,3pd) calculations for $CH_3COOH\cdots H_2SO_4$ at its global minimum of potential energy

Acetic-H_2SO_4			
Atom Number	x	y	z
C1	2.417502	-0.05407	-0.01545
O2	1.995543	1.181425	-0.09363
O3	1.682049	-1.02834	-0.04276
H4	1.011654	1.219334	-0.16017
C5	3.902855	-0.17063	0.114114
H6	4.371959	0.308731	-0.7429
H7	4.224556	0.364809	1.005192
H8	4.189548	-1.21352	0.171502
S9	-1.55086	0.06195	-0.0767
O10	-0.68217	1.186875	-0.2466
O11	-2.8256	0.039954	-0.68501
O12	-0.80346	-1.22008	-0.44568
H13	0.20417	-1.13305	-0.27136
O14	-1.73325	-0.04806	1.486672
H15	-2.49372	-0.61015	1.684579

Table C.9 ASA···H_2O [I] structural information from M06-2X/6-311++G(3df,3pd) calculations[*†]

ASA-H2O [I.]		M06-2X/6-311++G(3df,3pd)
S1-O2	1.40689	
S1-O3	1.5281	
S1-O4	1.42029	
S1-O6	1.63377	
O3-H8	1.03	
O4-H15	2.64743	
C5-O6	1.36192	
C5-O7	1.19504	
O7-H8	2.66771	
O7-H14	1.95292	
H8-O13	1.50865	
O13-H14	0.96951	
O13-H15	0.96308	
∠(S1-O3-H8)	110.23471	
∠(S1-O4-H15)	106.06356	
∠(O2-S1-O3)	110.04414	
∠(O2-S1-O4)	122.06506	
∠(O2-S1-O6)	102.82713	
∠(O3-S1-O4)	110.38695	
∠(O3-S1-O6)	102.2258	
∠(O3-H8-O13)	171.02118	
∠(O4-S1-O6)	107.11101	
∠(O4-H15-O13)	99.19079	
∠(C5-O7-H14)	144.24775	
∠(O6-C5-O7)	123.6981	
∠(O7-H14-O13)	142.4626	
∠(H8-O13-H14)	94.97543	
∠(H8-O13-H15)	105.22174	
∠(H14-O13-H15)	104.87384	

[*]All distances in Å.
[†]All angles in degrees.

Table C.10 ASA···H_2O [II] structural information from M06-2X/6-311++G(3df,3pd) calculations[*†]

ASA-H2O [II.]		
		M06-2X/6-311++G(3df,3pd)
S1-O2	1.40751	
S1-O3	1.54935	
S1-O4	1.41494	
S1-O6	1.6203	
O2-O14	2.43351	
O3-H8	0.97482	
O4-H15	2.41567	
C5-O6	1.37769	
C5-O7	1.19247	
O7-H8	2.06177	
O13-H14	0.96038	
O13-H15	0.9603	
∠(S1-O2-H14)	96.37147	
∠(S1-O3-H8)	108.78786	
∠(S1-O4-H15)	96.39242	
∠(O2-S1-O3)	107.8924	
∠(O2-S1-O4)	122.43191	
∠(O2-S1-O6)	104.70402	
∠(O3-S1-O4)	111.01874	
∠(O3-S1-O6)	101.79489	
∠(O3-H8-O7)	121.93482	
∠(O4-S1-O6)	106.85866	
∠(O4-H15-O13)	123.79911	
∠(C5-O7-H8)	106.036	
∠(O6-C5-O7)	122.32275	
∠(O13-H14-O2)	123.75808	
∠(H14-O13-H15)	104.54971	

[*]All distances in Å.
[†]All angles in degrees.

C.11 $CH_3COOH\cdots H_2SO_4$ structural information from M06-2X/6-311++G(3df,3pd) calculations[*†]

ASA-H2O [II.]	
	M06-2X/6-311++G(3df,3pd)
S1-O2	1.40751
S1-O3	1.54935
S1-O4	1.41494
S1-O6	1.6203
O2-O14	2.43351
O3-H8	0.97482
O4-H15	2.41567
C5-O6	1.37769
C5-O7	1.19247
O7-H8	2.06177
O13-H14	0.96038
O13-H15	0.9603
∠(S1-O2-H14)	96.37147
∠(S1-O3-H8)	108.78786
∠(S1-O4-H15)	96.39242
∠(O2-S1-O3)	107.8924
∠(O2-S1-O4)	122.43191
∠(O2-S1-O6)	104.70402
∠(O3-S1-O4)	111.01874
∠(O3-S1-O6)	101.79489
∠(O3-H8-O7)	121.93482
∠(O4-S1-O6)	106.85866
∠(O4-H15-O13)	123.79911
∠(C5-O7-H8)	106.036
∠(O6-C5-O7)	122.32275
∠(O13-H14-O2)	123.75808
∠(H14-O13-H15)	104.54971

[*]All distances in Å.
[†]All angles in degrees.

Appendix D: Supplemental Material for Chapter 4

Table D.1 Observed transitions for the parent isotopologue, $HCCCOOSO_2OH$

J′	K_a'	K_c'	J″	K_a''	K_c''	Observed Frequency [MHz]	Obs-Calc [MHz]
3	1	3	2	1	2	5338.979	0.000
3	0	3	2	0	2	5457.076	0.000
3	1	2	2	1	1	5589.498	0.000
2	1	2	1	0	1	5979.359	-0.001
2	1	1	1	0	1	6229.914	-0.001
4	1	4	3	1	3	7116.232	0.000
4	0	4	3	0	3	7266.248	0.000
4	1	3	3	1	2	7450.096	0.000
3	1	3	2	0	2	7676.750	0.000
3	1	2	2	0	2	8177.824	0.001
5	1	5	4	1	4	8891.523	0.002
5	0	5	4	0	4	9067.161	-0.006
5	1	4	4	1	3	9308.379	-0.011
4	1	4	3	0	3	9335.907	0.001
4	1	3	3	0	3	10170.843	0.001
6	1	6	5	1	5	10664.469	-0.008
6	0	6	5	0	5	10858.188	-0.004
6	2	5	5	2	4	10921.528	-0.001
6	2	4	5	2	3	10994.421	0.002
6	1	5	5	1	4	11163.674	-0.001
7	1	7	6	1	6	12434.796	-0.008
7	0	7	6	0	6	12638.180	-0.005
7	2	6	6	2	5	12736.393	-0.010
7	2	5	6	2	4	12851.093	0.002
7	1	6	6	1	5	13015.160	0.004
8	1	8	7	1	7	14202.285	-0.007
8	0	8	7	0	7	14406.737	-0.004
8	2	7	7	2	6	14548.800	-0.012
8	2	6	7	2	5	14716.678	0.010
8	1	7	7	1	6	14861.951	0.011

Table D.2 Observed transitions for the deuterated isotopologue, $HCCCOOSO_2OD$

J′	K_a'	K_c'	J″	K_a''	K_c''	Observed Frequency [MHz]	Obs-Calc [MHz]
3	1	3	2	1	2	5312.485	0.002
3	0	3	2	0	2	5434.772	0.001
3	1	2	2	1	1	5572.986	-0.001
4	1	4	3	1	3	7080.640	0.000
4	0	4	3	0	3	7235.413	-0.002
4	1	3	3	1	2	7427.793	0.002
5	1	5	4	1	4	8846.628	0.001
5	0	5	4	0	4	9026.923	-0.001
5	2	4	4	2	3	9068.412	-0.001
5	2	3	4	2	2	9115.160	-0.002
5	1	4	4	1	3	9280.024	0.000
4	1	3	3	0	3	10091.278	0.000
6	1	6	5	1	5	10610.043	0.000
6	0	6	5	0	5	10807.541	0.001
6	2	5	5	2	4	10877.759	0.003
6	2	4	5	2	3	10958.596	-0.001
6	1	5	5	1	4	11128.884	-0.002

Table D.3 Observed transitions for the ^{34}S isotopologue, $HCCCOO^{34}SO_2OH$

J′	K_a'	K_c'	J″	K_a''	K_c''	Observed Frequency [MHz]	Obs-Calc [MHz]
3	1	3	2	1	2	5309.309	0.000
3	0	3	2	0	2	5426.296	0.000
3	1	2	2	1	1	5557.299	-0.001
4	1	4	3	1	3	7076.721	-0.001
4	0	4	3	0	3	7225.419	0.001
4	1	3	3	1	2	7407.229	0.004
5	1	5	4	1	4	8842.212	0.001
5	0	5	4	0	4	9016.460	0.001
5	1	4	4	1	3	9254.900	0.001
6	1	6	5	1	5	10605.413	-0.001
6	0	6	5	0	5	10797.801	-0.001
6	2	5	5	2	4	10859.812	0.000
6	1	5	5	1	4	11099.633	-0.002

Table D.4 Cartesian coordinates for the minimum energy structure of the HCCCOOH···SO_3 van der Waals complex

Atom	X	Y	Z
S1	-1.524935	-0.120593	0.010886
O2	-1.936983	-0.902187	-1.087556
O3	-1.351654	1.293259	-0.205351
O4	-1.758723	-0.549727	1.335261
C5	1.331926	0.20694	-0.019515
O6	0.408338	-0.617268	-0.056221
O7	1.186549	1.487144	0.004286
H8	0.211042	1.695993	-0.045589
C9	2.690392	-0.265183	-0.002718
C10	3.810717	-0.677057	0.010009
C11	4.809486	-1.044486	0.021394

Table D.5 Cartesian coordinates for the HCCCOOH···SO_3 optimized transition state geometry corresponding to π_2+ π_2+σ_2 cycloaddition

Atom	X	Y	Z
S1	-1.388945	-0.164369	0.026165
O2	-1.987158	-0.977559	-0.953922
O3	-1.264521	1.263887	-0.354695
O4	-1.607895	-0.383682	1.403263
C5	1.259123	0.259125	-0.036403
O6	0.328103	-0.624786	-0.128337
O7	1.054097	1.486061	0.017538
H8	-0.11011	1.599081	-0.131679
C9	2.599952	-0.251674	-0.01013
C10	3.714755	-0.678055	0.014335
H11	4.709245	-1.056918	0.035457

Table D.6 Cartesian coordinates for the minimum energy structure of $HCCCOOSO_2OH$

Atom	X	Y	Z
S1	-1.255346	-0.19212	0.080457
O2	-1.982676	-1.303303	-0.372136
O3	-1.412263	0.940392	-0.972667
O4	-1.357552	0.328595	1.387646
C5	1.276042	0.33621	-0.035812
O6	0.309565	-0.615994	-0.137088
O7	1.056736	1.508996	0.005119
H8	-0.880505	1.706494	-0.689658
C9	2.586006	-0.266955	-0.012862
C10	3.679182	-0.746791	0.008607
H11	4.654056	-1.172362	0.028826

Table D.7 Vibrational Frequencies Used in the Calculation of Equilibrium Constants[a]

Molecule	**Vibrational Frequencies (cm^{-1})**
SO_3	506.6989, 527.4375, 527.4569, 1106.8185, 1422.3692, 1422.3789
H_2O	1574.4943, 3770.1572, 3867.9914
HCOOH	627.5706, 653.6345, 1041.7412, 1130.1276, 1280.5455, 372.5985, 1822.0771, 3006.5829, 3696.9804
CF_3COOH	40.7012, 232.7321, 239.7646, 383.6738, 420.5047, 497.6585, 576.277, 583.2998, 663.0726, 783.3429, 801.1812, 1145.9192, 1208.0186, 1209.0662, 1272.9989, 1413.2803, 1874.8839, 3707.5728
HCCCOOH	105.9531, 236.9225, 523.994, 576.1024, 591.5254, 705.4713, 743.7378, 765.7568, 814.9067, 1171.3332, 1338.7649, 1809.9133, 2203.3841, 3373.5145, 3709.6874
cis-H_2C=CHCOOH	109.416, 275.4703, 473.4473, 485.6305, 615.077, 627.0953, 819.2523, 827.9338, 1001.7772, 1005.3177, 1044.108, 1159.4701, 1256.3052, 1336.2332, 1405.7725, 1674.2103, 1808.4874, 3077.3444, 3128.3276, 3172.7924, 3718.1555
trans-H_2C=CHCOOH	106.9134, 285.8396, 474.3106, 523.412, 576.1121, 578.8281, 825.567, 828.6128, 997.9554, 1011.7391, 1013.4851, 1190.6362, 1270.7 1343.159, 1412.6692, 1666.9741, 1807.983, 3080.3999, 3129.8505, 3172.1813, 3726.9049
C_6H_5COOH	63.7872, 155.0351, 214.9714, 376.069, 401.7061, 421.3098, 486.552, 571.2524, 608.2967, 627.9586, 681.0176, 713.9006, 761.8671, 811.7348, 854.6088, 949.4845, 980.3887, 989.2642, 1002.7957, 1025.2512, 1072.8976, 1104.7621, 1142.4466, 1160.5274, 1185.3497, 1288.8681, 1305.6685, 1353.247, 1447.3661, 1491.0937, 1604.3315, 1622.7906, 1801.9399, 3105.6102, 3118.6664, 3125.6407, 3134.8945, 3142.0628, 3726.8952
$HCOOSO_2OH$	115.1681, 210.199, 224.5259, 327.3168, 391.589, 454.4644, 501.1311, 517.398, 543.7626, 704.8408, 798.0384, 898.9087, 1025.4064, 1117.5564, 1178.0747, 1249.0399, 1360.4832, 1480.802, 1804.2194, 3039.9509, 3593.9179
CF_3COOSO_2OH	33.659, 59.7617, 125.906, 130.0867, 213.4388, 240.9383, 301.7476, 339.3254, 388.0873, 411.9105, 443.3191, 487.4153, 516.1564, 538.544, 540.29,

	593.6691, 727.4515, 757.7737, 783.0713, 863.1836, 910.0831, 1128.9636, 1165.2222, 1225.013, 1254.4137, 1272.9407, 1348.1933, 1492.7524, 1859.3445, 3617.7411
$HCCCOOSO_2OH$	62.7881, 118.9511, 124.7129, 226.0294, 246.7874, 328.6845, 379.1342, 411.765, 455.124, 492.8376, 539.6013, 596.8604, 619.9755, 720.6421, 746.803, 763.4579, 788.222, 880.3429, 926.059, 1179.0156, 1188.8611, 1256.4507, 1480.9475, 1795.3924, 2207.914, 3368.8391, 3591.6384
s-trans $H_2C=COOSO_2OH$	54.611, 110.3278, 139.5927, 165.2104, 254.4213, 332.7197, 377.8441, 460.3911, 472.681, 488.9382, 525.0998, 543.9566, 563.4051, 637.6198, 786.3402, 826.1199, 872.4665, 918.7452, 1001.2534, 1007.9076, 1017.3845, 1189.7535, 1224.3922, 1266.6066, 1273.707, 1407.7028, 1471.6646, 1662.483, 1793.9665, 3085.9289, 3133.9245, 3178.4572, 3569.8813
s-cis $H_2C=COOSO_2OH$	60.6056, 100.589, 132.9482, 156.7229, 287.1394, 327.7048, 359.773, 391.007, 464.824, 478.5592, 527.5345, 547.5747, 587.9946, 682.6181, 776.4365, 817.0795, 871.4771, 918.396, 997.7614, 1016.8607, 1060.0354, 1148.0241, 1190.0348, 1250.3494, 1294.7075, 1400.1368, 1473.9538, 1666.4018, 1792.5309, 3081.7773, 3140.1422, 3177.7491, 3555.3507
$C_6H_5COOSO_2OH$	41.5257, 47.5203, 113.393, 123.4034, 165.1328, 228.1149, 292.1349, 344.2336, 385.0124, 400.1832, 430.3017, 449.0615, 485.4753, 506.728,, 544.0051, 579.9145, 607.3655, 675.9251, 677.2055, 709.4192, 782.596, 813.7524, 835.3058, 854.1723, 901.6926, 953.9271, 979.3023, 991.9123 1008.8679, 1024.9796, 1063.8378, 1088.3788, 1146.9377,1167.5987, 1192.227, 1232.9379, 1271.3208, 1293.7278, 1310.5185, 1449.6553, 1470.4909, 1490.2013, 1604.0114, 1620.3656, 1782.0937, 3110.111, 3123.2448, 3129.5692, 3137.9597, 3144.8564, 3555.6223
$SO_3–H_2O$	41.7197, 189.7902, 200.305, 205.9795, 494.118, 506.2818, 507.0287, 560.2235, 602.8162, 1102.405, 1403.6676, 1421.5156, 1558.0916, 3709.765, 3806.1054
$(H_2O)_2–SO_3$	17.557 162.6302, 207.6576, 240.1332, 286.4604, 293.2407, 334.0971, 357.5905, 512.1988, 526.9913, 544.4125, 555.9943, 569.7683, 797.8347, 1088.3691, 1130.3895, 1363.2186, 1419.1391, 1570.0905, 1577.2879, 2922.9689, 3659.8682, 3738.2539, 3811.2076

(a) The values in the table were obtained from the M06-2X/6-311++G(3df,3pd) level of theory and were scaled by a factor of 0.97.

Table D.8 Rotational Constants and Dissociation Energies Used in the Calculations of Equilibrium Constants [(a)]

Molecule	***A, B, C* [MHz]**	D_e **(hartree)[a]**
SO_3	10543.626, 10543.626, 5271.713	623.229702
H_2O	829677.55, 433104.86, 284560.02	76.377668
HCOOH	78320.692, 12236.909, 10581.709	189.599512
CF_3COOH	3903.273, 2518.972, 2088.704	526.420135
HCCCOOH	12277.865, 4161.592, 3108.099	265.632706
cis-H_2C=CHCOOH	11240.206, 4293.414, 3106.736	266.896944
trans-H_2C=CHCOOH	10860.909, 4430.007, 3146.567	266.896565
C_6H_5COOH	3919.808, 1236.906, 940.218	420.340862
$HCOOSO_2OH$	4541.770, 2026.889, 1926.781	812.858739
CF_3COOSO_2OH	2158.913, 591.945, 560.621	1149.675633
$HCCCOOSO_2OH$	3389.781, 957.114, 873.140	888.891850
s-trans H_2C=$COOSO_2OH$	2874.374, 1057.195, 909.673	890.159595
s-cis H_2C=$COOSO_2OH$	3667.119, 901.388, 842.265	890.159437
$C_6H_5COOSO_2OH$	2054.544, 384.145, 345.444	1043.604363
SO_3–H_2O	5215.536, 3975.785, 3939.703	699.622709
$(H_2O)_2$–SO_3	4612.963, 2011.670, 1922.849	776.021545

(a) Obtained at the CCSD(T)/CBS(D-T)//M06-2X/6-311++G(3df,3pd) level of theory.

Procedure for Calculating Equilibrium Constants

The procedure used to determine the pressure-dependent equilibrium constants and atmospheric abundances is detailed by Vaida et al.[179] and here. Using equilibrium statistical mechanics and thermodynamics,[178] vibrational and rotational constants, binding energies, and atmospheric inputs[179,183], we calculated $\Delta H°$, $\Delta S°$, $\Delta G°$, and K for seven carboxylic sulfuric anhydride molecules, *cis*-AcrSA, *trans*-AcrSA, BSA, FSA, PinicSA, PSA, and TFASA.

It can be shown that the enthalpy change for the formation of molecules or clusters from nonlinear monomeric constituents is given by,

$$\Delta H_T^o = -4RT + \Delta E_{T,vib}^o + BE \tag{D.1}$$

where $\Delta E_{T,vib}^o$ is the change in the vibrational contribution to internal energy upon complexation or formation (J/mol) and BE is the binding energy of the molecule or complex (J/mol). $\Delta E_{T,vib}^o$ can be determined by calculating $E_{T,vib}^o$ for the dimer and then subtracting the individual monomers, equation (D.2),

$$\Delta E_{T,vib}^o = E_{T,vib}^o(M_1 - M_2) - E_{T,vib}^o(M_1) - E_{T,vib}^o(M_2) \tag{D.2}$$

For a nonlinear polyatomic molecule, the vibrational contribution to the internal energy is given by,

$$E_{T,vib}^o = \frac{hcR}{k_B} \sum_{j=1}^{3n-6} \left\{ \widetilde{\nu_j} \left[\frac{1}{2} + (e^{\frac{hc\tilde{\nu}_j}{k_B T}} - 1)^{-1} \right] \right\} \tag{D.3}$$

where h is Planck's constant (J*s), c is the speed of light in a vacuum (cm/s), R is the universal gas constant (J K^{-1} mol^{-1}), k_b is Boltzmann's constant (J/K unless otherwise

stated), T is temperature (K), n is the number of atoms in the molecule, and $\tilde{\nu}_j$ is the jth vibrational constant (cm^{-1}).

Calculating the entropy change, $\Delta S°$, is slightly more complicated because not only do the vibrational frequencies need to be known, as it was for calculating the enthalpy, but the rotational constants for both the reactants and products need to be known as well. $\Delta S°$ is defined by,

$$\Delta S° = \Delta S°_{T,trans} + \Delta S°_{T,rot} + \Delta S°_{T,vib} + \Delta S°_{T,elec} \tag{D.5}$$

which show how the translational, rotational, vibrational, and electronic contributions affect the total change in entropy. The individual $\Delta S°_{T,x}$ terms (x = trans, rot, vib, or elec) are written as the product subtracted from each monomer, as shown in equation (D.6),

$$\Delta S^o_{T,x} = S^o_{T,x}(M_1 - M_2) - S^o_{T,x}(M_1) - S^o_{T,x}(M_2) \tag{D.6}$$

Each $\Delta S°_{T,x}$ term, summarized in eq. (D.7-D.10), is calculated using structural and spectroscopic information[137],

$$\Delta S°_{T,trans} = R\ ln\left[\left(\frac{2\pi m k_B T}{h^2}\right)^{3/2} * \frac{e^{5/2} k_B T}{P^o}\right] \tag{D.7}$$

$$\Delta S°_{T,rot} = R \ln\left[\left(\frac{T^3}{\theta_A \theta_B \theta_C}\right)^{1/2} * \frac{\pi^{1/2} e^{3/2}}{\sigma}\right], where\ \theta_A = \frac{\tilde{A}}{k_B}, etc. \tag{D.8}$$

$$\Delta S°_{T,vib} = R \sum_{j=1}^{3n-6} \left\{\frac{hc\tilde{\nu}_j}{k_B T} * (e^{\frac{hc\tilde{\nu}_j}{k_B T}} - 1)^{-1} - \ln(1 - e^{\frac{-hc\tilde{\nu}_j}{k_B T}})\right\} \tag{D.9}$$

$$\Delta S°_{T,elec} = R \ln \omega_{el} \tag{D.10}$$

The variables introduced in the above equations are defined as follows: m is the mass of the molecule (kg), k_B is the Boltzmann constant (Torr*m^3/K in eq. (D.7) and 1/cm^{-1}*K in eq. (D.8)), P^o is the standard reference pressure of 1 atm, σ is the molecular symmetry number, $\tilde{A}$ is the characteristic rotational constant in wavenumbers, and ω_{el} is the molecular ground-state degeneracy.

We were able to determine the standard Gibb's free energy change, $\Delta G°$, for the reaction by inserting our calculated values of $\Delta H°$ and $\Delta S°$ at different temperatures into equation (D.11) given below,

$$\Delta G° = \Delta H° - T\Delta S° \tag{D.11}$$

The temperature-dependent thermodynamic equilibrium constant, *K(T),* was also obtained, since the relation to $\Delta G°$ is as follows:

$$K(T) = e^{\frac{-\Delta G°}{RT}} \tag{D.12}$$